2018

THE DEVELOPMENT OF NOVEL NON-PEPTIDE PROTEASOME INHIBITORS FOR THE TREATMENT OF SOLID TUMORS

Zachary C. Miller

University of Kentucky, zach.miller@uky.edu

Author ORCID Identifier:

https://orcid.org/0000-0002-1193-7646

Digital Object Identifier: https://doi.org/10.13023/ETD.2018.177

STUDENT AGREEMENT:

I represent that my thesis or dissertation and abstract are my original work. Proper attribution has been given to all outside sources. I understand that I am solely responsible for obtaining any needed copyright permissions. I have obtained needed written permission statement(s) from the owner(s) of each third-party copyrighted matter to be included in my work, allowing electronic distribution (if such use is not permitted by the fair use doctrine) which will be submitted to UKnowledge as Additional File.

I hereby grant to The University of Kentucky and its agents the irrevocable, non-exclusive, and royalty-free license to archive and make accessible my work in whole or in part in all forms of media, now or hereafter known. I agree that the document mentioned above may be made available immediately for worldwide access unless an embargo applies.

I retain all other ownership rights to the copyright of my work. I also retain the right to use in future works (such as articles or books) all or part of my work. I understand that I am free to register the copyright to my work.

REVIEW, APPROVAL AND ACCEPTANCE

The document mentioned above has been reviewed and accepted by the student's advisor, on behalf of the advisory committee, and by the Director of Graduate Studies (DGS), on behalf of the program; we verify that this is the final, approved version of the student's thesis including all changes required by the advisory committee. The undersigned agree to abide by the statements above.

Zachary C. Miller, Student

Dr. Kyung Bo Kim, Major Professor

Dr. David Feola, Director of Graduate Studies

THE DEVELOPMENT OF NOVEL NON-PEPTIDE
PROTEASOME INHIBITORS FOR THE TREATMENT OF SOLID TUMORS

DISSERTATION

A dissertation submitted in partial fulfillment of the
requirements for the degree of Doctor of Philosophy in the
College of Pharmacy
at the University of Kentucky

By

Zachary C. Miller

Lexington, Kentucky

Director: Kyung Bo Kim, Ph.D., Associate Professor of Pharmaceutical Sciences

Lexington, Kentucky

2018

ABSTRACT OF DISSERTATION

THE DEVELOPMENT OF NOVEL NON-PEPTIDE
PROTEASOME INHIBITORS FOR THE TREATMENT OF SOLID TUMORS

The proteasome is a large protein complex which is responsible for the majority of protein degradation in eukaryotes. Following FDA approval of the first proteasome inhibitor bortezomib for the treatment of multiple myeloma (MM) in 2003, there has been an increasing awareness of the significant therapeutic potential of proteasome inhibitors in the treatment of cancer. As of 2017, three proteasome inhibitors are approved for the treatment of MM but in clinical trials with patients bearing solid tumors these existing proteasome inhibitors have demonstrated poor results. Notably, all three FDA-approved proteasome inhibitors rely on the combination a peptide backbone and reactive electrophilic warhead to target the proteasome, and all three primarily target the catalytic subunits conferring the proteasome's chymotrypsin-like (CT-L) activity.

It is our hypothesis that compounds with non-peptidic structures, non-covalent and reversible modes of action, and unique selectivity profiles against the proteasome's distinct catalytic subunits could have superior pharmacodynamic and pharmacokinetic properties and may bear improved activity against solid tumors relative to existing proteasome inhibitors. In an effort to discover such compounds we have employed an approach which combines computational drug screening methods with conventional screening and classic medicinal chemistry.

Our efforts began with a computational screen performed in the lab of Dr. Chang-Guo Zhan. This virtual screen narrowed a library of over 300,000 drug-like compounds down to

under 300 virtual hits which were then screened for proteasome inhibitory activity in an *in vitro* assay. Despite screening a relatively small pool of compounds, we were able to identify 18 active compounds. The majority of these hits were non-peptide in structure and lacked any hallmarks of covalent inhibition. The further development of one compound, a tri-substituted pyrazole, provided us with a proteasome inhibitor which demonstrated cytotoxic activity in a variety of human solid cancer cell lines as well as significant anti-tumor activity in a prostate cancer mouse xenograft model. We have also evaluated the *in vitro* pharmacokinetic properties of our lead compound and investigated its ability to evade cross-resistance phenomena in proteasome inhibitor-resistant cell lines.

We believe that our lead compound as well as our drug discovery approach itself will be of interest and use to other researchers. We hope that this research effort may aid in the further development of reversible non-peptide proteasome inhibitors and may eventually deliver new therapeutic options for patients with difficult-to-treat solid tumors.

Zachary C. Miller

April 27, 2018

THE DEVELOPMENT OF NOVEL NON-PEPTIDE PROTEASOME INHIBITORS FOR THE
TREATMENT OF SOLID TUMORS

By

Zachary C. Miller

Dr. Kyung Bo Kim
Director of Dissertation

Dr. David Feola
Director of Graduate Studies

April 27, 2018

To my parents, who have supported and encouraged me throughout my life, and who always fostered my love of learning and discovery. I could not have made it here without you both.

ACKNOWLEDGEMENTS

TABLE OF CONTENTS

iv

LIST OF FIGURES

Chapter 1   INTRODUCTION

1.1   Introduction and History of the Ubiquitin-Proteasome System (UPS)

The discovery of the biological system now referred to as the ubiquitin-proteasome system can be traced back to the 1940's when pioneering work by Schoenheimer showed that cellular proteins exist in a state of flux, being both continuously synthesized and continuously degraded. This corrected the prior view that cellular proteins were generally stable [1, 2]. In 1955, the discovery of a new organelle known as the lysosome was reported by de Duve [3]. The lysosome is an acidic, membrane-bound organelle containing a variety of hydrolytic enzymes capable of degrading cellular proteins. This discovery, along with additional studies into the function of the lysosome, lead to the belief that the lysosome was chiefly responsible for cellular protein turnover [2]. It would not be until the late 1970's that a more accurate picture of cellular protein degradation would begin to emerge with the discovery of the ubiquitin-proteasome system (UPS).

When discussing the discovery of the ubiquitin-proteasome system, the work done by Aaron Ciechanover, Avram Hershko, and Irwin Rose in the 1970's and 1980's is of particular importance. Their efforts formed the basis for our modern understanding of the UPS and for this work they were awarded the 2004 Nobel Prize in Chemistry. Although we now understand that the UPS plays a key role in cellular protein degradation, including the regulation of many important signaling proteins, this knowledge was acquired gradually thanks to the publication of many seminal papers in 1970's, 80's, and 90's. Much of this early work in unraveling the function of the ubiquitin-proteasome system was aided by the use of the rabbit reticulocyte system, a preparation from cells which lacked lysosomes yet which had the capability for ATP-dependent protein degradation [4]. In 1980, publications by Ciechanover et al. and Hershko et al. demonstrated that ATP-dependent protein degradation in the rabbit reticulocyte system relied on a small protein factor dubbed APF-1 which could be covalently linked to lysine ε-amino groups in target proteins via an isopeptide bond [5, 6]. This would result in the breakdown of those target proteins and the recycling of the APF-1 protein. Later that same year, APF-1 was positively identified as the widely-distributed 8.5 kDa protein ubiquitin [7]. By the mid-1980's it was known that a cascade of three enzymes was responsible for the ATP-dependent conjugation of ubiquitin to a target protein and there

was strong evidence that ubiquitination was the key signal for non-lysosomal protein degradation [8, 9].

At this point the protease or proteases responsible for the degradation of ubiquitin-tagged proteins were still unknown. Some of the first steps towards the discovery of the proteasome began with publications by Wilk et al. in 1979 and 1980 which reported the purification and characterization of an abundant neutral endopeptidase from bovine pituitaries. This endopeptidase was found to have an apparent molecular weight of 700 kDa and was believed to consist of multiple smaller subunits providing the protein complex with multiple distinct proteolytic activities [10, 11]. One of the major steps towards linking this protein complex with the ubiquitin tagging system came in 1986 when Hough et al. described the partial purification of a similar large proteolytic complex from rabbit reticulocyte lysate [12]. They demonstrated the ability of this complex to degrade ubiquitin-conjugated lysozyme in the presence of ATP, but not unconjugated lysozyme. This complex was dubbed the proteasome by Arrigo et al. in 1988 and in the following years numerous additional publications contributed to our modern understanding of the structure and function of the proteasome [13-16].

We now know that ubiquitin is a key posttranslational modification used in numerous biological systems beyond just protein degradation, such as DNA repair and endocytic trafficking [17, 18]. Although a target protein can be tagged with a single ubiquitin molecule (monoubiquitination), the use of polymeric chains of ubiquitin is more frequently observed and these polyubiquitin chains can adopt different structures based on the particular choice of lysine residue used to link them together [19]. These distinct structural conformations allow for recognition by a variety of ubiquitin receptors which determine the biological fate of the ubiquitinated or polyubiquitinated protein [20, 21].

As mentioned previously, the process of attaching one or more ubiquitin polypeptides to a target protein involves a cascade of three enzyme types known as E1, E2, and E3 (Figure 1.1). E1 proteins, also known as ubiquitin-activating enzymes, first use ATP to activate ubiquitin (Ub) via C-terminal adenylation. Next the E1 enzyme's catalytic cysteine (Cys) residue attacks the adenylated ubiquitin molecule, forming a E1~Ub complex via a thioester bond and releasing AMP. Once the E1 enzyme's Cys residue is loaded with a ubiquitin molecule, it can

interact with an E2 enzyme and ubiquitin can be transferred to a catalytically-active Cys residue on the E2 protein via a transthiolation reaction yielding a covalent E2~Ub complex. The third step in the ubiquitination cascade involves the E3 enzyme, also known as a ubiquitin ligase. The human genome encodes over 600 putative E3 enzymes, and it is believed that this diversity of E3 enzymes allows the ubiquitin system to interact with a wide array of substrates and thus to regulate a large number of biological processes [22, 23]. Most eukaryotic E3 enzymes fall into one of two families, the RING (Really Interesting New Gene) finger domain family or the HECT (Homologous to the E6AP Carboxyl Terminus) domain family. The majority of known E3 enzymes utilize a RING finger domain in which the E3 enzyme interacts with E2~Ub and mediates the direct transfer of ubiquitin from the E2 enzyme to the lysine side chain of a target protein [24]. HECT domain E3 enzymes instead utilize a catalytic Cys residue and an additional transthiolation step to yield a covalent E3~Ub complex. Now charged with ubiquitin, the HECT domain E3 can transfer its ubiquitin molecule to a target protein. Once a target protein has been covalently tagged with a single ubiquitin molecule via an isopeptide bond (dubbed 'initiation'), additional ubiquitin molecules can be attached to one of the lysine side chains present in the prior ubiquitin to build up a polyubiquitin chain via a step-wise process dubbed 'chain extension'. In most but not all cases, polyubiquitin chains are built up sequentially on the target protein, rather than being preassembled and attached in a single reaction [25]. Once a target protein has been polyubiquitinated, it is poised for a recognition by a variety of ubiquitin-binding proteins which can carry out further modifications to the polyubiquitin chain or mediate downstream functions such as protein degradation [26].
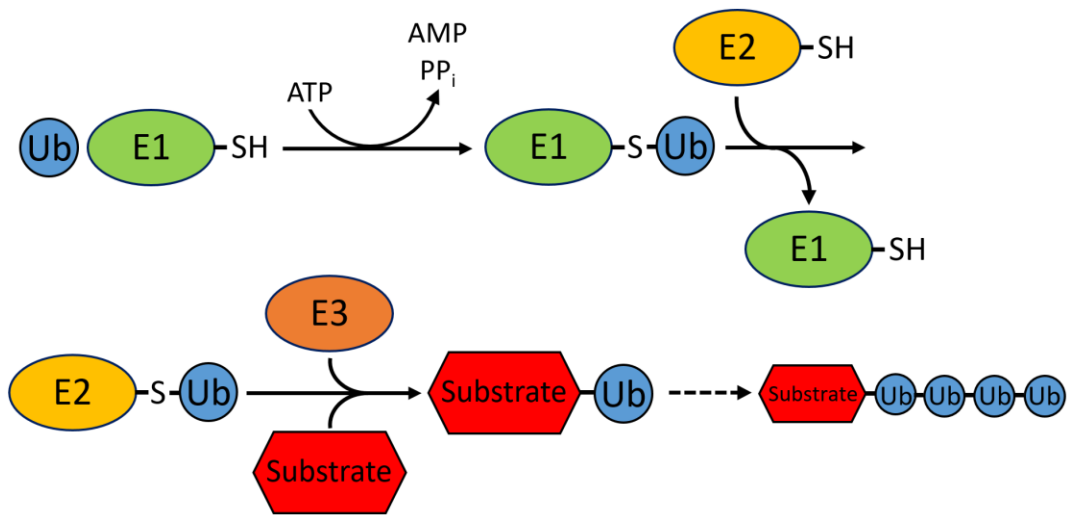
Figure 1.1   Substrate ubiquitination via ubiquitin cascade

Ubiquitination of a model substrate protein is mediated by E1, E2, and E3 enzymes. Repeated enzymatic cycles lead to the construction of a polyubiquitin chain on the target protein which serves as a signal for proteasomal degradation or other fates.

1.2   Structure and Function of the Proteasome

1.2.1   *The 20S Proteasome*

The canonical form of the proteasome in eukaryotes is known as the 26S proteasome, based on its sedimentation rate. This 26S proteasome is large protein complex, approximately 2.4 MDa, and can be dissociated into two main components, the 20S core proteasome particle and a 19S regulatory complex. The 20S core particle is responsible for the proteasome's proteolytic activity and has a molecular weight of approximately 700 kDa. The 19S regulatory complex handles recognition of substrate proteins and the subsequent transfer of these substrates into the 20S proteasome, and will be discussed in greater depth below.

Structurally, the 20S proteasome consists of a cylinder made from four stacked rings with each ring made from seven heteromeric subunits. X-ray crystallographic analysis has found that the mammalian 20S proteasome has an approximate overall length of 150 angstroms and an approximate diameter of 110 angstroms [27]. The cylinder is hollow internally, with the topmost and bottommost of the four stacked rings forming gates which segregate this space from the exterior environment. If we divide the cylinder horizontally between the two middle rings, we obtain two identical halves each consisting of 14 unique proteins forming two heptameric rings. In a complete 20S proteasome particle, the two outermost (top and bottom) rings are made from the α1-α7 subunits and are known as the alpha rings. The two inner rings are made from the β1-β7 subunits and are known as the beta rings (Figure 1.2). In total there are two copies each of 14 unique subunits, with subunits having individual molecular weights of approximately 20-30 kDa [28].

Functionally, the 20S proteasome contains three types of proteolytically-active subunits, the β1, β2, and β5 subunits located in the two inner beta rings [29]. The active sites of these subunits face inward, accepting peptide substrates from the proteasome's hollow inner chamber. By controlling which proteins enter its inner chamber, the proteasome is able to prevent non-specific degradation of cellular proteins [30]. These proteolytically-active subunits utilize an N-terminal threonine residue for their catalytic activity, placing them in the N-terminal nucleophile (Ntn) hydrolase family. These active threonine residues are initially masked by propeptide tails which serve both to prevent unregulated proteolytic

activity and which assist in assembly of the 20S proteasome complex [31]. The catalytically-active β1, β2, and β5 subunits also possess distinct substrate specificities from one another. Traditionally these substrate preferences have been described as caspase-like (C-L) for β1, trypsin-like (T-L) for β2, and chymotrypsin-like (CT-L) for the β5 catalytic subunit. This is to say that the β1, β2, and β5 catalytic subunits generally prefer acidic, basic, and hydrophobic amino acids in the P1 position of their substrates, respectively [29, 32]. As a whole, a 20S proteasome particle contains six proteolytically active subunits (two copies each of the β1, β2, and β5 subunits) which degrade peptides which have entered its interior chamber. Each catalytic subunit contains regions known as specificity pockets which interact with the amino acid side chains of peptide substrates. Peptide-based inhibitors of catalytic subunits also possess side chains which interact these specificity pockets. Differences in these specificity pockets provide the catalytic β-subunits with unique substrate preferences and also facilitate the design of subunit-selective proteasome inhibitors [33, 34]. Using the nomenclature described by Schechter and Berger, substrates have their residues or side chains labelled P1, P2, P3, etc. moving away from the scissile bond towards the peptide's N-terminus. On the other side of the scissile peptide bond, residues or side chains are labelled P1', P2', P3', etc. moving towards the peptide's C-terminus [35]. Similarly the proteasome subunit's specificity pockets which interact with these residues or side chains are labelled S1, S2, S3, etc. and S1', S2', S3', etc. [36].

Once a peptide substrate is bound to the active site of a β1, β2, or β5 subunit, the catalytic cycle can occur. Based on the quantum mechanical/molecular mechanical free energy calculations (QM/MM-FE) published by Wei et al. in 2013, the cycle is believed to begin with a water-assisted proton transfer from the catalytic N-terminal threonine's oxygen (Thr1O$^\gamma$) to the N-terminal threonine's free amino group (Thr1N) yielding a zwitterion. Now activated, the negatively charged Thr1O$^\gamma$ attacks the carbonyl carbon of the substrate's amide bond to generate a tetrahedral intermediate which, following a proton transfer, releases the C-terminal portion of the substrate leaving behind an acyl-enzyme intermediate. Next this intermediate undergoes nucleophilic attack by water which eventually leads to the release of the N-terminal portion of the substrate as well as the regeneration of the catalytic Thr1 residue [37]. The end result of this catalytic cycle is that proteins which are fed into the proteasome's inner chamber are cleaved into smaller peptides. Kisselev et al. measured the

degradation products produced when 26S proteasomes purified from rabbit muscle were incubated with non-ubiquitinated casein and chemically-denatured IGF, ovalbumin, and lactalbumin. The resulting peptides ranged from approximately 3-22 residues with a log-normal distribution and mean lengths of 6.5-9.0 residues. The high processivity of the proteasome is believed to result from the fact that the exit of small peptides from the proteasome's inner chamber is diffusion-controlled [38].

1.2.2   *The 19S Proteasome Regulatory Complex*

The work of recognizing polyubiquitinated substrate proteins, unfolding them, and then translocating them into the 20S proteasome's inner chamber is handled by the 19S regulatory particle, also known as PA700 [39]. Evidence suggests that the 20S proteasome itself may be capable of degrading oxidized or damaged proteins, but the ability of cellular proteasomes to efficiently degrade ubiquitinated proteins requires the presence of the 19S regulatory particle [40]. The overall structure of the 19S regulatory particle consists of a lid subcomplex and a base subcomplex, and it is via this base subcomplex that the 19S particle interacts with the 20S proteasome's alpha ring to form the larger 26S proteasome [41]. Due to the 20S proteasome's two symmetrical halves, it is possible for 19S regulatory caps to simultaneously bind to both ends of the 20S proteasome forming a "19S-20S-19S" complex, also referred to as the 30S proteasome [42]. For simplicity, the term "26S proteasome" is frequently used to refer indiscriminately both to 19S-20S and 19S-20S-19S proteasome complexes.

The 19S lid consists of at least nine non-ATP dependent subunits: Rpn3, Rpn5, Rpn6, Rpn7, Rpn8, Rpn9, Rpn11, and Rpn12. The 19S base consists of a ring of six homologous AAA-ATPase subunits known as Rpt1-6 as well as the non-ATP dependent subunits Rpn1, Rpn2, Rpn10, and Rpn13 [28, 39] (Figure 1.2). The ATP-dependent Rpt subunits are believed to be involved in the unfolding of client proteins as well as the opening of the gate which otherwise blocks the free entry of substrates into the 20S proteasome's inner chamber. The Non-ATPase Rpn-type proteins serve a variety of functions such as binding polyubiquitin (e.g. Rpn10 and Rpn13), interfacing with external ubiquitin-binding proteins (e.g. Rpn1), or cleaving ubiquitin off of client proteins in order to recycle ubiquitin for reuse [43-46]. Due to its

complexity and dynamic nature, some elements of the structure and the function of the 19S regulatory particle are not well understood and are generally beyond the scope of this work.

1.2.3   *The Immunoproteasome and Thymoproteasome*

In addition to the β1, β2, and β5 catalytic subunits found in the 20S proteasome, four additional catalytic proteasome subunits are encoded in the human genome. These additional catalytic subunits are all believed to be involved in immune function and occur only in jawed vertebrates [47]. The first three additional subunits are the β1i, β2i, and β5i catalytic subunits which are the respective homologues of the β1, β2, and β5 subunits. The β1i, β2i, and β5i subunits have 59-71% amino acid sequence identity to their respective constitutive homologues [48]. When present in the cell, the β1i, β2i, and β5i catalytic subunits are capable of incorporating into newly-formed 20S proteasomes in place of the β1, β2, and β5 subunits giving rise to immunoproteasomes (Figure 1.4). The immunoproteasome is so named due to its presence in a wide variety of immune system cells and due to its ability to be induced upon exposure to certain inflammatory cytokines such as tumor necrosis factor alpha (TNF-α) and interferon gamma (IFN-γ) [49]. Amino acid substitutions in the specificity pockets alter the substrate specificity of the immunoproteasome and allow it to generate an alternative repertoire of peptide products. Although all of the mechanisms by which the immunoproteasome modulates immune function are not fully understood, it is known that the expression of immunoproteasome catalytic subunits leads to increased production of peptides with a hydrophobic C-terminal amino acid and decreased production of peptides with an acidic C-terminal amino acid [50, 51]. An increase in N-terminally extended peptides has also been reported [52]. These alterations in the proteasome's cleavage pattern are consistent with the requirements for N-terminal trimming of potential antigens by ER aminopeptidase 1 (ERAP1) as well as the requirements for peptide binding to MHC Class I molecules [53-55]. Although there are known cases in which specific antigenic peptides are produced more readily by constitutive proteasomes, increased immunoproteasome expression generally leads to an increase in MHC Class I antigen presentation [56]. Additional evidence for the immunoproteasome's role in antigen presentation and other facets of immune function come from observations of altered immune responses when one or more immuno-subunits are genetically knocked out [57-59]. Alterations in immunoproteasome

expression or activity have also been implicated in various pathophysiological conditions including cancer, inflammatory diseases, and neurodegenerative diseases making it an important area of research [60-63].

The fourth and most recently discovered alternative catalytic subunit is β5t, a homologue of the β5 catalytic subunit with 50% amino acid sequence identity [48]. β5t is expressed specifically in cortical thymic epithelial cells (cTEC's) where it is incorporated along with β1i and β2i to form thymoproteasomes. These thymoproteasomes have been shown to function in the positive selection of CD8+ T-cells via the generation of an altered repertoire of peptides which are displayed by MHC Class I proteins. The β5t subunit exhibits reduced chymotrypsin-like activity and it has been hypothesized that this may aid in T-cell positive selection by generating weakly-bound or unstable peptide-MHC I complexes, however there is as yet little data available to verify this hypothesis [64, 65]. The precise mechanisms by which β5t expression aids CD8+ T-cell maturation are still an area of active research.
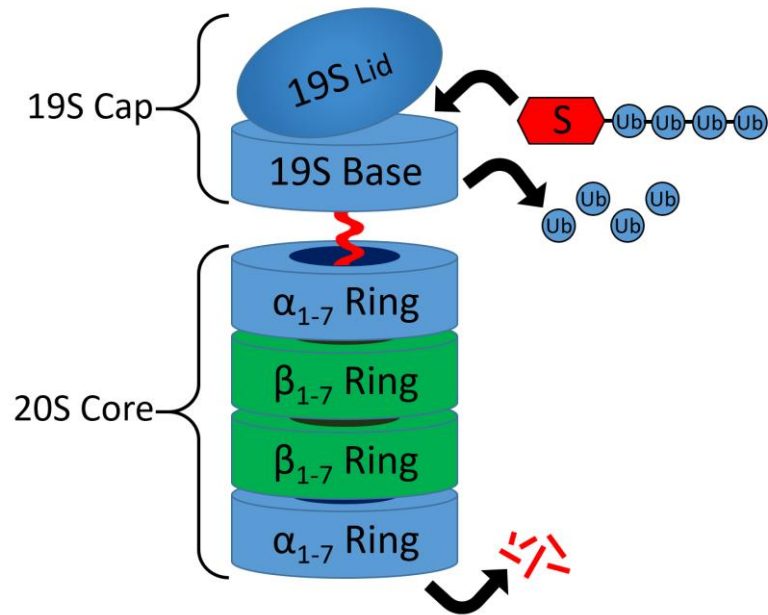
Figure 1.2   Structural diagram of the 26S proteasome

The 26S proteasome consists of a 20S core particle and one or two 19S regulatory caps affixed at either end. The 20S core particle is constructed from four hepta-heteromeric rings, two α-rings and two β-rings. The 19S regulatory cap consists of a lid component and a base component. Polyubiquitinated substrates are recognized, unfolded, and degraded into short polypeptides by the 26S proteasome complex. Polyubiquitin tags are released as free ubiquitin monomers.
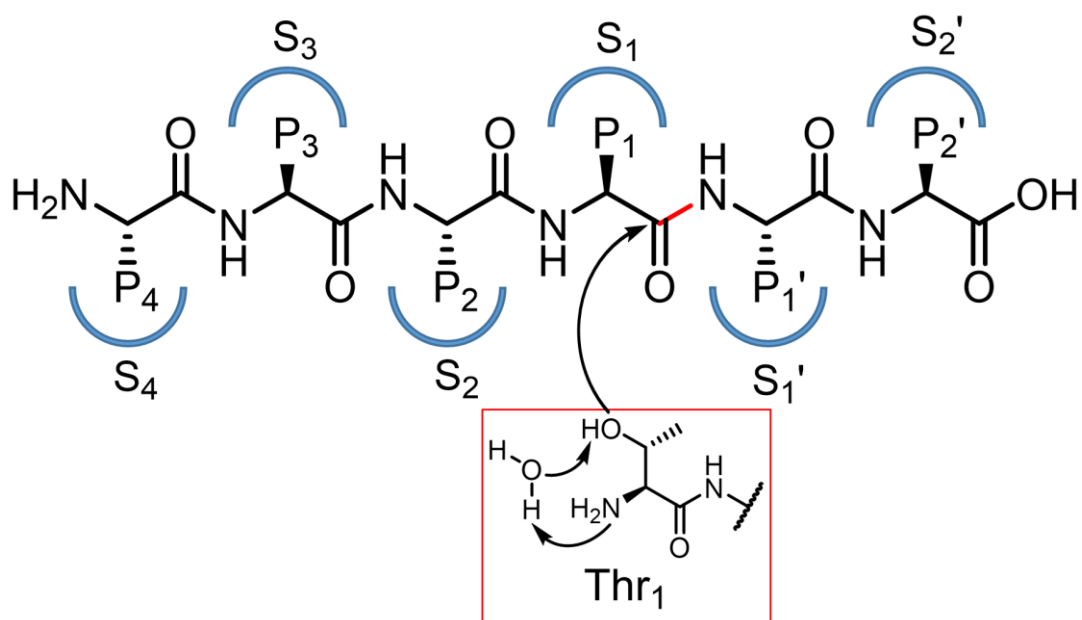
Figure 1.3   Proteasome catalytic site and Schechter and Berger nomenclature

A hypothetical substrate peptide containing side chain substituents P1-P4 and P1'-P2' interacting with the corresponding catalytic β-subunit specificity pockets denoted by blue semicircles, labeled S1-S4 and S1'-S2'. The scissile peptide bond is shown in red, with the catalytic β-subunit's Thr1 residue positioned to attack the adjacent carbonyl carbon yielding a tetrahedral intermediate followed by peptide bond hydrolysis.
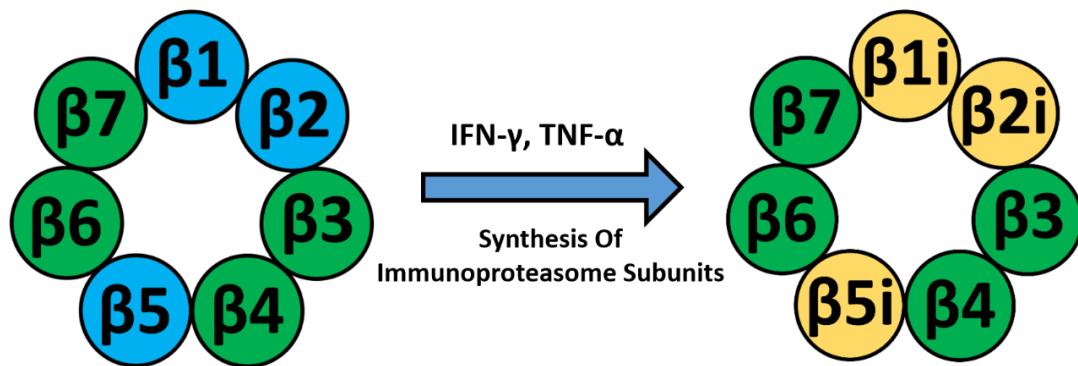
Figure 1.4   Cross-sectional view of constitutive and immunoproteasome β-rings

A cross-sectional diagram of proteasome and immunoproteasome β-rings containing three catalytically-active β-subunits (β1, β2, and β5 or β1i, β2i, and β5i) as well as four catalytically-inactive β-subunits. Exposure to IFN-γ or TNF-α triggers the synthesis of immunoproteasome catalytic subunits followed by their incorporation into newly synthesized proteasomes.

1.3   Deubiquitination

Before concluding our introduction to the ubiquitin-proteasome system, the reversible nature of ubiquitin tags must be discussed. As with most posttranslational modifications, ubiquitination is not an irreversible process and specific enzymes known as deubiquitinases (DUBs) exist to trim or remove mono- and polyubiquitin tags from proteins. Over 70 DUB's are encoded in the human genome and they perform a number of key functions within the ubiquitin-proteasome system. These include the production of free ubiquitin from newly-synthesized polymeric precursor proteins, the recycling of ubiquitin from proteins to be degraded, and the removal of ubiquitin tags from proteins preventing their degradation [66]. DUB's also regulate non-proteasomal functions of ubiquitin tags such as DNA damage repair and endocytic trafficking of cell-surface receptors [67, 68]. DUB proteins are critical for the normal function of the ubiquitin-proteasome system and also act to regulate the half-lives of specific substrate proteins including key signaling proteins such p53, NF-κB pathway proteins, and Myc [69-71].

1.4   The Discovery and Development of Proteasome Inhibitors

The impetus to develop new and improved proteasome inhibitors has existed since the beginning of proteasome research. Initially proteasome inhibitors were used as tools to probe the proteasome's function and its role in the cell, but by the late 1990's there was evidence that proteasome inhibitors may have therapeutic potential for a number of indications. These included genetic diseases which involved protein degradation, immune and inflammatory diseases, skeletal muscle wasting, and cancer [72]. Known proteasome inhibitors will be discussed in this section, classified by warhead pharmacophore.

1.4.1   *Peptide Aldehyde Inhibitors*

Many early studies on proteasome inhibition utilized peptides with a C-terminal aldehyde moiety which were already well known as inhibitors of serine (Ser) and cysteine (Cys) proteases [73-75]. Theory suggests that small molecules which act as analogues of a

protease's transition state will bind more tightly than substrates, thus occupying the enzyme's active site and consequently inhibiting the enzyme's activity. [76]. In the case of the proteasome catalytic subunits, the initial reaction between the catalytic threonine residue and a peptide substrate yields a tetrahedral acyl-enzyme intermediate. A subsequent hydrolysis step uses a water molecule to release the N-terminal portion of the substrate and regenerates the catalytic threonine nucleophile. When a peptide aldehyde reacts with the proteasome's catalytic residue, a reversible covalent bond is formed yielding a tetrahedral hemiacetal. This hemiacetal is believed to mimic the transition state which occurs naturally in the hydrolysis step of the proteasome's peptidase reaction. Peptide aldehyde inhibitors bind tightly and competitively inhibit proteasome catalytic subunits. The most common aldehyde proteasome inhibitors were designed based on di-, tri-, or tetrapeptides with a hydrophobic P1 residue. Aldehyde-based inhibitors of note include Z-LLF-CHO (Z = carboxybenzyl, CHO = aldehyde), LLnL (N-acetyl-LL-norleucine-aldehyde), and MG-132 (Z-LLL-CHO) (Figure 1.5). These compounds all act as slow-binding reversible inhibitors of the proteasome's chymotrypsin-like activity. The drawbacks of these compounds included their rapid metabolism of peptide aldehydes to inactive carboxylic acids in living cells, their generally low potency, and the rapid reversibility of their inhibition [77].

1.4.2 *Peptide Boronic Acid Inhibitors*

Later work focused both on the development of alternative 'warheads' to replace the aldehyde moiety. A 1998 publication by Adams et al. was one of the first to report the usefulness of peptidyl boronic acids as proteasome inhibitors [78]. While boron is not commonly utilized in medicinal chemistry, peptide boronic acid analogues are known for their ability to inhibit a number of different serine proteases via the formation of coordinate or dative covalent bonds between the boron atom and the protease's catalytic nucleophile [79]. Using a C-terminal boronic acid pharmacophore to target the proteasome's catalytic threonine residue, Adams et al. described the optimization of a series of tripeptide boronic acids using natural and unnatural amino acids. Via this method they were able to generate highly potent inhibitors of the 20S proteasome's chymotrypsin-like activity. They identified several inhibitors with Ki values in the 0.01 to 0.025 nM range, and Adams et al. demonstrated as much as 2,500-fold improvement in potency when replacing an aldehyde warhead with a

boronic acid warhead. Adams et al. also tested several other potential warheads such as ketobenzoxazole or di-keto ester warheads, however boronic acids were found to give the highest inhibitory potency and additionally offered superior selectivity for the proteasome over other protease families when compared to aldehyde inhibitors. As proven by X-ray crystallographic analysis of a peptide boronic acid bound to the 20S proteasome published by Groll et al. in 2006, a tetrahedral adduct is formed when the Thr1Oγ nucleophile attacks the boron atom. Groll et al. also rationalized the greater selectivity of peptide boronic acid inhibitors for Thr and Ser proteases over Cys proteases via the Lewis hard-soft acid-base (HSAB) theory [80]. Due to sulfur's lower density of charge as compared to oxygen, it is theorized to react slower and to form a weaker bond with boron-based warheads. Evidence also shows that boronic-acid proteasome inhibitors are capable of achieving high potency and relatively slow target dissociation rates. The FDA-approved boronic acid proteasome inhibitors, bortezomib and ixazomib (Figure 1.5), were found to have K_I values of 0.55 and 0.93 nM against the β5 catalytic subunit, respectively, as well as β5 dissociation half-lives of 110 and 18 minutes, respectively [81]. Chronologically, bortezomib and ixazomib were the 1st and 3rd proteasome inhibitors to receive FDA approval, and will be discussed in greater detail below. Other boronic acid-based proteasome inhibitors of note include the MG-262, the boronic acid analogue of MG-132, and delanzomib, an orally-available inhibitor whose development for the treatment of multiple myeloma was discontinued following poor phase I/II clinical trial results [82].

1.4.3   *β-Lactone Inhibitors*

The next class of proteasome inhibitors to receive significant attention was the β-lactones. In 1995 Fenteany et al. identified the proteasome β5 catalytic subunit as the primary binding target of the Streptomyces metabolite lactacystin (Figure 1.5). Additional experiments revealed that several proteasome catalytic subunits can be covalently and irreversibly labeled by an active β-lactone compound which is formed when lactacystin, itself inactive, undergoes intramolecular nucleophilic attack releasing N-acetylcysteine as a byproduct. This active compound, referred to as omuralide or clasto-lactacystin β-lactone, covalently modifies the Thr1 residue of multiple proteasome catalytic subunits causing potent and irreversible inhibition of the proteasome's chymotrypsin-like activity as well as l inhibition

of its trypsin-like and caspase-like activities [83-85]. Analogues of omuralide were studied and one compound known as PS-519 was tested preclinically and in a phase I clinical trial for use as a neuroprotective agent in acute stroke [86]. Interest in β-lactone proteasome inhibitors was rekindled in 2003 with the discovery of the natural product proteasome inhibitor salinosporamide A produced by a marine actinomycete bacteria [87]. Sharing the same core structure as omuralide, salinosporamide A consists of a β-lactone ring fused to a γ-lactam ring (Figure 1.5). Salinosporamide A was found to inhibit the 20S proteasome approximately 35-fold more potently than omuralide and, unlike omuralide, had potent activity against all three proteasomal activities (CT-L, T-L, and C-L) [88]. Due to its inhibitory activity against the proteasome as well as potent cytotoxic activity against cancer cell lines, salinosporamide A was entered into clinical trials as an anticancer agent first under the name NPI-0052 and later as marizomib by Nereus Pharmaceuticals [89, 90]. Marizomib has been investigated in multiple phase I and phase I/II clinical trials beginning in 2006. Following the acquisition of marizomib by Celgene Corporation in late 2016, positive results from a more recent phase I trial of marizomib with pomalidomide and dexamethasone in relapsed and refractory MM were published in the British Jounral of Haematology [91]. A total of 38 patients were treated with intravenous marizomib at doses of 0.3, 0.4, or 0.5 mg/m^3. A 53% ORR was observed, with two patients (6%) achieving a very good partial response (VGPR). Treatment was well tolerated with neutropenia being the most common grade 3 or higher adverse event (29%). Another potential application of marizomib is in the treatment of malignant gliomas. In rats injected with ^{3}H-marizomib, radioactivity levels in the CNS indicated that marizomib concentrations were approximately 30% of the steady-state blood concentration. Dosing healthy cynomolgus monkeys with oral marizomib produced significant reductions in pre-frontal cortex proteasome activity, further demonstrating marizomib's ability to cross the blood-brain barrier [92]. A phase III trial of marizomib in combination with temozolomide and radiotherapy in glioblastoma patients is anticipated to begin in April 2018 [93].

1.4.4 *Peptide Vinyl Sulfone Inhibitors*

Peptide vinyl sulfones are a class of compounds originally known for their covalent irreversible inhibition of cysteine proteases via the Michael reaction. In this case the catalytic

cysteine residue acts as a nucleophile and attacks the vinyl sulfone at its electrophilic β-carbon atom [94]. In 1997, Bogyo et al. reported the synthesis and evaluation of Z-L$_3$VS, a tripeptide compound with a C-terminal vinyl sulfone warhead which reacts with the proteasome's catalytic Thr1 residues thus inhibiting multiple catalytic activities of the proteasome [95] (Figure 1.6). This initial publication noted that peptide vinyl sulfones were more easily synthesized than β-lactone-based inhibitors and inhibited their targets irreversibly, unlike aldehyde and boronic acid-based compounds. These characteristics made it possible to tag vinyl sulfone inhibitors with labels such as biotin or radioiodine thus irreversibly labeling the proteasome catalytic subunits. Although peptide vinyl sulfones have not been pursued as candidates for therapeutic use, they have been used as activity-based probes of the proteasome in a number of academic studies. Notable examples include an in-depth study of proteasomal substrate specificity using radiolabeled vinyl sulfones by Nazif et al. and a publication by Verdoes et al. which showed that a fluorophore-labeled vinyl sulfone inhibitor could penetrate living cells and tag active proteasomes for visualization [96, 97].
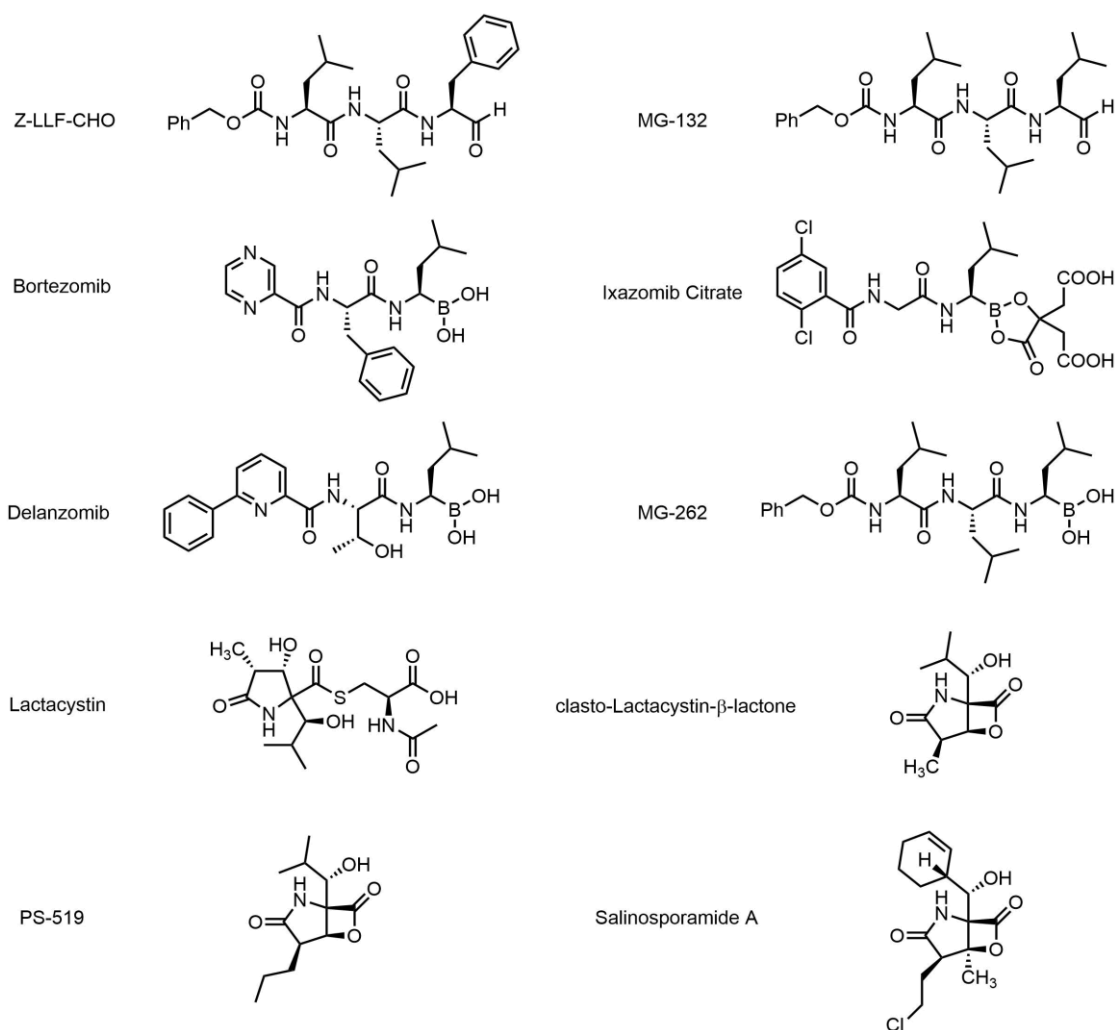
Figure 1.5   Chemical structures of aldehyde and β-lactone proteasome inhibitors

Z-LLF-CHO and MG-132 are peptide aldehyde inhibitors. Bortezomib, ixazomib citrate, delanzomib, and MG-262 are peptide boronic acid inhibitors. Clasto-Lactacystin-β-lactone, PS-519, and salinosporamide A are β-lactone inhibitors. Lactacystin is an inactive precursor which forms the active β-lactone via the elimination of N-acetylcysteine and intramolecular attack.

1.4.5 *Peptide Epoxyketone Inhibitors*

Peptide epoxyketone proteasome inhibitors were first discovered as natural products. Eponemycin and epoxomicin were both discovered at Bristol-Myers Squibb in Tokyo based on their activity against B16 murine melanoma. Eponemycin, first reported in 1990, was produced by a Streptomyces strain whereas epoxomicin, reported in 1992, was produced by an uncharacterized actinomycete strain [98, 99]. Both compounds contain a C-terminal α',β'-epoxyketone moiety and a peptide backbone capped with an N-acyl group (**Figure 1.6**). In order to uncover the biological targets of these compounds, a group working under Dr. Craig Crews at Yale University first synthesized an analogue of eponemycin in which the unsaturated dehydroleucine residue was replaced with a normal leucine residue [100]. After confirming that this compound, dihydroeponemycin, retained biological activity, a probe compound bearing an N-terminal biotin group was synthesized. Upon incubating this probe compound with lysed murine lymphoma cells, two biotin-tagged proteins were captured via an affinity column. Protein sequencing identified these proteins as the immunoproteasome catalytic subunits β1i and β5i [101]. Treating purified bovine 20S proteasomes with the unlabeled compound dihydroeponemycin confirmed its ability to inhibit all three proteasomal catalytic activities in a competitive and irreversible fashion. A similar effort using biotinylated epoxomicin also identified proteasome and immunoproteasome catalytic subunits as the sole binding partners of epoxomicin. In this case β2, β5, β2i, and β5i were identified as bound by the epoxomicin-based probe compound [102]. Soon after, X-ray crystallographic analysis of epoxomicin bound to the proteasome revealed the formation of a 6-membered morpholino ring between the inhibitor and the active Thr1 residue [103]. More recently, high-resolution X-ray structures of human 20S proteasomes treated with three different peptide epoxyketone inhibitors instead revealed a 7-membered 1,4-oxazepane ring between the each inhibitor and the catalytic Thr1 residue, thus leading to a revised mechanism for action for epoxyketone proteasome inhibitors [104]. As described in a 2016 review article by Carmony et al., proteasome inhibition by peptide epoxyketones is believed to be a two-step process which begins with an attack of Thr1O$^\gamma$ on the epoxyketone carbonyl carbon followed by an attack of Thr1N on the epoxide ring's β-methylene carbon leading to epoxide ring opening and formation of the 7-membered ring [105]. This final

adduct is stable thus providing irreversible inhibition of the catalytic site. Peptide epoxyketone inhibitors have been utilized as tool compounds in a number of studies. Examples include the use of fluorescent BODIPY-tagged epoxyketone proteasome inhibitors as imaging probes for specific catalytic subunits and the use of fluorophore-tagged epoxyketones as FRET pairs to examine the makeup of proteasomes which include mixtures of immuno- and constitutive catalytic subunits [106, 107]. A peptide epoxyketone of significant note is carfilzomib, a synthetic analogue of epoxomicin with potent anti-myeloma activity which was the 2nd proteasome inhibitor to receive FDA approval [108] (Figure 1.6).
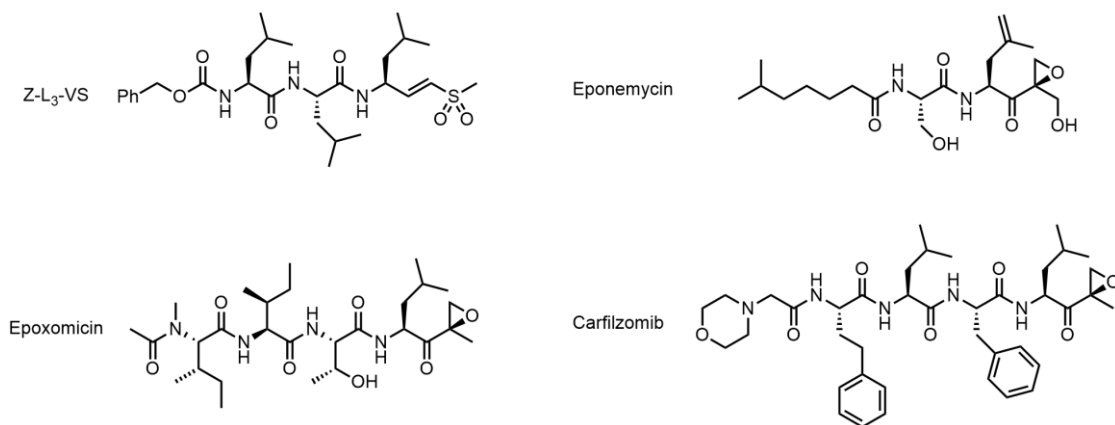
Figure 1.6 Chemical structures of vinyl sulfone and epoxyketone proteasome inhibitors Z-L$_3$-VS is a peptide vinyl sulfone inhibitor. Eponemycin, epoxomicin, and carfilzomib are peptide epoxyketone inhibitors.

1.5   The Development of Subunit-Selective Proteasome Inhibitors

Due to the multi-subunit nature of the proteasome, genetic knockouts of individual catalytic subunits may have undesired consequences such as increased incorporation of the homologous immunoproteasome catalytic subunit in their place or an overall decrease in the assembly of 20S proteasomes. Because chemical inhibition of specific proteasome catalytic subunits does not appear to affect the overall structure of the 20S proteasome or its assembly, it has been a preferred method for studying the function of individual catalytic subunits. There is also the potential that specific proteasome catalytic subunits may play pathological roles in diseases which could be inhibited by small molecules. Thus there has been an ongoing drive to develop subunit-selective proteasome inhibitors.

1.5.1   *Chymotrypsin-like (β5/β5i) Selective Inhibitors*

Both the constitutive β5 and the β5i immunoproteasome catalytic subunits contribute to the proteasome's chymotrypsin-like (CT-L) activity, albeit with some alterations in substrate preference between them such as a greater tolerance for a P1 Ala substituent for β5 and a greater tolerance for a P3 Pro substituent for β5i. Inhibitors which non-selectively target the β5 and β5i catalytic subunits are some of the oldest and best-studied proteasome inhibitors, going back to early peptide aldehyde inhibitors such as MG-132 which target both β5 and β5i in large part due to the presence of a hydrophobic leucine residue at the inhibitor's P1 position. The FDA-approved peptide epoxyketone carfilzomib is a potent inhibitor of β5 and β5i with IC_{50}'s of 0.89 and 1.3 nM, respectively, and demonstrates >13-fold selectivity over other catalytic subunits when measured in cell lysate [32].

1.5.2   *Trypsin-like (β2/β2i) Selective Inhibitors*

Unlike the β1i and β5i immuno-subunits, β2i is reported to have no differences in its substrate binding pockets relative to its counterpart β2 except for the substitution of Asp53Glu, a residue which contributes to the character of the S1 pocket [34]. Due to the

presence of a negatively-charged residue in the S1 pocket, both subunits prefer to cleave substrates with positively-charged residues in the P1 position. Due to their similar binding pockets the β2 and β2i catalytic subunits are likely to have highly similar substrate specificities and thus the task of creating fluorogenic substrates or inhibitors which selectively target β2 or β2i is very difficult. Although inhibitors containing a P1 Arg residue have long been known to preferentially inhibit proteasomal trypsin-like activity, peptides containing highly-charged amino acids such as Arg are also more likely to suffer from poor cell permeability [109]. Data from Mirabella et al. provide examples of known T-L-selective inhibitors and may also exemplify this effect on permeability. Two tripeptide epoxyketones known as NC-012 and NC-022 were tested against purified 26S proteasomes as well as intact H929 cells. NC-012 and NC-022 are tripeptide epoxyketones with the peptide sequence N-acetyl-Arg-Leu-Arg and hydroxymethylbenzoyl-Val-Ser-Arg. While NC-012 was more potent than NC-022 in purified proteasomes (~0.1 μM vs. ~0.3 μM), NC-012 showed significantly lower potency against whole cells (~8 μM vs. ~0.02 μM) [110]. Both compounds demonstrated >100x selectivity for trypsin-like (T-L) activity versus chymotrpysin-like (CT-L) and caspase-like (C-L) activity, and NC-022 showed minimal off-target activity in whole cells at doses up to 30 μM. Nonetheless these compounds still suffered from reportedly poor stability due to cyclization reactions with the Arg side chain, variable cell permeability, and difficult synthesis. A more recent paper from Mirrabella et al.'s group sought to overcome these issues by switching to a non-guanidino P1 substituent and a vinyl sulfone warhead [111]. Their lead compound known as LU-102 utilized L-leucine residues at the P2 and P3 positions combined with a non-natural 4-aminomethylphenyalanine residue in the P1 position to achieve an IC_{50} of 3.8 nM against purified proteasomes and potent and selective inhibition of T-L activity in whole cells. More recently there has been a report of a pair of inhibitors selective for β2 over β2i and vice versa with reported selectivity ratios of greater than 10:1 for both compounds [112]. Interestingly these two compounds have significant structural differences utilizing different C-terminal warheads, different substituents at the P1, P2, and P3 positions, and different N-terminal caps. To date the selectivity of these two compounds has only reported via an activity-based profiling method in Raji cell lysates so further evaluation of their selectivities via multiple methods is warranted.

1.5.3   *Caspase-like (β1) Selective Inhibitors*

When comparing the β1i catalytic subunit to the β1 subunit, there are significant differences in the S1 specificity pocket of β1i, including the Arg45Leu substitution, which reduce the pocket's affinity for acidic amino acid side chains and decrease its size [34]. These alterations result in the β1i subunit having greatly reduced C-L activity as compared to β1 and a concomitant increased its chymotrpysin-like activity. This also aligns with the report by Blackburn et al. that the synthetic peptide substrates Z-Leu-Leu-Glu-AMC and Ac-Pro-Ala-Leu-AMC (AMC = aminomethylcoumarin) act as specific substrates of β1 and β1i, respectively [113]. A publication by Kisselev et al. in 2003 examined the relative preference of the β1 catalytic subunits for substrates containing Asp or Glu in the P1 position and found that the Asp-containing peptide Ac-GPLD-AMC was hydrolyzed approximately two-fold faster than the corresponding Glu-containing substrate. Via the use of a positional scanning library of proteasome substrates, Ac-nLPnLD-AMC (nL = norleucine) was identified as a good substrate of β1 and the corresponding C-terminal aldehyde was identified as a potent inhibitor of β1 with a Ki of 0.40 μM [114]. Unfortunately, due to the generally rapid metabolism of aldehydes in living cells, the usefulness of this compound *in vivo* is likely to be limited. In 2016, data on a peptide epoxyketone inhibitor of β1 known as LU-001c were published [112]. Structurally, LU-001c is azidoacetyl-APnLD-ek (ek = epoxyketone) and had an IC_{50} of 65.5 nM against β1 in Raji cell lysates and an IC_{50} of >1000 nM against all other catalytic subunits. Unfortunately, no inhibition was detected when live cells were treated with LU-001c suggesting a lack of cell permeability. Due to the apparent requirement of an acidic P1 residue for high potency and specificity towards β1 and the apparent negative effect of acidic residues on peptide cell permeability, a novel strategy may be necessary to create a β1 inhibitor which is suitable for *in vivo* use.

1.5.4   *β1i-Selective Immunoproteasome Inhibitors*

Following the observation that the peptide epoxyketone natural product eponemycin and its dihydro analogue demonstrated a preference for β1i over other subunits, our laboratory examined the structure-activity relationship (SAR) for β1i inhibition using eponemycin

analogues [115]. A series of N-acyl dipeptide epoxyketones were synthesized which were closely related to eponemycin but which included a variety of substituents at the P1' hydroxyl group. The lead compound, dubbed UK-101, utilized a P1 Leu residue, a P2 Ala residue, and a tert-butyldimethylsilyl (TBDMS) group at the P1'-OH position. This compound completely inhibited the binding of an activity-based probe to the β1i subunit at 1 μM but did not significantly inhibit other catalytic subunits at concentrations of up to 10 μM. More recent data on UK-101's IC_{50}'s against constitutive and immunoproteasome catalytic subunits was obtained using a set of fluorescently-tagged activity-based probes selective for the β1, β1i, β5, and β5i subunits. These experiments showed that UK-101 was highly selective for β1i as compared to β1, with an IC_{50} ratio of 144:1, but had only moderate selectivity for β1i over β5 with a 10:1 selectivity ratio [116]. Our group has also investigated the previously-reported caspase-like inhibitor YU-102 (Ac-GPFL-epoxyketone) and found it to have β1i:β1 and β1i:β5 selectivity ratios of 4.2:1 and >100:1 when measured using subunit-selective fluorogenic peptide substrates (unpublished data) [117]. Via modification of the P2, P4, and N-terminal substituents we were able to generate compounds with improved potency (β1i IC_{50} = 28 nM) and greater β1i:β1 selectivity (20.8:1).

A report of efforts to optimize peptide epoxyketones for β1i selectivity was published by de Bruin et al. in 2014 [116]. Based on an initial scaffold similar to YU-102, utilizing P3 Pro and P1 Leu residues, they identified a tetrapeptide compound LU-001i as a highly specific inhibitor of β1i. In particular, the modifications of the P3 Pro residue to 4,4-difluoroproline and of the P1 Leu residue to cyclohexylglycine resulted in significant improvements to selectivity, albeit with a minor loss in potency. LU-001i was reported to have a 252-fold selectivity for β1i over β1 and a >200-fold selectivity for β1i over β5 and β5i. LU-001i is likely to be a useful probe of β1i function and has already been used to investigate the effects of several FDA-approved proteasome inhibitors on β1i activity in primary cells from acute lymphocytic leukemia patients [112].
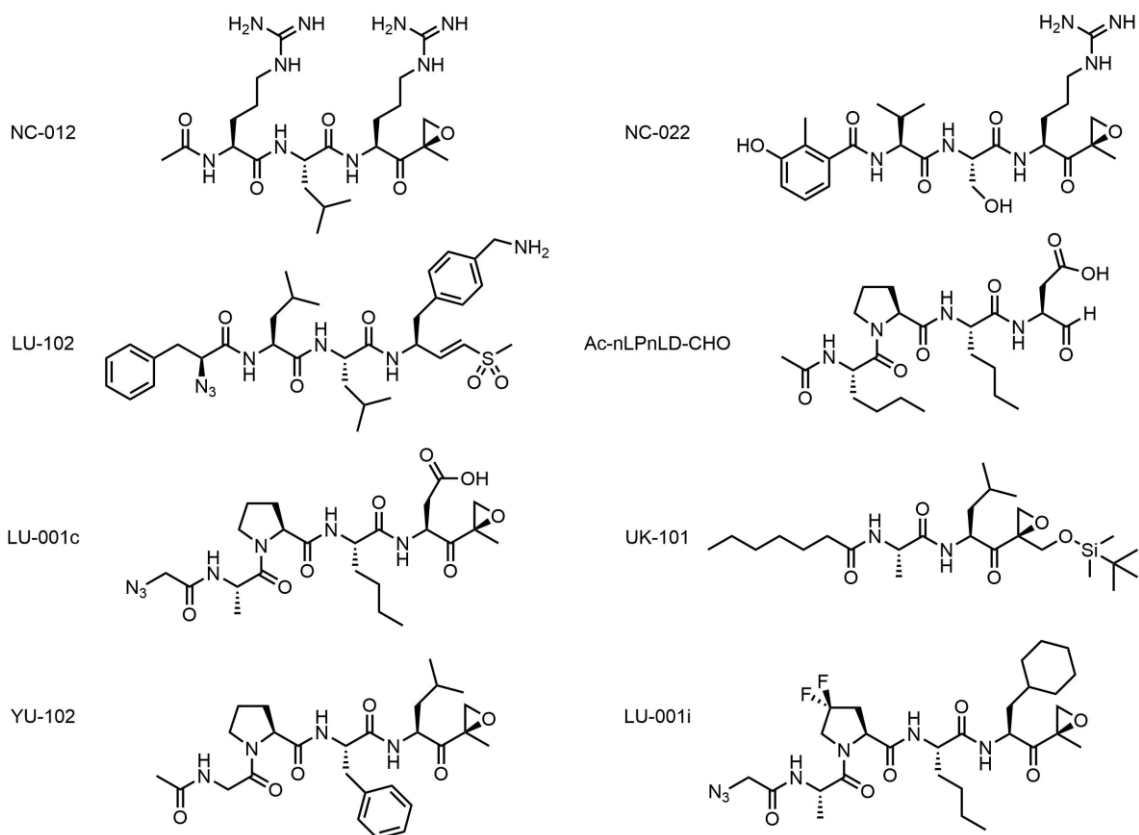
Figure 1.7 Chemical structures of inhibitors targeting β2/β2i (T-L activity), β1, and β1i

NC-012, NC-022, and LU-012 selectively inhibit the proteasome's trypsin-like (T-L) activity which is conferred by the β2 and β2i catalytic subunits. Ac-nLPnLD-CHO and LU-001c selectively inhibit the constitutive proteasome β1 subunit. UK-101, YU-102, and LU-001i selectively inhibit the immunoproteasome β1i subunit with varying degrees of selectivity.

1.5.5   *β5i-Selective Immunoproteasome Inhibitors*

A medicinal chemistry effort undertaken by Proteolix Inc. resulted in a β5i-selective peptide epoxyketone inhibitor known as IPSI (immunoproteasome-selective inhibitor) or later as PR-924 (Proteolix compound #924) (Figure 1.8). As described in their 2009 publication, the potency and selectivity of IPSI was determined via an assay known as ProCISE in which a combination of a non-selective irreversible biotin-tagged inhibitor and subunit-specific antibodies allows for the measurement of all six proteasome catalytic subunit activities in cell lysates [118]. IPSI had an IC_{50} of 22 nM against β5i and 132-fold selectivity over β5. Selectivity against other catalytic subunits was greater than 300-fold in all cases. This initial report on IPSI also showed that a β5i-selective concentration (270 nM) of IPSI did not significantly reduce the cell viability or induce caspase-3/7 activity in several hematologically-derived cancer cell lines. Although a later publication did demonstrate that IPSI/PR-924 was cytotoxic in established cell lines and primary samples of multiple myeloma, the inhibitor concentrations required to observe these effects were in the non-selective range (≥1 μM).

PR-957 is a second Proteolix-developed β5i-selective inhibitor (Figure 1.8). Although PR-957, later known as ONX 0914, is less potent and less selective than PR-924, in our laboratory's observations it has substantially better aqueous solubility, as might be expected based on structural differences between the two compounds [119]. A 2009 Nature Medicine publication showed that i.v. administration of PR-957 in mice inhibited blood and tissue β5i activity, altered immune response, and significantly reduced severity of disease symptoms in a mouse model of rheumatoid arthritis while producing minimal toxicity [119]. Investigations into the potential therapeutic applications of β5i inhibitors in autoimmune disease are ongoing [63].
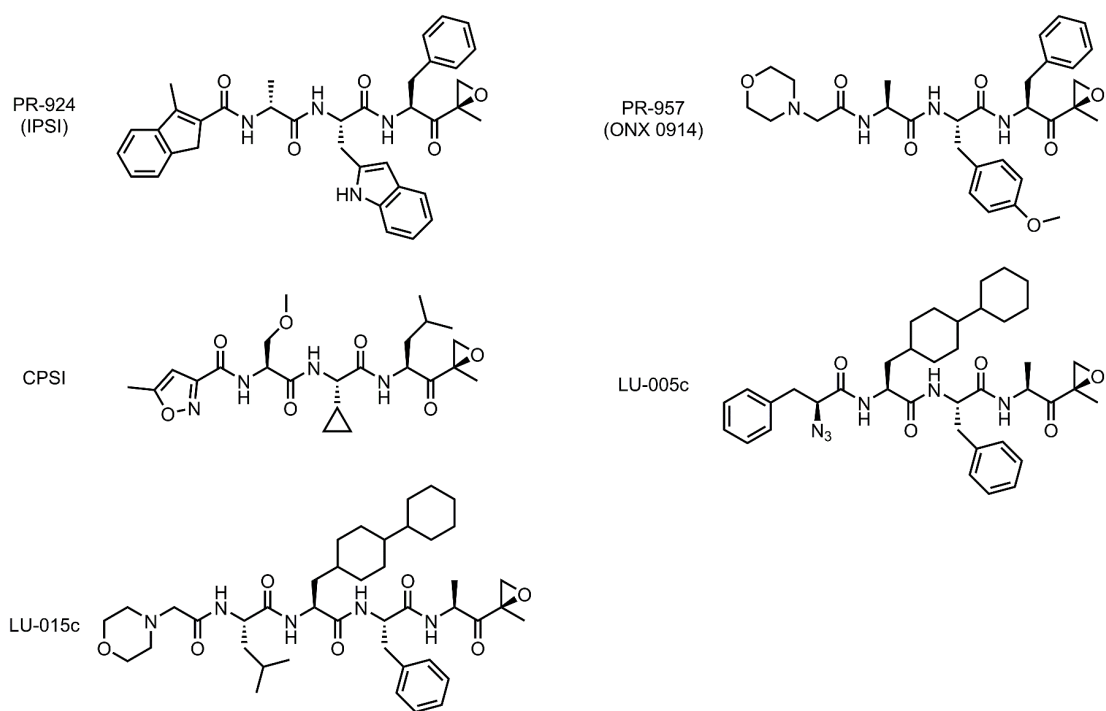
Figure 1.8   Chemical structures of inhibitors targeting the β5 and β5i subunits

PR-924 (IPSI) and PR-957 (ONX 0914) are β5i-selective epoxyketones. CPSI, LU-005c, and LU-015c are β5-selective peptide epoxyketones.

1.5.6 *β5-Selective Proteasome Inhibitors*

CPSI (Constitutive proteasome selective inhibitor) is a β5-selective inhibitor discovered by Proteolix Inc. as a part of their efforts to design an orally-bioavailable analogue of carfilzomib (Figure 1.8) [120]. Assayed using ProCISE, CPSI had a β5 IC_{50} of 17 nM and moderate selectivity over β2i and β5i (13- and 21-fold, respectively). As was the case for IPSI, CPSI alone at a selective dose (180 nM) did not cause cell death or induce caspase-3/7 activity, whereas non-selective inhibitors such as carfilzomib or a combination of IPSI plus CPSI did [118]. These data support the overarching hypothesis that the inhibition of an individual proteasome catalytic subunit is not sufficient to effectively induce cell death. LU-005c and LU-015c are a pair of related peptide epoxyketone inhibitors which specifically inhibit β5 (Figure 1.8). Using Raji cell lysates, LU-005c was determined to have a β5 IC_{50} of 22.9 nM with IC_{50}'s of >1000 nM against all other catalytic subunits. Due to a lack of any observed inhibition in intact cells, LU-015c was developed by replacing LU-005c's N-terminal cap with the hydrophilic 2-morpholino acetic acid cap found in the FDA-approved proteasome inhibitor carfilzomib and by extending the inhibitor's length via the insertion of an L-leucine residue in the P4 position. Although these modifications reduced potency by 6.5-fold and resulted in a somewhat less favorable β5:β5i selectivity ratio of 52:1, it did result in a compound which was suitable for use in intact cells such as live primary leukemia cells [112].

1.6   The Clinical Development of Proteasome Inhibitors

Although we now know that the ubiquitin-proteasome system is involved in a multitude of diseases, a key motivation for the early development of proteasome inhibitors was their potential ability to treat muscle wasting. The path to the first FDA-approved proteasome inhibitor began with research into the role of the ubiquitin-proteasome system in muscle wasting conducted in the lab of Alfred L. Goldberg at the Harvard Medical School. A review article by Mitch and Goldberg published in the New England Journal of Medicine in 1996 summarizes several studies which identified increased activity of the UPS in animal models of various catabolic states [121]. They also identified a number of important human

conditions which may involve pathological muscle wasting such as AIDS, Cushing's syndrome, neuromuscular disease, and cancer. Mitch and Goldberg hypothesized that partial pharmacological inhibition of the proteasome could limit excessive proteolysis in these conditions without excessively impairing cellular function. Based on this hypothesis, research to develop proteasome inhibitors suitable for clinical use began.

1.6.1 *Bortezomib*

In an effort to develop and commercialize proteasome inhibitors as therapies in muscle wasting diseases, Goldberg founded Myogenics in 1993. It was at Myogenics where some of the notable peptide aldehyde inhibitors of the proteasome such as MG-115 and MG-132 were discovered and it was these compounds that would eventually serve as the basis for the first FDA-approved proteasome inhibitor bortezomib [122]. Julian Adams was hired as head chemist in 1994, and research into boronic acid-based proteasome inhibitors was conducted under his lead. This quickly led to the discovery of the dipeptidyl boronic acid known originally as MG-341 which would eventually become the first FDA-approved proteasome inhibitor, not for the treatment of muscle wasting diseases, but rather for an entirely different application.

A 1994 Cell publication by Goldberg and Tom Maniatis of Harvard University showed that proteasome plays an essential role in the activation of the NF-κB transcription factor via both the degradation of the inhibitory factor IκBα and the processing of the inactive p105 precursor protein to the active protein product p50 [123]. In live HeLa cells, peptide aldehyde proteasome inhibitors were able to cause a large reduction in NF-κB activation following stimulation. Due to NF-κB's critical role in immune response and inflammation, it was a drug target of significant interest [124]. Based in part upon these observations, Myogenics shifted its focus from muscle wasting to inflammation and changed their name to ProScript to reflect this new focus. Alongside this rebranding, the proteasome inhibitor previously known as MG-341 was renamed to PS-341. It was also in 1994 that Avram Hershko, Nobel Prize winner for this research into the UPS, suggested to Goldberg that ProScript should investigate the potential applications of proteasome inhibitors as anticancer therapies. Although there was little published information linking proteasome function to cancer at that time, ProScript

began investigating cancer as a potential therapeutic area for proteasome inhibitors, while reportedly maintaining interest in inflammation and NF-κB as well.

Two significant studies which were among the first to support the effectiveness of proteasome inhibitors were published in 1999. These two publications resulted from collaborations between ProScript researchers and scientists at the National Cancer Institute (NCI) and the Dana-Farber Cancer Institute, respectively. The first of these papers detailed the results of 13 boronic acid proteasome inhibitors which had been screened against the NCI's panel of 60 cancer cell lines known as the NCI-60 [125]. Although these compounds spanned a wide range of proteasome inhibitory activity (Ki = 0.1-2300 nM), there was high degree of correlation between each compound's activity against purified 20S proteasomes and its average growth inhibitory activity against the NCI-60 panel. Of these compounds, PS-341 was the most potent against the cell line panel with an average growth inhibitory concentration (GI_{50}) of 6.3 nM. Following these results, PS-341 was tested against mice bearing tumor xenografts. This study showed that a single i.v. injection of 0.3 mg/kg PS-341 could significantly inhibit proteasome activity in white blood cells and in PC-3 tumor cells. Four direct injections of 1 mg/kg PS-341 into PC-3 tumors on a daily or weekly schedule significantly reduced tumor volume as compared to vehicle. A publication by Teicher et al. published three months later demonstrated similar results: PS-341 was cytotoxic to cancer cells both *in vitro* and in mouse models with relatively high potency [126].

Following the promising preclinical results of PS-341, human clinical trials were begun. A number of phase I clinical trials of PS-341 were conducted, using patients with solid tumors as well as patients with hematological cancers. According to Adams et al. in a 2002 review, data from approximately 200 patients treated in phase I trials indicated that PS-341 was well tolerated but with reports of low-grade fever, fatigue, thrombocytopenia, and in some cases, peripheral neuropathy [127]. Adams et al. also noted anecdotal reports of efficacy in non-small cell lung cancer, melanoma, and multiple myeloma.

PS-341 changed ownership twice during its clinical development, first from ProScript to LeukoSite in 1999. Several months later LeukoSite was purchased by Millenium Pharmaceuticals for reasons unrelated to PS-341, and PS-341's development was deemed a low priority [122]. According to previously-cited review by Sanchez-Serrano, it was a single

promising result in a multiple myeloma patient, a 47-year old woman with advanced disease who achieved complete remission as a part of the phase I trial conducted at the University of North Carolina [122, 128]. During its clinical development at Millenium, PS-341 received the nonproprietary name bortezomib and was eventually marketed under the brand name Velcade®.

Phase II clinical trials of PS-341 examined its efficacy in several different cancer types, but in hindsight it is multiple myeloma which is of the most interest due to the eventual FDA approval of PS-341 to treat relapsed and refractory multiple myeloma. SUMMIT was a phase II open-label non-randomized trial of bortezomib which enrolled 202 patients with relapsed multiple myeloma which was refractory to the last agent used in 91% of patients. Patient enrollment was performed between February and December 2001. Bortezomib was dosed intravenously at 1.3 mg per square meter of body-surface area (mg/m^3) twice weekly for two weeks per 21-day cycle. Bortezomib was used as a single agent except in patients with progressive or stable disease after four cycles who were eligible to receive supplemental dexamethasone (Dex). Among the evaluable patients, the overall response rate (ORR) was 35% with 4% (n=7) of patients achieving complete response (CR) and 6% (n=12) of patients achieving a near-complete response (nCR). The median duration of response (DOR) for patients achieving any response was 12.7 months. Median overall survival for the entire population was 17.0 months [129]. Compared to historical response and survival data in similar patient populations, bortezomib's activity was promising.

In May 2003, FDA fast-track approval for the use of bortezomib in relapsed and refractory multiple myeloma patients was granted based primarily on data from the phase II SUMMIT trial. Further evidence of bortezomib's activity in relapsed multiple myeloma (MM) was provided by the 669-patient randomized APEX trial which compared bortezomib versus high-dose Dex. Combined complete and partial response (CR and PR) rates were 38% and 18% for bortezomib and Dex, respectively. Median times to progression were 6.22 and 3.49 months, respectively. After one year of follow-up, there was a significantly greater rate of overall survival (p=0.003) in patients treated with bortezomib (80% rate) as compared to high-dose Dex (66% rate). Although bortezomib treatment was associated with a number of adverse events, publication such as the 2005 review by Bladé et al. already deemed it a "safe and highly effective drug to be added to the current treatment strategies for multiple

myeloma" [130]. By 2004 bortezomib was already seeing significant clinical use in with annual sales of $143 million in the US and bortezomib continues to see significant clinical use today.

1.6.2 *Carfilzomib*

The second proteasome inhibitor to receive FDA approval was carfilzomib. The development of carfilzomib can be traced back to the discovery of the natural product epoxomicin in 1992 by Bristol-Myers Squibb Japan. Due to its potent *in vivo* activity against murine melanoma, the lab of Craig Crews at Yale University began evaluating epoxomicin as a modulator of tumor growth signaling pathways. Based on the hypothesis that epoxomicin's epoxyketone group was responsible for covalently modifying target proteins, the Crews lab synthesized a biotin-labeled analogue of epoxomicin and used it to pull down potential target proteins. This experiment revealed that the proteasome's catalytic subunits were covalently modified by epoxomicin, and further work found that epoxomicin had exceptional selectivity for the proteasome over other common proteases. This excellent selectivity is now believed to be the result of a unique two-step inhibition mechanism in which epoxomicin or similar peptide epoxyketones are able to covalently modify both the catalytic Thr1Oγ atom as well as the N-terminal amino group forming a six-membered morpholino ring. Such a reaction would not be possible with a non-N-terminal nucleophile protease.

Further work in the Crews lab focused on the optimization of epoxomicin's anticancer activity via traditional medicinal chemistry [131]. By modifying the P2, P3, and P4 amino acid side chains they arrived at a tetrapeptide epoxyketone dubbed YU-101. According to a 2013 retrospective by Crews and his former mentee Kim, YU-101 had better potency against the proteasome and more potent antitumor activities than bortezomib [132]. Based upon YU-101's superior potency and reports of bortezomib's ongoing successes in clinical trials, Proteolix Inc. was established to develop YU-101 as an anticancer therapeutic. Work at Proteolix identified that, as with many other highly-hydrophobic peptides, YU-101 has poor water solubility (< 1 μg/mL) that could reduce its usefulness as a therapeutic agent. Further medicinal chemistry efforts were undertaken at Proteolix to optimize YU-101's solubility, yielding the lead compound PR-171 via swapping YU-101's N-terminal acetyl cap for the more polar and ionizable 2-morpholinoacetic acid group [133].

In a 2007 publication by Demo et al. of Proteolix, PR-171 was reported to have greater than 1000-fold improved water solubility relative to YU-101 while retaining potent inhibitory activity against proteasome chymotrypsin-like activity (IC_{50} = 6 nM). PR-171 also demonstrated potent cytotoxic activity in a variety of cell lines with hallmark signs of proteasome inhibition such as polyubiquitin accumulation and upregulation of p21. Moving onto studies in mice, Demo et al. established that PR-171 could be administered to mice on two consecutive days (QDx2) to achieve a cumulative inhibition of proteasomal activity without excessive toxicity. This is in contrast to the typical clinical and preclinical use of bortezomib in which the drug is dosed on days 1 and 4 of each week, allowing for recovery of proteasome activity between doses. When comparing consecutively-dosed PR-171 to non-consecutively dosed bortezomib in three groups of mice bearing different types of human tumor xenografts, 5 mg/kg PR-171 was found to have a significantly greater effect on tumor volume than 1 mg/kg bortezomib well remaining well-tolerated [133].

Based on positive preclinical results, Proteolix moved forward with phase I clinical trials of PR-171 under the generic name carfilzomib. Starting in the fall of 2005, two phase I dose-escalation trials of single-agent carfilzomib were conducted in patients with relapsed or refractory hematologic malignancies with a QDx5 and a QDx2 dosing cycle, respectively. The results of these studies established a three-week QDx2 dosing cycle with one week of rest (days 1, 2, 8, 9, 15, and 16 per 28-day cycle) as the preferred schedule and established the safety of carfilzomib i.v. infusions at doses up to 27 mg/m^3. During the course of the QDx2 phase I PX-171-002 trial, strong anti-myeloma activity was identified in five MM patients treated with 27 mg/m^3 carfilzomib. Adverse reactions were also noted at this dose including cyclic thrombocytopenia and transient increases in creatinine consistent with an infusion-like reaction [134].

Going forward, an open-label phase II pilot study of carfilzomib in patients with relapsed and refractory multiple myeloma was conducted (PX-171-003) with 46 enrolled patients as reported by Jagannath et al. in 2012 [135]. Based on early results from the PX-171-002 dose-escalation study, a dose of 20 mg/m^3 was chosen. Patients received 20 mg/m^3 carfilzomib twice per week on consecutive days as a 2-minute i.v. infusion. Low-dose dexamethasone was administered prior to carfilzomib during the first cycle and as needed thereafter. Based on data from 42 evaluable patients, single-agent carfilzomib had activity deemed encouraging.

Specifically, 7 patients achieved PR (16.7%), 3 patients achieved MR (7.1%), and 17 patients had stable disease (SD, 40.5%). The ORR was 16.7% and the median duration of response was 7.2 months for the ORR population, favorable results in the context of this heavily pre-treated population with a 100% rate of exposure to bortezomib and a 91% rate of exposure to lenalidomide (Len). Later results from PX-171-002 identified that the true maximum tolerated dosage was greater than expected, 27 mg/m^3. Based on this new knowledge, PX-171-003 was expanded with an additional 266 patients who were dosed at 20 mg/m^3 for the first cycle followed by 27 mg/m^3 in additional cycles. The reduced dose in cycle 1 was intended to mitigate previously-reported first-dose infusion reactions. According to the ASH abstract published Siegel at al. in 2010, the ORR was 24% and the median DOR was 7.4 months [136]. As with the pilot study, this patient population was heavily pretreated with a median of 5 lines of prior therapy.

An additional phase II study (PX-171-004) was conducted with a population consisting mainly of bortezomib-naïve patients. The results for bortezomib-naïve and bortezomib-treated patients were published separately, however I will only discuss the former here. A total of 129 bortezomib-naïve patients were treated using single-agent carfilzomib in two separate cohorts. 94 patients in cohort 1 received carfilzomib at a steady dose of 20 mg/m^3. A second cohort of 70 patients received carfilzomib at the 20/27 mg/m^3 stepped dose mentioned above. The ORR was 42% and 52% in cohorts 1 and 2, respectively. The median time-to-progression (TTP) and median DOR was 13.1 months and 8.3 months in cohort 1. Neither median TTP nor median DOR were reached in cohort 2 with a median time to follow-up of 11.5 months. The results compared favorably to the 38% ORR reported for single-agent bortezomib in the phase III APEX trial [137].

Amidst carfilzomib's clinical development Proteolix was acquired by Onyx Pharmaceuticals in late 2009 with large payments contingent upon the expected FDA approval of carfilzomib. Onyx sought FDA accelerated approval for carfilzomib (trade name Kyprolis®) for the treatment of relapsed and refractory MM in 2012 based upon phase II efficacy data. Onyx additionally presented safety data from a total of 768 patients treated in phase I and II studies. Serious adverse events probably related to carfilzomib treatment were rare with the most common being pneumonia in 4% of patients and congestive heart failure in 3% of

patients. On July 20th, 2012, Carfilzomib was granted accelerated FDA approval with an ongoing phase III ASPIRE trial to confirm the drug's clinical benefit and safety [108].

The randomized phase III ASPIRE trial (PX-171-009) examined carfilzomib in combination with the immunomodulatory agent lenalidomide and high-dose dexamethasone versus Len and high-dose Dex alone. ASPIRE enrolled 729 patients with relapsed MM who had received one to three prior therapies. Patients previously treated with bortezomib were eligible for the trial as long as they did not experience disease progression during bortezomib treatment. Progression-free survival was significantly greater in the carfilzomib group at 26.3 months versus 17.6 months in the control group. The ORR was 87% with carfilzomib and 67% without carfilzomib. Although median overall survival was not reached in either group, the 24-month overall survival was significantly higher in the carfilzomib group by 8.3 percentage points (p=0.04). Although the carfilzomib group experienced a greater rate of grade 3 or higher adverse events and a greater rate of serious adverse events, they experienced fewer deaths during or shortly after treatment, and reported higher quality of life. The ASPIRE trial thus established the safety and efficacy of carfilzomib in relapsed MM as part of a three-drug regimen [138].

More recently, the phase III trial ENDEAVOR trial directly compared carfilzomib plus dexamethasone versus bortezomib plus dexamethasone in patients with relapsed or refractory MM [139]. As per its prescribing information, bortezomib was dosed at 1.3 mg/m^3 on days 1, 4, 8, and 11 per 28-day cycle. Based on new clinical data supporting the safety of higher doses of carfilzomib when given as a slow infusion, carfilzomib was dosed 20 mg/m^3 on the first cycle and 56 mg/m^3 on subsequent cycles as a 30-minute infusion. The median PFS in the carfilzomib group was 18.7 months, a significant increase relative to the bortezomib groups median PFS of 9.4 months (p<0.0001). Interim data suggests that this larger difference in progression-free survival is present regardless of patients' prior exposure to bortezomib. Median duration of response in the carfilzomib group was more than double that of the bortezomib group (21.3 vs. 10.4 months). Although patients treated with carfilzomib experienced a greater rate of grade 3 or higher adverse events, they experienced significantly fewer grade 2 or higher events of peripheral neuropathy, a known serious side effect of bortezomib treatment. While cardiac failure was more common in carfilzomib-treated patients, a sub-study using serial echocardiograms found no evidence of cumulative

cardiac injury or ventricular dysfunction in the carfilzomib group. An interim analysis of overall survival for ENDEAVOR was published in Lancet Oncology in October 2017. The OS of carfilzomib-treated patients was significantly longer than that of bortezomib-treated patients (47.6 vs. 40.0 months, p=0.010) [140]. Taken as a whole, these results identify a significant efficacy gap between these two drugs in favor of carfilzomib and establish carfilzomib as a standard of care in the treatment of relapsed or refractory multiple myeloma.

1.6.3 *Ixazomib*

A third proteasome inhibitor, ixazomib, was approved for clinical use by the FDA in 2015 under the brand name Ninlaro® for the treatment of relapsed multiple myeloma. Ninlaro® is the first orally-administered proteasome inhibitor to reach the market. Structurally, ixazomib is an N-capped dipeptide boronic acid whose boronic acid pharmacophore can be esterified with citric acid to form the prodrug ixazomib citrate. Ixazomib itself is a potent inhibitor of the proteasome's β5 and, to a lesser extent, β1 catalytic subunits (IC_{50} = 3.4 nM and 31 nM). Like bortezomib, ixazomib is a slowly-reversible inhibitor of the proteasome, but its dissociation rate is significantly faster ($t_{1/2}$ = 110 and 18 minutes). Ixazomib citrate is reported to be immediately hydrolyzed to yield ixazomib upon exposure to aqueous solutions or plasma. Preclinical studies showed that ixazomib citrate had good oral bioavailability in mice and produced proteasome inhibition in blood cells and in tumor cells following i.v. administration. Twice-weekly oral doses of ixazomib citrate were shown to significantly reduce tumor volume in a mouse xenograft model of prostate cancer. When injected, ixazomib citrate was more efficacious than bortezomib in two preclinical models of lymphoma [81]. Notably, i.v. ixazomib had a better ratio of tumor:blood proteasome inhibition than bortezomib, suggesting that ixazomib has good distribution in tumor tissues. In humans, ixazomib citrate has oral bioavailability of 58% and has a terminal half-life of 9.5 days allowing for once-weekly dosing. Ixazomib citrate was approved based on a double-blind phase 3 trial of 722 multiple myeloma patients of ixazomib, lenalidomide, and dexamethasone versus Len and Dex only. Patients received 5.7 mg of ixazomib citrate which is equivalent to 4 mg ixazomib once per week for three weeks per 28-day cycle. ORR was 78% for ixazomib versus 72% for control, with the rate of VGRP at 48% and 39%, respectively. Notably the median time of PFS was 20.6 months in the ixazomib group versus 14.7% in the

control group. It should be noted that, as with bortezomib, patients taking ixazomib had a higher rate of peripheral neuropathy as compared to control (27% versus 22%) but the rate of grade 3 peripheral neuropathy was low at 2% [141].

1.7   Unmet Clinical Needs and Drawbacks of Approved Inhibitors

From the first clinical trials of bortezomib over 15 years ago to today, proteasome inhibitors have significantly changed the way that multiple myeloma is treated and have had a tremendous impact on patient survival and well-being. Despite this, there is still room for improvement. To date, proteasome inhibitors are FDA-approved only for the treatment of multiple myeloma and mantle cell lymphoma, diseases which represent less than 3% of new cancer cases in the US [142, 143]. Additionally, currently-approved proteasome inhibitors have several drawbacks such as undesired adverse events, susceptibility to drug resistance, and less than ideal pharmacokinetic properties. Efforts to develop proteasome inhibitors having strong activity in solid tumors or which avoid the drawbacks of existing inhibitors could help many more patients.

1.7.1   *Clinical Trial Results in Non-Myeloma Cancers*

While proteasome inhibitors have played a significant role in improving patient outcomes in MM, they have seen little success in treating other types of cancer. Although bortezomib is approved for use in mantle cell lymphoma, their use in general is largely restricted to MM. During the preclinical development of bortezomib, it was clear that it had potent activity in a wide variety of cancer cell lines and bortezomib's average growth inhibitory potency (GI_{50}) in the NCI's 60 cell line panel was excellent at just 7 nM. Furthermore, cell lines which were highly sensitive to bortezomib originated from a variety of cancer types including leukemia, colon cancer, melanoma, and renal cancer. Bortezomib also demonstrates cytotoxic activity in mouse models of a number of different cancer types including prostate cancer, colon cancer, melanoma, and adult T-cell leukemia, among others [125, 144-146]. Despite these signs of activity against a variety of non-myeloma cancers, many of the clinical trials of proteasome inhibitors in patients with these cancers have been relatively unsuccessful.

A phase I study of bortezomib and gemcitabine in 31 patients with advanced solid tumors identified only one patient with an objective response and seven patients with stable disease following treatment. Although the treatment's observed toxicities were considered to be manageable, the MTD for bortezomib in this study was 1.0 mg/m^3, lower than in MM patients [147]. A phase I/II study of bortezomib and docetaxel in 83 patients with androgen-independent prostate cancer demonstrated that this combination was well tolerated with no dose-limiting toxicities at doses up to 1.6 mg/m^3. However according to the study authors, the bortezomib/docetaxel combination therapy showed anti-tumor activity similar to that expected for docetaxel monotherapy. Among the 45 patients evaluable according to RECIST criteria, three patients had a confirmed partial response and no patients had a complete response [148]. A phase II study of single-agent bortezomib in 25 patients with advanced urothelial carcinoma identified no objective responses [149]. A phase II clinical trial of single-agent bortezomib in 29 patients with advanced biliary tract cancers also identified no confirmed partial or complete responses [150]. As for hematologic cancers other than MM, a phase II study of bortezomib in patients with adult T-cell leukemia or lymphoma was published in 2015. A partial remission was observed in 1 of 15 patients and the authors concluded that bortezomib's activity was not very promising in this population [151]. While there have been clinical trials in which bortezomib exhibited more promising activity in solid tumors, none have warranted the undertaking of a large-scale phase III trial to compare a proteasome inhibitor to the current best-in-class therapies for these diseases.

As with bortezomib, there is data which suggests that carfilzomib has preclinical activity in cancers besides MM such as lung cancer and colon cancer [152, 153]. Although carfilzomib was first tested in humans much more recently than bortezomib, data from a phase I/II trial of carfilzomib in patients with advanced solid tumors has been published. Among the 12 evaluable patients in the phase I dose-escalation study, two patients had confirmed partial responses and two patients had stable disease [154]. Of the 51 evaluable patients in the phase II dose expansion study, no patients achieved a partial response or better after four or more cycles of carfilzomib therapy and 11 patients had stable disease after four or more cycles of therapy. Although there is relatively little available data to examine the efficacy of carfilzomib in solid tumors, the lack of large scale clinical trials of carfilzomib in non-myeloma cancers is telling in it of itself.

One phase I dose-escalation and dose-expansion study of IV ixazomib in patients with advanced non-hematologic cancer has been published [155]. Among 92 evaluable patients who received at least one cycle of ixazomib, one patient with head and neck cancer achieved a partial response. 30 patients achieved stable disease with 8 of those patients maintaining stable disease for at least 4 cycles. The study authors noted that the antitumor activity of ixazomib was limited and was comparable to observations of bortezomib's and carfilzomib's lack of activity in patients with advanced solid tumors.

Overall, the poor activity of currently-approved proteasome inhibitors in non-myeloma cancers is disappointing considering their highly promising preclinical activity. Considering the significant positive impact of proteasome inhibitors on the multiple myeloma treatment landscape, efforts to understand the poor efficacy of bortezomib, carfilzomib, and ixazomib in patients with solid cancers are laudable.

1.7.2 *Adverse Event Profiles of Approved Proteasome Inhibitors*

The FDA-approved proteasome inhibitors bortezomib, carfilzomib, and ixazomib share a number of adverse events which may or may not be intrinsic properties of proteasome-inhibiting drugs. Adverse event (AE) data collected from clinical trials indicates that gastrointestinal AEs such as diarrhea, constipation, and vomiting are commonly reported (>20% incidence) with all three drugs. Nausea and fatigue are also commonly reported during treatment with these three proteasome inhibitors. While these AEs are very common, their severity is typically low. Thrombocytopenia, a reduction in platelet count, is also commonly reported for all three drugs but was more frequently severe or life-threatening (grade 3/4) with incidence rates of 15%, 24%, and 26% for carfilzomib, bortezomib, and ixazomib, respectively. Research on the effects of bortezomib on platelet function indicate that bortezomib transiently reduces platelet production by megakaryocytes but does not decrease the lifespan of circulating platelets [156].

In addition to these common adverse events, each drug has undesired effects which are specific to that drug and could be related to off-target activity. In clinical trial data encompassing 663 patients, 35% of patients treated with single-agent bortezomib

experienced peripheral neuropathy versus 4% of patients treated with dexamethasone. The rate of grade 3 and 4 peripheral neuropathy in these groups was 7.6% and 0.3%, respectively. The propensity of bortezomib to cause peripheral neuropathy frequently leads to dose modification and impacts patient quality of life [157]. In contrast to bortezomib, the rate of peripheral neuropathy in patients treated with a carfilzomib-containing regimen was only 11%, one percentage point above the incidence rate in the control group. Patients treated with ixazomib also experienced a relatively low rate of peripheral neuropathy at 28% versus 21% in the control group. Only 2% of patients treated with ixazomib experienced grade 3 or higher peripheral neuropathy. According to research published by Arastu-Kapur et al., bortezomib's inhibition of the neuronal serine protease HtrA2/Omi may be responsible for the high incidence of this adverse event. This research found that bortezomib was capable of potently inhibiting several serine proteases such as cathepsin G and chymase. Using a database mining approach, HtrA2/Omi was identified as a protease which was both likely to be inhibited by bortezomib and played a key role in neuronal function. Further investigation revealed that bortezomib but not carfilzomib inhibited HtrA2/Omi with a low nanomolar IC_{50} [158]. Considering its key role in neuronal survival and function, bortezomib's off-target inhibition of HtrA2/Omi may be the key cause of bortezomib-induced peripheral neuropathy.

Carfilzomib treatment has been associated with cardiovascular adverse events including new or worsening cardiac failure and myocardial infarction. In a randomized trial of carfilzomib plus lenalidomide and dexamethasone versus Len and Dex alone the rate of cardiac failure events was 6.4% and 4.1%, respectively among 781 total patients [138]. In a randomized trial of carfilzomib plus Dex versus bortezomib plus Dex, the rate of cardiac failure events was 8% and 3%, respectively. Higher than expected incidences of renal insufficiency and acute renal failure have also been reported in patients treated with carfilzomib. Although the mechanism by which carfilzomib impacts cardiac function is still unknown, the topoisomerase-II inhibitor and iron chelating agent dexrazoxane has been reported to protect mice from carfilzomib-induced cardiotoxicity, potentially via a reduction in reactive oxygen species (ROS).

Currently available safety data from patients treated with ixazomib has not shown high rates of cardiac adverse events or of serious peripheral neuropathy. While patients treated with

ixazomib did experience an increased incidence of eye disorders as compared to control (26% versus 16%), the vast majority of these adverse reactions were not severe [159].

Although additional research is needed to determine the underlying causes of these adverse events, the development of novel proteasome inhibitors which avoid some of these agent-specific adverse events such as peripheral neuropathy or cardiotoxicity could reduce the number of patients who are forced to discontinue PI therapy due to these undesired drug reactions.

1.7.3   *Resistance to Proteasome Inhibitors*

Resistance to proteasome inhibitor therapies represents a significant impediment to their effectiveness in the treatment of cancer. While proteasome inhibitors have strong anti-myeloma activity, especially when combined with other agents, they remain ultimately incapable of curing MM due in large part to the emergence of drug resistance. In clinical practice, a significant fraction of patients do not respond to PI therapy and many other patients who do initially respond will experience relapse during therapy. While some mechanisms of drug resistance are likely to be unique to individual PI drugs, evidence of cross-resistance between the peptide-based inhibitors bortezomib and carfilzomib has been observed. Based on data from the phase II PX-171-003 trial of carfilzomib in bortezomib-treated patients, carfilzomib exhibits reduced activity in this patient group as compared to bortezomib-naïve patients [160]. While this difference could reflect the more advanced state of disease in these patients, it may also indicate the development of cross-resistance in bortezomib-treated patients. In order to better understand the potential mechanisms of proteasome inhibitor resistance in patients, significant preclinical research has been undertaken. Though the exact mechanisms of clinical PI resistance remain largely unknown, preclinical studies have revealed several likely candidates. The phenomenon of PI resistance has been studied both in models of multiple myeloma as well in solid cancers, thus these mechanisms may explain the poor activity of current PI's in patients bearing solid tumors as well as observed PI resistance in MM patients. Such mechanisms include overexpression or mutation of proteasome catalytic subunits, increased drug efflux from cells, altered proteasome activity and expression, and alterations in the unfolded protein response (UPR).

1.7.4   *Resistance via Overexpression or Mutation of Proteasome Subunits*

Overexpression of the *PSMB5* gene which encodes the proteasome β5 catalytic subunit have been reported in several preclinical models of proteasome inhibitor resistance. A 2008 report by Lu et al. investigated the characteristics of a bortezomib-resistant Jurkat cell line developed by over 6 months of continuous exposure to bortezomib. This highly-resistant JurkatB5 line overexpressed *PSMB5* at the mRNA level. Total chymotrypsin-like activity was increased, suggesting increased protein levels of active β5. Amplification of the *PSMB5* gene was also detected [161]. Another 2008 report by Oerlemans et al. examined several THP-1 cell lines which acquired bortezomib resistance via long-term continuous exposure. The THP-1/Btz$_{100}$ cell line exhibited a 79-fold increase in the IC$_{50}$ value for bortezomib cytotoxicity but no significant cross-resistance to a panel of other chemotherapeutic agents. The THP-1/Btz$_{100}$ cell line did, however, have significant cross-resistance to several other proteasome-targeting peptide aldehydes. Cross-resistance was especially marked in the case of 4A6, a cytotoxic peptide believed to specifically target the β5 subunit. The β5 catalytic subunit was highly overexpressed in these resistant cell lines and siRNA-mediated silencing of *PSMB5* led to a significant restoration of bortezomib sensitivity. Additionally, an Ala49Thr mutation in the β5 catalytic subunit protein was identified in highly-resistant THP-1 cells [162]. Ala49 is positioned in the S1 binding pocket, a key factor in determining the β5 catalytic subunit's interactions with inhibitors [34, 80]. Additional studies have confirmed the existence of the β5 Ala49Thr mutation in other bortezomib-resistant cell lines as well as several other mutations such as Ala50Val, Cys52Phe, and Met45Ile, all of which occur in or near the S1 binding pocket and may be hypothesized to interfere with bortezomib's ability to bind to the subunit. Using yeast proteasomes with engineered mutations to their catalytic subunits, Huber et al. demonstrated that mutations to Ala49, Met45, and Cys52 can reduce the ability of bortezomib and carfilzomib to inhibit their catalytic activity, by over 20-fold in some cases [163]. Considering that the β5 subunit is the key target of bortezomib and most cytotoxic proteasome inhibitors, we can also hypothesize that the mutations in the *PSMB5* gene which reduce proteasome inhibitor binding affinity without significantly affecting normal catalytic activity may protect the cell from proteasome inhibitors. Notably, an inhibitor which targets the non-catalytic α7 proteasome subunit retains full activity in

bortezomib-resistant THP-1 cells which overexpress mutated *PSMB5* [164]. This suggests that these cells remain fully reliant on proteasome function for cell survival. Although one case study has identified *PSMB5* mutations in a single bortezomib-treated patient, several other larger scale studies have failed to do so, suggesting that *PSMB5* mutations may not play a significant role in clinical resistance to bortezomib [165-167].

1.7.5   *Resistance via Increased Drug Efflux*

A 2012 publication by Verbrugge et al. examined the impact of a number of drug efflux transporters on sensitivity to four proteasome inhibitors using cell line models. The most notable result was with the CEM/VLB cell line which overexpressed P-glycoprotein (P-gp, also known as MDR1). This cell line had only a modest resistance to bortezomib relative to a control cell line (4.5-fold), but was highly resistant to the three epoxyketone inhibitors tested. The resistance factors were 114-fold, 23-fold, and 162-fold for carfilzomib, ONX 0912, and ONX 0914, respectively. Cell lines overexpressing the MRP1 through MRP5 or BCRP transporters did not have greater than 2.5-fold increased sensitivity to any of the proteasome inhibitors tested. In CEM/VLB, co-treatment with a peptide inhibitor of P-gp greatly reduced resistance to all three epoxyketone PI's [168]. A publication from our group confirmed these findings by identifying increased P-gp expression in H23 and DLD-1 cell lines which had acquired carfilzomib resistance. Treatment with verapamil, a known P-gp inhibitor, restored sensitivity to near that of the parental cell lines [169]. In a recent publication by Besse et al., MM cells were isolated from patients first during their initial response to carfilzomib therapy and then later during consecutive disease progression under carfilzomib therapy. Evaluating these samples for paired gene expression identified significant increases in the expression of the ABCB1 (P-glycoprotein) gene. Deletion of the ABCB1 gene by CRISPR/Cas9 editing in carfilzomib-resistant AMO cells resulted in an 8-fold increase in carfilzomib sensitivity as well as a 7-fold increase in sensitivity to the epoxyketone PI oprozomib. Patients newly-diagnosed with plasma cell leukemia (PCL), an aggressive form of MM, were also found to overexpress ABCB1 within circulating plasma cells. Overexpression of P-glycoprotein in the carfilzomib-resistant AMO cell line model directly resulted in increased carfilzomib efflux and decreased proteasome inhibition [170]. Additionally there is evidence to suggest that P-gp plays a role in resistance to other anti-myeloma agents such as vincristine and doxorubicin,

and that P-gp expression is likely to be increased in patients who have been treated with these agents [171, 172].

1.7.6 *Resistance via Altered Proteasome Activity and Expression*

As discussed previously, increased expression of the β5 catalytic subunit targeted by bortezomib and carfilzomib is a mechanism of drug resistance in preclinical models. Additionally, more complex changes in the expression and activity levels of the six proteasome and immunoproteasome catalytic subunits have been observed in cell line models of proteasome inhibitor resistance. In a 2011 publication Suzuki et al. examined the expression levels of all six catalytic subunits in HT-29 cells with acquired bortezomib resistance. After 14 days of withdrawal from bortezomib these cells maintained a 28-fold bortezomib resistance factor and when compared to parental cells had significantly increased expression of five catalytic subunits: β1, β2, β5, β1i, and β5i. Measurements with fluorogenic peptide substrates confirmed increased catalytic activity of the CT-L, T-L, and C-L activities. Interestingly, despite the fact that the β1 and β2 subunits are not potently inhibited by bortezomib, their expression was increased to a similar degree as β5. Additionally the β5i subunit showed the highest-fold upregulation, over five times greater than the low-level expression observed in parental HT-29 cells [173]. Measurements of catalytic subunit protein expression levels in the bortezomib-resistant THP-1 cell line by Verbrugge et al. also identified altered expression of multiple subunits, however the specific pattern was different. In this case, while β1, β2, β5 protein levels were upregulated (approx. 2-fold), β1i was significantly downregulated and β2i and β5i were not significantly altered. Looking specifically at cell lines of hematologic origin, Niewerth et al. generated bortezomib-resistant sub-lines of RPMI-8226, THP-1, and CCRF-CEM which exhibited bortezomib resistance factors of 40- to 150-fold [174]. Sequencing of the PSMB5 gene revealed that all three resistant cell lines carried the Ala49Thr mutation. As compared to their parental counterparts, the resistant THP-1 and CEM cell lines showed an overall increase in proteasome content and increases in the relative proportions of the β1, β2, and β5 subunits in the overall pool of catalytic subunits. In contrast, RPMI-8226 only experienced minor increases in overall proteasome content and relative β1/β2/β5 content, but this may be due to its higher basal levels of constitutive proteasome expression. Treating these three resistant cell lines with IFN-γ lead to the upregulation of the β1i and β5i subunits at the mRNA and

protein levels as well as moderate decreases in constitutive catalytic subunit expression levels. A corresponding decrease in C-L activity and increases in β5i-specific and β1i-specific catalytic activities were observed. These alterations were significantly more pronounced than in parental cells treated with IFN-γ. Treatment with IFN-γ significantly restored bortezomib sensitivity in all three cell lines. Notably, siRNA-mediated silencing of β5i blocked this effect but β1i silencing did not. Niewerth et al. hypothesized that downregulation of β5i may be a determinant of bortezomib resistance and that IFN-γ-mediated upregulation of β5i may drive the assembly of immunoproteasomes or may facilitate the generation of hybrid proteasomes which combine β5i with constitutive catalytic subunits. Whether this relationship between β5i expression and bortezomib resistance is due simply to the displacement of mutated β5 from proteasomes, or whether β5i-containing proteasomes have an intrinsic resistance to the effects of bortezomib is unknown [174]. Further research has also indicated that the relative expression levels of proteasome and immunoproteasome catalytic subunits may be predictive of response in some patients with acute leukemia [175, 176]. While overall it is clear that alterations in expression and activity levels of proteasome catalytic subunits is a feature in several cell line models of acquired resistance, the magnitude of the clinical relevance of this fact is still unknown.

1.7.7   *Resistance via the Unfolded Protein Response*

Recent research has highlighted alterations in the unfolded protein response (URP) as a potential non-proteasomal mediator of resistance to proteasome inhibitors. The UPR is a stress response pathway which is activated following the accumulation of unfolded or improperly folded proteins within the endoplasmic reticulum (ER). UPR activation can have a protective effect via the downregulation of protein synthesis and upregulation of pathways which aid in protein folding and protein degradation. Alternatively, UPR activation can activate apoptosis leading to cell death under certain circumstances. The UPR consists of three major signaling arms, the PERK arm, the ATF6 arm, and the IRE1 arm. The IRE1 arm is of particular interest in this context. IRE1 is an endoplasmic reticulum (ER) transmembrane protein which has a luminal domain which senses ER stress and a cytoplasmic RNase domain which initiates downstream signaling via the splicing of XBP1 mRNA to yield the XBP1s mRNA. This mRNA is then transcribed to yield XBP1s protein, a bZIP family transcription

factor which acts on a number of target genes [177]. Although it has been known for some time that PI's can both induce the UPR and inhibit Xbp1s signaling, the role of the UPR and IRE1/XBP1s specifically in proteasome inhibitor resistance was not explored in detail until more recently [178]. In 2011 Zhu et al. reported the results of an RNAi screen of the druggable genome which sought genes which would sensitize KMS11 myeloma cells to bortezomib when silenced. Upon reanalyzing this data in search of compounds which had an opposite protective effect, the *IRE1* gene was identified as a top candidate [179]. This was a surprising finding considering that IRE1 signaling was thought to help restore homeostasis in the face of ER stress. As the *XBP1* gene was not tested in the original screen, additional experiments were performed which revealed that *XBP1* silencing also induced bortezomib resistance in six different MM cell lines. Using gene expression data from a phase III trial of bortezomib the authors found a correlation between downregulation of the IRE1-XBP1 signaling pathway and poor clinical response to bortezomib. Further studies identified the presence of Xbp1s⁻ pre-plasmablasts in primary MM samples which are intrinsically insensitive to bortezomib and which become enriched following PI therapy. As with MM cells which have been *XBP1*-silenced, these XBP1s⁻ plasmablasts exhibit reduced immunoglobulin secretion suggesting that these cells are less sensitive to ER stress and accordingly less sensitive to proteasome inhibition due to a reduced basal ER load. This hypothesis has gained additional credence with the finding that high *XBP1* expression is a prognostic indicator of better outcome in MM patients treated with bortezomib [180]. While XBP1s may play a significant role in the sensitivity to MM to proteasome inhibitors, it is unlikely to play a role in the sensitivity or resistance of other cancer types to PI considering the interaction between XBP1s function and plasma cell maturation and immunoglobulin secretion.

Overall, these potential mechanisms of a resistance still require significant clinical validation to determine their relevance in the clinic both for the treatment of MM with proteasome inhibitors as well as for the potential application of proteasome inhibitor in non-myeloma cancers. Nonetheless there may be the potential to develop novel proteasome inhibitors which lack cross-resistance to existing FDA-approved PI's, or which have activity in intrinsically insensitive cancer types due to their novel properties.

1.7.8   *Pharmacokinetic Properties of Approved Proteasome Inhibitors*

Although bortezomib, carfilzomib, and ixazomib are effective in the treatment of myeloma, they have pharmacokinetic (PK) properties which may negatively impact their activity in solid tumors. Though bortezomib, carfilzomib, and ixazomib are known to be active in a number of xenograft models of solid tumors, there are important differences between these models and solid tumors found in human patients. As compared to human solid tumors, mouse xenograft tumors are significantly different in terms of tumor-immune system interaction and in terms of tumor microenvironment and tumor architecture [181]. These differences can significantly alter drug function leading to cases where drugs are significantly more or less effective in human patients than would be expected based on mouse xenograft models. Although there has been research into the pharmacokinetic properties of bortezomib, carfilzomib, and ixazomib in both humans and animals, very little of it has focused on the behavior of the drug within solid tumors in particular. What research is available and the overall pharmacokinetic properties of these drugs will be discussed below.

Bortezomib is a slowly-reversible proteasome inhibitor with an *in vivo* half-life of 76-108 hours at the standard 1.3 mg/m^3 dose. Bortezomib's volume of distribution is large (498 to 1884 L/m^2), potentially indicating good distribution to peripheral tissues [182]. Plasma bortezomib concentrations peaked at 223 ng/mL (580 nM) following i.v. administration of 1.3 mg/m^3 bortezomib with average plasma concentrations dropping below 10 ng/mL (26 nM) by one hour post-dose. Peak inhibition of blood CT-L (chmyotrpysin-like) proteasome activity following 1.3 mg/m^3 of i.v. bortezomib was 69.3% on average with inhibition levels falling to approximately 45% and 25% at 6 and 24 hours post-dose, respectively [183]. It should be noted that high apparent volume of distribution is reflective of rapid clearance of bortezomib in systemic circulation, but not necessarily an indication of drug distribution to various organs including solid tumor tissues. The major elimination route of bortezomib is via oxidative deboronation catalyzed by P450 enzymes found predominantly in the liver [184, 185]. This reaction yields two stereoisomeric carbinolamide metabolites which lack the boronic acid pharmacophore required for covalent inhibition of the proteasome.

A publication by Clemens et al. identified massive intracellular accumulation of bortezomib in nine different multiple myeloma cell lines which appeared to be independent of influx transporter activity [186]. Following incubation with 1 nM bortezomib, intracellular drug

concentration rose rapidly in the first four hours and remained elevated until 48 hours post-dose while extracellular concentrations gradually declined. After one hour the intracellular bortezomib concentration was 43-fold higher than the extracellular concentration on average. The peak intracellular concentration of bortezomib differed significantly between cell lines but the median concentration was 271 nM giving an intracellular/extracellular concentration ratio of well over 1000-fold. Incubating cells with 5 nM or 25 nM of bortezomib yielded even higher peak intracellular concentrations, however the increase was less than proportional (2.9x and 4.8x relative to 1 nM). Although the mechanism of this significant drug accumulation was not determined, bortezomib's high-affinity binding to the proteasome was proposed by the authors as one potential factor. If intracellular bortezomib accumulation occurs in other cell types found in the body, it could impact bortezomib's ability to reach solid tumor cells.

It should also be noted that the architecture of solid tumors itself can impair drug distribution [187]. Cancer cells within tumors may grow more rapidly than the blood vessels which supply them leading to poor vascularization and giving rise to cells which are isolated from blood vessels creating a hypoxic environment. When combined with increased glycolysis due to the Warburg effect, tumor pH is decreased as well. Solid tumors may also suffer from high interstitial fluid pressure and a lack of lymphatic flow. These factors can lead to low drug concentrations in significant portions of the tumor.

A 2009 paper published by researchers at Millennium Pharmaceuticals remarked that bortezomib exposure and pharmacodynamic profiles varied across different tumor xenograft models [188]. As such they sought to study bortezomib's efficacy in two xenograft models with a known disparity in bortezomib sensitivity, CWR22 and H460. Both cell lines are sensitive to bortezomib *in vitro* with IC_{50}'s of 4.0 and 7.4 nM, respectively, in a 48-hour cell viability assay. Next they studied the effects of twice-weekly i.v. bortezomib in nude mice bearing CWR22 or H460 tumors. Peak bortezomib concentrations (Cmax) and AUC_{0-48h} values measured in blood were similar in both groups with the H460 group having a 7.9% higher Cmax and a 1.6% higher AUC_{0-48h} as compared to the CWR22 group. In contrast, the intra-tumoral concentration of bortezomib differed greatly between the two groups. Peak tumor bortezomib concentration was 4.8-fold higher and bortezomib AUC_{0-48h} was 3.1-fold higher within CWR22 xenograft tumors than H460 tumors. Peak inhibition of tumor β5-specific

proteasome activity was approximately 40% in the CWR22 group but was less than 10% in the H460 group. Using average tumor volume reduction as a marker of drug efficacy, bortezomib treatment significantly reduced tumor volume CWR22-bearing mice but not in H460-bearing mice. Dynamic contrast-enhanced MRI was used to measure the distribution of a contrast-agent into the core of CWR22 and H460 tumors which found significantly reduced signal in H460 tumors. Micro computed tomography (MicroCT) vascular casting confirmed that H460 tumors were poorly vascularized in their core regions as compared to CWR22 tumors. The authors concluded that prominent differences in tumor vasculature and architecture may result in reduced tumor concentrations of bortezomib and consequently reduced bortezomib efficacy in poorly vascularized tumors. Whether these results translate to human solid tumors is yet unknown.

In contrast to bortezomib or ixazomib, carfilzomib is rapidly eliminated from the body. In a study of three solid tumor patients dosed with 20 mg/m^3 carfilzomib via a short i.v. infusion, an average peak plasma drug concentration of 2,760 ng/mL (3,830 nM) was achieved immediately after dosing [189]. Plasma carfilzomib concentrations declined rapidly thereafter with a half-life of 1.0 ± 0.6 hours (mean ± S.D.). At four hours post-dose the average plasma concentration of carfilzomib was below 0.2 ng/mL (<0.3 nM). Average plasma clearance of carfilzomib exceeded typical hepatic blood flow, suggesting the involvement of extrahepatic clearance mechanisms [190]. Analysis of patient plasma samples identified three major metabolites, M14, M15, and M16. Metabolites M14 and M15 are N-terminal fragments of carfilzomib which are formed via peptide bond hydrolysis of carfilzomib at the P3-P4 and P2-P3 peptide bonds, respectively. M16 is the diol of carfilzomib formed via epoxide ring opening. These metabolites are believed to be formed by the actions of peptidase(s) and epoxide hydrolase(s). In contrast, metabolites formed via P450 enzymes were only detected at very low levels. An *in vitro* study using rat tissue homogenates has confirmed that carfilzomib metabolism is not restricted to the liver and that lung, kidney, and heart tissues all possess the ability to rapidly degrade carfilzomib to its inactive metabolites [191]. Although carfilzomib is metabolized rapidly, it achieves a prolonged pharmacodynamic response via its irreversible covalent binding to the proteasome. In RPMI-8226 and HT-29 cell lines treated with a one-hour pulse of 32 nM bortezomib or carfilzomib, the degree of inhibition of proteasomal CT-L activity after 24 or 72 hours was

equal or greater in cells treated with carfilzomib as compared to bortezomib [133]. In BALB/c mice treated with 1 mg/kg bortezomib or 5 mg/kg carfilzomib, blood CT-L inhibition (approx. 90%) was similar in both groups after one hour. Differences in tissue CT-L inhibition between two groups at one hour post-dose were minor. Recovery of whole blood CT-L activity was much faster in bortezomib-treated mice, returning to 100% of control at +72 hours. In contrast, whole-blood CT-L activity was still below 25% of control at +72 hours in carfilzomib-treated mice. Proteasomal CT-L activity also recovered more quickly with bortezomib in heart tissue when measured at +24 hours. Interestingly, in rats dosed with 8 mg/kg i.v. carfizomib, ≥90% inhibition of proteasome CT-L activity was observed in heart, lung, and adrenal tissues at 2 hours post-dose. However liver CT-L activity was inhibited to a lesser degree, approximately 70%, despite prior confirmation that carfilzomib is well-distributed to the liver [133]. The authors suggest that competition between the proteasome and carfilzomib-metabolizing enzymes may reduce its activity in the liver. This suggests that tissues which express high levels of carfilzomib-metabolizing enzymes may be more resistant to its effects.

As described previously, ixazomib is a reversible proteasome inhibitor which dissociates from the proteasome more rapidly than bortezomib. The pharmacokinetics of 2 mg/m^3 oral ixazomib (as ixazomib citrate) were evaluated in 31 patients with multiple myeloma [192]. On average, a peak drug plasma concentration of 49 ng/mL (136 nM) was achieved at 0.65 hours after dosing on day 1. The terminal half-life was evaluated following the third dose (cycle 1 day 11) and was found to be 116 hours, slightly longer than that of bortezomib. Due to its long elimination half-life, significant inter-dose accumulation of ixazomib was already observed by cycle 1 day 11 where an accumulation ratio of 3.09 was calculated. Although there is, as yet, relatively little data concerning ixazomib's pharmacodynamics in humans with solid tumors, a publication by Kupperman et al. provides extensive data comparing ixazomib and bortezomib in mouse models [81]. Ixazomib displayed a blood volume of distribution of 20.2 L/kg in mice, over four-fold greater than for bortezomib. Ixazomib's effects were evaluated in mice bearing CWR22 human prostate xenograft tumors or WSU-DLCL2 human lymphoma tumors. Both drugs were dosed intravenously at the MTD, however the MTD for ixazomib was determined to be much higher than for bortezomib (14 and 0.8 mg/kg, respectively). Despite this discrepancy in dose, the peak inhibition of blood β5 activity

was slightly greater in animals treated with bortezomib. Of particular interest is the peak inhibition of tumor β5 activity which was much greater in ixazomib-treated mice. Specifically, bortezomib achieved peak inhibition levels of 44.8% and 27.6% in the CWR22 and WSU-DLCL2 groups, respectively, whereas ixazomib achieved levels of 69.1% and 77.0%, respectively. This relationship was mirrored when evaluating 0-24 hour area under the effect vs. time curve for proteasome inhibition (AUEC). Although the AUEC in blood was greater for bortezomib, tumor AUEC was much higher for ixazomib for both tumor types. Accordingly, the treatment to control ratios for tumor volume with ixazomib were slightly better than bortezomib in CWR22-bearing mice and much better in WSU-DLCL2-bearing mice. Although the concentration of ixazomib within the tumors was not measured, it is plausible that ixazomib's ability to achieve greater pharmacodynamics effects in tumors without causing greater proteasome inhibition in blood may be due to an improved drug penetration and partitioning into solid tumors ratio as compared to bortezomib.

In conclusion, we have evidence that tumor architecture can negatively impact bortezomib's efficacy in mouse models of poorly vascularized solid tumors and that this effect is most likely due to poor partitioning of bortezomib into such tumors. There is also evidence that ixazomib achieves greater intratumoral proteasome inhibition in xenograft-bearing mice than bortezomib at their respective MTDs. Whether this difference is due to differences in proteasome binding kinetics, membrane permeability, susceptibility to drug transporters, or other factors is not yet known. In the case of carfilzomib, research indicates that carfilzomib can be rapidly metabolized to inactive compounds by a wide variety of bodily tissues and that tissues which metabolize carfilzomib more rapidly show decreased proteasome inhibition by carfilzomib. Whether these properties are a factor in carfilzomib's poor activity in humans with solid tumors is unknown. At a fundamental level, we know that proteasome inhibitors must be well-distributed to tumor cells and must reach their targets before being metabolized in order to exert a therapeutic effect.

1.8   Non-Peptide and Non-Covalent Proteasome Inhibitors

As discussed above, proteasome inhibitors have proven activity against a variety of solid cancer cell lines and against preclinical animal models of solid cancers. Unfortunately, clinical trials of bortezomib and carfilzomib in patients with solid tumors have yielded disappointing results. The poor activity of these drugs in patients with solid tumors could be attributed to a number of factors such as insufficient maximum tolerated dose, poor drug penetration into solid tumors, high drug efflux from solid cancer cells, or the rapid acquisition of drug resistance via changes in proteasome catalytic subunit expression levels or other mechanisms. The discovery of structurally-novel proteasome inhibitors could alleviate these issues. The vast majority of existing proteasome inhibitors utilize a peptide backbone and a reactive C-terminal warhead, a simple recipe that tends to yield potent proteasome inhibitors. In contrast, the potential for non-peptide-based non-covalent inhibitors of the proteasome has gone largely unexplored. Prior research examining non-covalent inhibitors of the proteasome (either peptide-based or non-peptide-based) is recounted below.

1.8.1   *Prior Discoveries in the Area of Non-Peptide Inhibitors*

Non-covalent proteasome inhibitors have long been sought after as a solution for the promiscuity of many types of reactive warheads such as aldehydes, vinyl sulfones, and boronic acids. An early report of non-covalent peptide inhibitors of the proteasome was published by Lum et al. in 1998. These compounds consisted of a hydrophobic dipeptide core which is N- and C-terminally capped with aromatic substituents. One of the compounds reported, CVT-600 consisted of a L-Leu-D-Leu dipeptide with a C-terminal aminobenzyl cap and a substituted indanone acetic acid cap at the N-terminus (Figure 1.9). At a concentration of 10 μg/mL (~18 μM), CVT-600 inhibited 20S proteasome chymotrypsin-like (CT-L) activity by >90% with minimal inhibition of proteasome T-L or C-L activities and with minimal inhibition of the non-proteasomal protease calpain I [193]. According to a second publication by Lum et al., an analogue of CVT-600 dubbed compound 28 bearing an altered C-terminal cap achieved a proteasome CT-L IC_{50} of 0.14 μM (Figure 1.9) [194]. For comparison, the CT-L IC_{50} of CVT-600 according to this publication was 0.93 μM. Although these compounds were

not directly proven to act as non-covalent inhibitors, their ability to retain inhibitory activity with a wide variety of C-terminal substituents suggests a non-covalent mechanism.

Research into non-covalent proteasome inhibitors was further advanced with the discovery of the proteasome-inhibiting natural product TMC-95A produced by the fungus *Apiospora montagnei*. Reported by Koguchi et al. in 2000, TMC-95A is a macrocyclic peptide containing a biaryl junction between tyrosine and tryptophan side chains with a total molecular weight of 678.7 Da (Figure 1.9). It was found to be a potent inhibitor of 20S proteasome catalytic activities with IC_{50}'s of 5.4, 60, and 200 nM against the CT-L, C-L, and T-L activities, respectively [195, 196]. Unlike all other previously known inhibitors, X-ray crystallographic analysis of TMC-95A in complex with yeast 20S proteasome found no covalent bond with the proteasome's catalytic Thr1 residues but rather a network of hydrogen bonds between the inhibitor and proteasome catalytic subunit residues including Ser20, Thr21, Gly23, and Ala49. A hydrogen bond with Thr1Oγ was identified as well as hydrophobic interactions in the S1 and S3 specificity pockets which may drive the inhibitor's specificity for CT-L activity [197].

Efforts by researchers at Millenium Pharmaceuticals have employed a more systematic approach to discover structurally-novel proteasome inhibitors. According to their 2010 publication, they conducted an extensive screen of approximately 352,000 small molecule compounds using a cell-based assay in which a tetra-ubiquitin luciferase reporter accumulates following ubiquitin-proteasome system inhibition [113]. Of 611 confirmed hits, the majority were peptide boronic acids or E1 inhibitors with 191 previously unknown proteasome inhibitors. These active compounds were assayed for their ability to inhibit purified 20S proteasome using a fluorogenic β5-specific substrate (Ac-WLA-AMC). While most of the test compounds did not inhibit the 20S proteasome, a series of four N,C-di-capped tripeptides were identified as potent inhibitors of 20S proteasome β5 activity. Compound 1, utilizing a tri-homophenylalanine core, had IC_{50}'s of 16 and 8.9 nM against 20S β5 and 20S β5i activity, respectively, and >1000x selectivity for β5/β5i over all over catalytic subunits (Figure 1.9). The results of kinetic analysis were consistent with non-covalent reversible binding. In the tetra-ubiquitin luciferase accumulation assay in MDA-231 cells, compound 1 had a higher EC_{50} than bortezomib (690 vs. 240 nM) and a lower maximal induction (52- vs. 340-fold). Compound 1 also displayed cytotoxic activity against a variety of cancer cell lines,

but with potencies on the order of 10-fold less than bortezomib. With assistance from an X-ray crystallographic structure of compound 1 bound to yeast 20S proteasomes, compound 1 was optimized to generate analogues with improved *in vitro* and cellular potency, most notably compound 16 with 20S β5 and β5i IC$_{50}$'s of 1.2 and 1.1 nM, respectively, as well as greatly improved potency in all cell-based assays including cytotoxicity. Non-covalent inhibitors with >10x selectivity for β5 over β5i and vice versa were also described. In conclusion, this work demonstrated that peptide-based non-covalent inhibitors could achieve *in vitro* potencies within an order of magnitude of bortezomib, significantly better than previously reported compounds such as CVT-600 or TMC-95A. While the reported results are promising, the pharmacokinetic properties of these compounds as well as their performance in animal models of solid cancers remain unknown.

A 2009 publication by Kazi et al. describes a discovery of a non-peptide proteasome inhibitor [198]. In an effort to discover novel proteasome inhibitors, Kazi et al. screened 3,229 small molecules comprising three small compound libraries curated by the NCI for their ability to inhibit purified 20S proteasome CT-L activity. Among eight hits, compound PI-083 (NSC-45382) was the most potent with an IC$_{50}$ of 1 μM (Figure 1.9). PI-083 also inhibited proliferation and induced apoptosis in several solid cancer cell lines in. IC$_{50}$ values for a 72-hour MTT assay ranged from 1.7 to 11 μM across 10 solid cancer cell lines. In a mouse xenograft model using MCF-7 and A549 solid cancer cell lines, twice-weekly dosing of 1 mg/kg PI-083 produced significantly lower tumor volumes than 1 mg/kg of bortezomib. Testing was not performed to determine whether PI-083 forms a covalent bond with the proteasome or whether its inhibition is reversible. The authors did, however, generate a plausible model of the PI-083:proteasome complex via molecular docking. They note that their study could not rule out a covalent mechanism of action for PI-083 where the naphthoquinone chloro substituent could potentially be displaced via an attack by the catalytic Thr1 residue's hydroxyl group leading to the formation of a covalent complex.

A subsequent 2010 publication examined the structure-activity relationship for PI-083 and its analogues and provided further insight into its mechanism of action [199]. A dialysis experiment was performed to examine the reversibility of PI-083 binding to purified 20S proteasomes. Immediately after the start of dialysis, an initial test showed that proteasome CT-L activity was at approximately 12% of control. Proteasome activity rose gradually as

dialysis continued reaching approximately 24% of control at 2 hours and approximately 35% of control after 18 hours. In contrast bortezomib-treated proteasomes showed <5% activity at the start of dialysis reaching approximately 15% after 18 hours. Based on the slow return of proteasome activity in PI-083-treated proteasomes, the authors concluded that PI-083 is likely to act as a covalent reversible inhibitor. As in their previous publication, molecular modeling suggests that the naphthoquinone's chloro substituent is poised to be displaced by the Thr1 nucleophile forming a carbon-oxygen covalent bond between PI-083 and the proteasome's β5 catalytic subunit. This publication also demonstrated the design, synthesis, and testing of over 50 analogues of PI-083, based on traditional medicinal chemistry as well as molecular modeling. Unfortunately, none of the tested compounds provided an improvement in potency as compared to PI-083. In further support of the role of the naphthoquinone 2-chloro substituent, changes from chlorine to hydrogen or to a methyl group lead to a severe loss of activity. In general modifications of the sulfonamide's N-pyridyl group to other heteroaromatics such as to 2-thiazole were the best tolerated with a 3.3-fold reduction of CT-L inhibitory potency in this case. The discovery of another novel structural class of proteasome inhibitors was reported by Gallastegui et al. in 2012, this time both reversible and non-covalent [200]. As in many previously reported efforts, a library of small molecule of compounds was screened in vitro for their ability to inhibit proteasomal fluorogenic peptide hydrolysis. This screen identified an N-hydroxyurea compound dubbed 'compound 1' which was previously reported as an inhibitor of 5-lipoxygenase and is structurally similar to the FDA-approved 5-lipoxygenase inhibitor zileuton (Figure 1.9). Compound 1 was a relatively weak inhibitor of yeast proteasome CT-L activity (K_i = 23 μM) but appeared to have at least moderate specificity for yeast CT-L activity over yeast T-L or C-L activities. Interestingly, compound 1 is structurally dissimilar from the majority of known proteasome inhibitors and an X-ray crystallographic structure of compound 1 bound to yeast 20S proteasome revealed a unique binding mode. This structure revealed no interactions between the N-hydroxyurea moiety and the catalytic Thr1 residue indicating a non-covalent mechanism of action. The compound's propynyl-benzene group was shown to extend into a novel sub-pocket of the S1 substrate binding pocket with the 3,3-methylbutoxy group interacting with a novel sub-pocket of the S3 binding pocket. In order to determine a structure-activity relationship for this scaffold and improve inhibitor potency, the authors synthesized 50 analogues of compound 1 with guidance from molecular docking studies.

Modifying the 3,3-methylbutoxy group to a 1-adamantyl ether as well as introducing a methyl group at the carbon adjacent to the hydroxylated nitrogen yielded a racemic mixture with an inhibitory potency over 200-fold greater than the initial hit, compound 1. Testing of the individual enantiomers yielded compounds 9 and 10 with S and R configurations at methyl substituted carbon (Figure 1.9). Compound 10, the R-isomer, was found to be an extremely potent inhibitor of yeast CT-L activity with a K_i value of 34 nM (IC$_{50}$ = 340 nM). Unfortunately, this series of compounds has not been studied in further publications with regards to activity against cancer cell lines or animal models of cancer. Depending on the pharmacokinetic characteristics of compound 10, it could be a promising lead for further development.

One final series of novel proteasome inhibitors of note are the oxadiazole-isopropylamide compounds discovered via additional efforts from the researchers based at the University of South Florida and Moffitt Cancer Center who previously reported the discovery of PI-083 and related compounds. The effort to discover and characterize this series of compounds was reported in two articles published in 2013 and 2014 [201, 202]. They began with a larger-scale screen for compounds which inhibited the CT-L activity of purified 20S rabbit proteasomes, this time using a 50,000 compound library. Compound 1, dubbed PI-1833, was identified as a potent hit with an IC$_{50}$ of 0.60 μM against proteasome CT-L activity (Figure 1.9). Several series of analogues of PI-1833 were synthesized and tested for their ability to inhibit proteasome activity *in vitro*. Modification of the amide N-isopropyl group to several other alkyl groups resulted in loss of activity, with N-isobutyl and N-ethyl groups retaining the most potency. The next modifications were targeted at the two p-methylphenyl groups located at either ends of PI-1833. An extensive series of analogues was synthesized and tested, and in this case a number of modifications were well tolerated with some yielding improved potency relative to the lead compound. Exchanging the R^2 p-methylphenyl group for a m-pyridine group yielded a 2.7-fold improvement in potency. Combining this modification with a p-(n-propyl)phenyl group in the R^1 position yielded compound 43, later dubbed PI-1840 (Figure 1.9). This was the most potent compound of the series with an IC$_{50}$ of 0.027 μM. Modifications of the central portion of the molecule, such as an amide-to-urea change or an ether-to-amine change, were also tested but resulted in significant loss of activity. Notably PI-1840 had IC$_{50}$'s of >100 μM for proteasomal C-L and T-L activities suggesting a strong binding preference for proteasomal CT-L subunits (β5 and/or β5i) over

other catalytic subunits. When tested for its ability to inhibit proteasomal CT-L activity in intact MDA-MB-468 cells, PI-1840 had a nearly 10-fold higher potency than PI-1833 (IC_{50} = 0.37 vs. 3.5 μM), suggesting that PI-1840 retains acceptable cellular permeability. PI-1840 likewise demonstrated an improved ability to inhibit MDA-MB-468 proliferation by approximately 10-fold as compared to PI-1833.

Although PI-1840 was not further validated in the 2013 publication by Ozcan et al. [201], this series of compounds was further explored in a subsequent publication [202]. Interestingly, when PI-1840 was assayed for its ability to inhibit purified 20S human immunoproteasome CT-L activity, the IC_{50} was 2.17 μM, more than 100-fold less potent when as compared to its IC_{50} against 20S rabbit constitutive proteasome. This is significant in that it may demonstrate the potential for non-peptide non-covalent inhibitors to specifically target individual constitutive or immunoproteasome subunits. However, as PI-1840 was not tested against human constitutive proteasome, the possibility exists that some or all of this difference in potency could be related to the minor sequence differences between human and rabbit proteasomes. To conclusively determine whether PI-1840 acts as a covalent inhibitor, purified 20S rabbit proteasome was incubated with PI-1840 or with lactacystin as a positive control. Tryptic digests were analyzed via LC-MS/MS. In the lactacystin-treated sample, a *clasto*-lactacystin-modified TTTLAFK peptide was identified, originating from the N-terminus of the β5 catalytic subunit. Modified β1 or β2 N-terminal peptides were not observed. In the case of the PI-1840-treated proteasomes, only unmodified β1, β2, and β5 N-terminal sequences were observed indicating that PI-1840 inhibits the β5 catalytic subunit without covalently modifying it. A dialysis experiment was also performed to compare the reversibility of PI-1840 and the control compound lactacystin. Whereas lactacystin-treated proteasomes only recovered approximately 10% activity after 18 hours of dialysis, proteasomes treated with PI-1840 recovered approximately 25% activity in 4 hours with activity being fully restored after 18 hours. Next, their efforts turned to studying the effects of PI-1840 in cell line models. As in their previous publication, the ability of PI-1833 and PI-1840 to inhibit proteasome CT-L activity in intact MDA-MB-468 cells was tested. Again PI-1840 was shown to be approximately 10-fold more potent than PI-1833, but the absolute potencies were lower (IC_{50} = 1.55 vs. 11.6 μM) than those reported in the 2013 publication by Ozcan et al. A 120-hour MTT assay was used to measure PI-1840's potency against several

solid cancer cell lines. IC_{50} values ranged from 2.2 μM against the breast cancer cell line MDA-MB-231 to 45.2 μM in the renal cell carcinoma cell line RXF 397. PI-1840 was then compared to bortezomib in a nude mouse xenograft model of solid cancer using MDA-MB-231 cells. PI-1840 was dosed daily for 14 days at 150 mg/kg via intraperitoneal injection. Bortezomib was dosed at 1 mg/kg i.p. twice weekly for two weeks. During the 14-day treatment period, the tumor volume for bortezomib-treated animals was not significantly different than for the vehicle-treated control group. In contrast, animals treated with PI-1840 had significantly lower tumor volume than the control group ($p < 0.05$). It should be noted that the total dose for PI-1840 was over 500-fold greater than for bortezomib, and that that PI-1840-treated animals did still experience a net growth in tumor volume (+69%) during the 14-day treatment period. In conclusion, PI-1840 has been demonstrated to be a potent non-peptide non-covalent reversible inhibitor of proteasomal β5 activity. While low-micromolar doses of PI-1840 did inhibit cell viability in a 120-hour MTT assay, measurements of CT-L activity from intact cells treated with PI-1840 showed less inhibition than might be expected for a compound with nanomolar potency *in vitro*. Specifically, 59% inhibition was observed when MDA-MB-213 cells were treated with 20 μM PI-1840 for 2 hours. The observed inhibition was in the 85-90% range for several cell lines, but there was not a clear correlation between CT-L inhibition and MTT assay potency. There are several possible explanations for these discrepancies. One possibility is poor cellular permeability, or the metabolism of PI-1840 within cancer cells. PI-1840's high selectivity for the β5 subunit could also reduce its cytotoxic activity as selective β5 inhibitors have been demonstrated to be less cytotoxic than combined inhibitors of β5 and β5i [118]. Another potential factor is the reversible nature of PI-1840 which can effect assays of proteasome activity. When cells are treated with a reversible proteasome inhibitor, lysed, centrifuged, and then diluted in assay buffer, the drug concentration is likely to be reduced by dilution as compared to the original intracellular drug concentration. Considering that PI-1840 appears to be a slowly-reversible inhibitor in dialysis experiments, drug molecules may dissociate from the proteasome between the collection of intact cells and the final CT-L activity assay, effectively reducing the inhibitory effect of the PI-1840 in these types of assays relative to its activity in intact live cells. Lastly, it would be useful to perform animal pharmacokinetic and pharmacodynamics studies of PI-1840 to determine whether it remains effective at doses lower than 100 mg/kg daily and

to determine its rate of clearance, route of metabolism, and its ability to enter into xenograft tumors.

In summary, while a number of non-covalent proteasome inhibitors have been identified, only a small number have been validated in animal models and shown to demonstrate anticancer activity *in vivo*. Though other research groups continue to make progress towards the development of efficacious non-peptide non-covalent inhibitors, we feel there is still significant room for further improvement and understanding in this area.
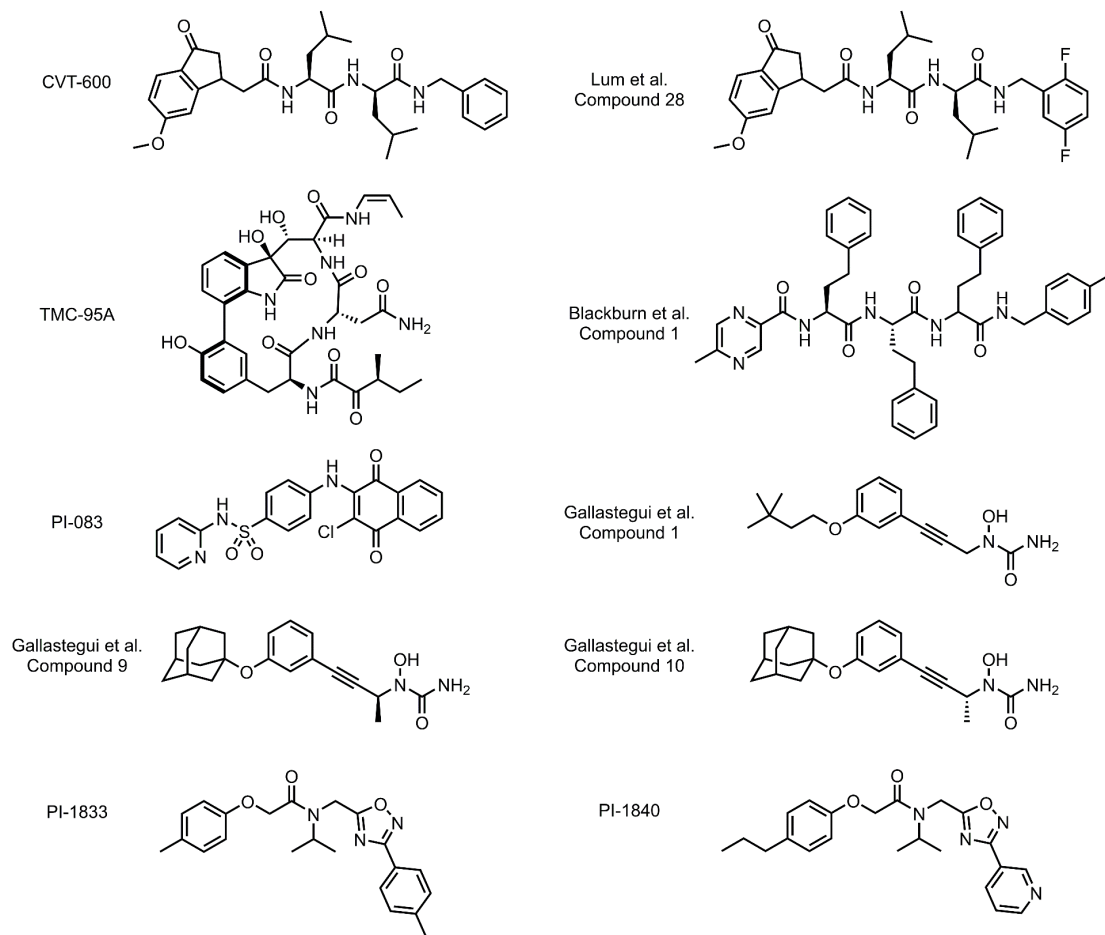
Figure 1.9   Chemical structures of non-peptide and non-covalent proteasome inhibitors

See accompanying text in section 1.8.1 for additional information on these non-peptide and/or non-covalent inhibitors of the proteasome.

1.9   Summary and Rationale for Further Research

From early research in the late 1970's to today, our collective knowledge of the ubiquitin-proteasome system has grown in leaps and bounds enabling the development and FDA approval of three proteasome inhibitors for the treatment of multiple myeloma. Collectively, bortezomib, carfilzomib, and ixazomib have seen widespread clinical use, contributed to significant improvements in MM patient well-being, and have achieved combined annual sales in excess of $3.5 billion USD. According to a wide array of preclinical experiments, conventional proteasome inhibitors such as bortezomib and carfilzomib are active not only against MM cell lines but also exhibit potent cytotoxic and antiproliferative activity against a broad spectrum of cancer cell lines including colon, pancreatic, renal, and lung cancer cell lines. Bortezomib and carfilzomib also have proven activity in mouse xenograft models of a number of solid cancer types. Furthermore, the proteasome is believed to be essential for the survival of all cells and there exists a strong mechanistic rationale for the cytotoxic activity of proteasome inhibitors in solid cancer cells. Despite these promising preclinical results, a large number of clinical trials of bortezomib and carfilzomib in patients with various solid cancers have shown disappointing results.

It is our belief that there exists an opportunity to develop novel proteasome inhibitors with improved clinical activity in a variety of solid tumor types. Although proteasome inhibitors have contributed to major improvements in the survival and well-being of multiple myeloma patients, myeloma represents only approximately 2% of annual US new cancer cases and approximately 2% of annual US cancer deaths. When taken together, solid cancers account for the vast majority of new cancer cases in the US and caused over 400,000 deaths in the US in 2016 [203]. Although the treatment landscape is unique for each type of cancer, there are a number of solid cancer types with high mortality rates and there exists a significant need for improved therapeutic options for these patients [204, 205]. This work was undertaken with the goal of identifying novel inhibitors which could serve as a starting point for a new generation of proteasome inhibitors with superior clinical activity against solid cancers as compared to existing FDA-approved proteasome inhibitors.

Chapter 2   HYPOTHESIS AND SPECIFIC AIMS

The main goal of this research was to discover and develop novel non-peptide non-covalent proteasome inhibitors with improved activity against solid cancers as compared to conventional proteasome inhibitors such as bortezomib or carfilzomib. In clinical trials, bortezomib and carfilzomib have shown poor activity against solid cancers despite promising activity in preclinical studies.

Although the reasons for this discrepancy between clinical trial experience and pre-clinical data are as yet unknown, it is our hypothesis that it results from sub-optimal pharmacokinetic and pharmacodynamic properties, examples of which include rapid metabolic inactivation of active drug, poor drug distribution into solid tumors, or off-target activities which limit the maximum tolerated dose. We also hypothesize that these sub-optimal properties may stem from the common structural heritage of conventional proteasome inhibitors: a peptide backbone combined with a reactive covalent warhead.

By avoiding these structural features, we believe that there exists an opportunity to develop proteasome inhibitors with improved pharmacokinetic and pharmacodynamic properties which may exhibit improved activity in patients with solid tumors. It is our hypothesis that compounds with non-peptidic structures, non-covalent and reversible modes of action, and unique selectivity profiles against the proteasome's distinct catalytic subunits could have superior pharmacodynamic and pharmacokinetic properties and may bear improved activity against solid tumors relative to existing peptide-based covalent proteasome inhibitors. We also hypothesize that non-peptide inhibitors could offer additional benefits such as higher oral bioavailability and lower cost of manufacture.

As described previously, there have already been a number of efforts to discover and develop non-peptide and/or non-covalent inhibitors of the proteasome. Unfortunately, all of these efforts suffer from one or more shortcomings. These include compounds with a peptide-based structure or covalent mechanism of action, a lack of validation in cell culture or animal models of solid cancers, poor potency or activity in cell culture or animal models, or a lack of data on drug pharmacokinetics.

We have made efforts to avoid these issues in our own work, with the ultimate goal of delivering a compound or structural scaffold potentially suitable for clinical use in the treatment of solid cancers. Such a discovery could provide much needed therapies for the many forms of solid cancer in which treatment options are limited and life expectancies are short.

Aim 1. Use a two-stage computational and *in vitro* screening method to identify structurally-novel proteasome inhibitors from a large chemical library. High-throughput screening of small molecules against a receptor or enzyme target is a traditional method for drug discovery but this method can be prohibitively expensive due to the need for automated robotic systems and the use of large amounts of purified enzyme and the large number of test compounds which must be synthesized or purchased. In order to avoid these costs, we turned to an *in silico* screening approach to pre-select compounds with a high likelihood of binding the proteasome's catalytic subunits, thus improving hit rate. We collaborated with Dr. Chang Guo-Zhan and postdoctoral researcher Dr. Vinod Kasam due to their expertise and experience in the area of structure-based virtual screening methods.

Aim 2. Evaluate potential hit compounds and use traditional medicinal chemistry methods to generate an optimized lead compound based on its activity *in vitro* and in cell culture. Compounds identified via structure-based virtual screening were assayed *in vitro* for their ability to inhibit the activity of β5 and β5i catalytic subunits present in purified constitutive and immunoproteasomes. Compounds with positive inhibitory activity were profiled against other proteasome and immunoproteasome catalytic subunits and were tested for cytotoxic activity against human cancer cell lines in cell culture. Traditional medicinal chemistry was performed to design and synthesize analogues of the most promising hit compound. Compound analogues were assayed initially for *in vitro* for proteasome inhibitory activity and later for their cytotoxic activity in cell culture.

Aim 3. Perform a detailed evaluation of the optimized lead compound using cell culture models of solid cancer cell lines, models of PI-resistant solid cancers, and mouse xenograft models of solid cancers. A lead compound was selected from among the synthesized analogues based on its *in vitro* and cellular potency and was evaluated for reversible proteasome inhibition using a jump dilution assay. Cell line models of bortezomib- and

carfilzomib-resistant solid cancers were used to quantify cross-resistance between traditional peptide-based covalent proteasome inhibitors and the lead compound. An *in vitro* assay of compound metabolism by pooled human hepatocytes was used to compare the potential metabolic stability of the lead compound with a conventional proteasome inhibitor. Lastly, to evaluate the lead compound's activity *in vivo*, a mouse xenograft model of human prostate cancer was with bortezomib serving as positive control.

Chapter 3   MATERIALS AND METHODS

Portions of the methods described below have been published previously [206, 207].

3.1   Structure-Based Virtual Screening

A structure-based virtual screening (SBVS) method was used to identify potential proteasome-inhibiting small molecules from a large compound library. Compounds identified as being most likely to bind proteasome catalytic subunits were then tested for proteasome inhibitory activity *in vitro*. All computational modeling was performed by Dr. Vinod Kasam under the direction of Dr. Chang-Guo Zhan at the University of Kentucky.

3.1.1   *Protein Preparation and Binding Site Definition*

A structure-based virtual screening (SBVS) method to identify potential proteasome-inhibiting small molecules began with the preparation of a homology model of the human β5i catalytic subunit. As a crystal structure of human β5i was not available, the SWISS-MODEL workspace was used to generate a homology model from the human β5i sequence (FASTA P28062) and a BLAST search was used to identify a suitable template with an available X-ray crystallographic structure. In this case the human constitutive β5 subunit was chosen as the preferred basis for the homology model. The generated homology model was then quality checked using a Ramachandran plot assessment via PRO-CHECK. As the β5i ligand binding site is constructed both from β5i as well as the adjacent β6 protein, models of both proteins were used in subsequent steps. Due to the availability of pre-existing X-ray crystal structures, homology modeling was not required for the β6 non-catalytic subunit.

In order to define the β5i-β6 binding site, a previously-published model of the peptide epoxyketone inhibitor UK-101 bound to β5-β6 was aligned to β5i-β6 and the UK-101 ligand was transferred to the β5i-β6 model. Next hydrogen atoms were added to the β5i-β6:UK-101 model to assign protonation states and energy minimization was performed with a small number of steps to relax UK-101 and β5i-β6 side chains to more energetically-favorable positions. β5i-β6 histidine side chains were evaluated individually and assigned as being

protonated at the δ-position or at the ε-position. The β5i-β6 binding site was then defined as encompassing all β5i or β6 atoms within 10 Å of the UK-101 ligand.

3.1.2   *Homology Model Validation*

Further validation of the homology model was performed using a set of 16 peptide-based non-covalent inhibitors with known IC_{50}'s against β5i as reported by Blackburn et al. in 2010 [113]. These 16 compounds were first built in the SYBYL 6.9 molecular modeling package. Molecular docking of the β5i binding site and the 16 compound was performed using the GOLD suite with 50 poses generated per compound. GoldScore was then used to assess pose fitness and select an ideal protein-ligand binding pose which would serve as the initial structure for energy minimization followed by molecular dynamics (MD) simulation. Molecular dynamics simulations of the 16 peptide compounds with the β5i binding site were performed using the sander module of Amber9 with the Amber ff03 force field. Protein-ligand complexes were neutralized, solvated, energy minimized and heated prior to running MD simulations for 1 ns total time with a 2 fs time step. Once a stable MD trajectory was obtained, 100 snapshots of the protein:ligand complex were obtained with 1 fs intervals between snapshots. Next, binding free energy calculations were performed using the molecular mechanics-Poisson-Boltzman surface area (MM-PBSA) method. Specifically, the binding free energy was calculated for each of the 100 snapshots and averaged to yield a calculated ΔG_{bind} value. For each snapshot, the binding free energy was calculated as the difference between the protein-ligand complex free energy and the unbound protein free energy and the unbound ligand free energy. When comparing the calculated binding free energies of the 16 peptide compounds with their experimentally-derived binding free energies, there was a positive linear correlation with $R^2 = 0.973$.

3.1.3   *Selection of the Best β5i Binding Site*

The molecular dynamics simulation of the binding between compound 16 and the β5i binding site was chosen as the starting point for further simulations due to compound 16's superior binding affinity among the 16 tested non-covalent inhibitors. An additional 1 ns MD

simulation of compound 16 with the β5i binding site was performed under the conditions described above. Snapshots were taken every 10 ps and binding energy was calculated with the MM-PBSA method. Those snapshots with the best MM-PBSA energies were then visualized manually. As peptide based proteasome inhibitors are known to form β-sheet-like hydrogen bonds with β5i residues Ser21, Gly47, and Ala49 and β6 residue Asp125, interactions with these residues were considered to be of additional importance for the selection of potential inhibitory compounds [80, 208, 209]. After categorizing the best-scoring snapshots based on these key residue interactions, the snapshots from 341 ps, 591 ps, and 931 ps were considered candidates for final selection. The sixteen non-covalent peptide inhibitors were then docked with these three snapshots using the methods described above and the MD simulation snapshot taken at 341 ps was selected due to its ability to best reproduce the binding poses of these 16 compounds.

3.1.4   *Conformations of Chemical Compounds*

The University of Cincinnati Genome Research Institute (UC-GRI) chemical compound library was chosen for this virtual screening due to its availability to University of Kentucky researchers in accordance with a collaborative research agreement and the large number of drug-like compounds available within the library. The UC-GRI compound library database contains the structural information for 345,447 compounds which are available upon request as DMSO solutions. The OMEGA tool (OpenEye Software) was used to systematically generate multiple conformations from each 2D structure and to discard high-energy conformations. The maximum number of conformations per compound was set at 250 and a root mean square deviation (RMSD) of 0.8 Å was used to discard duplicate conformers. A total of approximately 2.1 million confirmations were generated and stored in a single binary file.

3.1.5   *Rigid Molecular Docking*

Initial rigid molecular docking was performed using FRED 2.2.5 (OpenEye Software) using the conformations generated by OMEGA as input. FRED utilizes an exhaustive search that scans rotations and translations of each ligand conformation within the negative image of the

active site at a given resolution, 0.5 Å in this case. A smooth Gaussian shape fitting function was used to optimize the contact between the ligand surface and protein surface, and any ligand poses which clashed with the protein were rejected. Both the ligand poses and the protein were held rigid during this process. Conformations which survived this initial shape fitting processes were then passed to scoring functions. A series of three optimization filters were employed consisting of hydroxyl group rotamer optimization, rigid body optimization, and torsion optimization. In order to identify the ideal scoring function or functions, a preliminary docking trial was conducted using the set of 16 non-covalent peptide inhibitors. Scoring functions were chosen based on their ability both to reproduce known binding modes and to match the rank order of experimentally-determined compound β5i IC_{50} values. Exhaustive docking using ChemGauss3, ChemScore optimization, pose selection via consensus scoring (ShapeGauss, ChemGauss3, PLP, ChemScore), and lastly compound selection via ChemGauss3 and Chemscore produced the best results with the test set of 16 compounds and was accordingly chosen for high-throughput virtual screening. The overall database of approximately 2.1 million conformations was split into sub-groups of 15,000 conformations each. FRED docking of sub-groups were performed in parallel and in-house using distributed computing. The results from all sub-groups were merged and the 250,000 best binding poses from non-redundant compounds were selected. Compounds were selected solely based on ChemGauss3 and ChemScore docking score without other constraints.

3.1.6   *Flexible Molecular Docking*

The 250,000 best binding poses obtained from rigid molecular docking were subjected to flexible docking using Amber9 software. Preprocessing was performed by Amber9's Antechamer module prior to flexible docking. General Amber Force Fields (GAFF) parameters were used for ligands and Amber ff03 parameters were used for the β5i-β6 protein binding site for molecular mechanics and molecular dynamics simulations. The overall procedure for flexible docking began with energy minimization of the protein-ligand complex in which all atoms are allowed movement. Specifically, we employed the steepest decent and conjugate gradient methods for 100 and 2400 iterations, respectively, on all atoms of each β5i:ligand complex. This was followed by a 20 ps MD simulation where the ligand and protein side

68

chains within 12 Å of the ligand were allowed to move. The protein backbone was restrained using a harmonic potential of 50 kcal•mol^{-1}• Å^{-2}. A cutoff distance of 12 Å was used when calculating non-bonded interactions. A distance-dependent dielectric constant of $\varepsilon(r)=4r$ was used to mimic the effect of solvent. Following the 20 ps simulation, the final MD snapshot was fully energy minimized prior to calculating the binding free energy (ΔG_{bind}) via molecular mechanics-Poission-Boltzmann surface area (MM-PBSA) and molecular mechanics-generalized Born surface area (MM-GBSA) methods as implemented within Amber9. A list of the top 10,000 compounds each from the MM-PBSA scoring function and the MM-GBSA scoring function were generated independently. After removing duplicates, the two lists were combined to yield a single list of 15,000 top compounds intended for further study.

3.1.7   *Identification of Key Interactions and Manual Visualization*

Compounds were next filtered based on the presence of at least one hydrogen bonding interaction with β5i residues Ser21, Gly47, and Ala49 or β6 residue Asp125. This produced a set of approximately 3000 compounds which were evaluated by manual visualization in VIDA (OpenEye Software) using the binding mode of Blackburn et al. compound 16 as a template. Compounds with multiple hydrogen bonds to previously listed 'key residues' and high similarity the binding pose of Blackburn et al. compound 16 were given highest priority. A total of 288 compounds were then selected for *in vitro* measurement of proteasome β5 and β5i inhibitory activity.

3.2   Screening and *in Vitro* Measurement of Inhibitory Activity

The 288 selected compounds from structure-based virtual screening were provided as 10 mM DMSO solutions in four 96-well polypropylene storage plates and were stored at -20° C when not in use. Due to limited quantities, compounds were used as is without further purification. *In vitro* measurements of β5 and β5i inhibitory activity were performed in 96-well polystyrene plates (Greiner Bio-One) with a final volume of 100 µL per well. First each well was loaded with 20S proteasome assay buffer (20 mM Tris-HCl, 0.5 mM EDTA, 0.035% w/v SDS). Next test compounds were added at a final concentration of 5 µM via 0.4 µL of 1.25

mM DMSO stock solution. In some wells epoxomicin at 1 μM was used as a positive control or 0.4 μL DMSO as a negative control. Next 50 ng of purified human 20S constitutive proteasome or immunoproteasome (Boston Biochem) was added to each well for the measurement of β5 or β5i activity, respectively. Plates were then allowed to incubate for 1 hour at room temperature in the absence of light to allow slow-binding or irreversible inhibitors to act. 40 mM DMSO stock solution of Suc-LLVY-AMC fluorogenic proteasome substrate (Bachem) was diluted into 20S proteasome assay buffer to form a 1 mM solution of Suc-LLVY-AMC. In order to initiate the β5 or β5i activity assay, 10 μL of the Suc-LLVY-AMC solution was added per well via multichannel pipette to yield a final substrate concentration of 100 μM. Final DMSO concentration was 0.65% v/v in all wells. Na Ra Lee provided assistance in conducting this initial screening.

Following the initial 288-compound screen which utilized Suc-LLVY-AMC as a substrate, subunit-specific fluorogenic substrates were used to monitor proteasome inhibition, excluding the case of the β2 and β2i subunits, for which no specific substrate exists. For measuring activity of the β1, β1i, β2/β2i, β5, and β5i subunits we used 100 μM Ac-nLPnLD-AMC, 100 μM Ac-PAL-AMC, 200 μM Boc-LRR-AMC (R&D Systems), 20 μM Ac-WLA-AMC, and 100 μM Ac-ANW-AMC, respectively. Note that 0.35% w/v SDS was excluded from the proteasome assay buffer when measuring β2 or β2i with Boc-LRR-AMC due to its ability to precipitate this substrate. Ac-nLPnLD-AMC, Ac-PAL-AMC, Ac-WLA-AMC, and Ac-ANW-AMC were synthesized in house.

The inhibition of proteasome activity was monitored by the fluorescence of free 7-amino-4-methylcoumarin (AMC) which is released following the proteasomal hydrolysis of Suc-LLVY-AMC by the β5 or β5i subunit. This was done using a SpectraMax M5 plate reader (Molecular Devices). Each well in a 96-well plate was checked for fluorescence once per minute for a 90-minute period. The excitation wavelength was 360 nm and the emission wavelength was 460 nm. A cutoff filter was employed at 420 nm to improve signal to noise ratio. For each well, proteasome activity was calculated by taking the slope of a linear regression of the fluorescent signal (RFU) versus time (min) data set using GraphPad Prism. Percent activity remaining for any given compound was determining by dividing the slope (RFU/min) in the presence of the compound by the slope in the absence of inhibitor (DMSO control). Positive control wells containing 1 μM epoxomicin were used for normalization.

Proteasome inhibition assays were also performed using cell lysates a source of proteasomes. RPMI-8226 cells were permeabilized using a buffer containing 0.025% digitonin as well as 50 mM Tris-HCl, 250 mM sucrose, 5 mM MgCl2, 1 mM dithreitol, 0.5 mM EDTA, and 2 mM ATP at pH 7.5 [210]. Cells were then centrifuged at 21,000g for 15 minutes in a refrigerated (4°C) rotor and the supernatant was collected and assayed for protein concentration using the Bradford assay (Bio-Rad). Single-use aliquots of supernatant were stored at -80°C prior to use. Each microtiter well contained 3 μg of total RPMI-8226 protein. Chymotrypsin-like (β5/β5i activity) was monitored using 100 μM Suc-LLVY-AMC as substrate. Caspase-like activity was monitored using 100 μM of Z-LLE-AMC (R&D Systems). Trypsin-like activity was monitored using 100 μM of Boc-LRR-AMC. Proteasome inhibition assays using cell lysate were otherwise performed as described in the previous paragraphs. Detergent (0.035% w/v SDS) was omitted when measuring trypsin-like activity due to its propensity to precipitate positively-charged peptide substrates.

3.3   Cell Culture and Development of Drug Resistant Cell Lines

Human cancer cell lines BxPC-3, H358, H23, LNCaP, Panc-1, and RPMI 8226 were obtained from the ATCC (American Type Culture Collection) and maintained in media as recommended by ATCC, either DMEM or RPMI 1640 (Gibco) supplemented with 10% fetal bovine serum (Atlanta Biologicals) and 1 mM sodium pyruvate (Sigma-Aldrich). All media contained 1.5 g/L sodium bicarbonate. Cells were maintained in a 37ºC water-jacketed incubator with 5% CO_2 in air atmosphere. All cell lines were cultured every 3 days. For adherent cell lines, rinsing with HBSS solution (Gibco) followed by treatment with 0.05% trypsin-EDTA solution (Gibco) was used to dissociate cells from cell culture vessels prior to splitting and re-plating on new vessels. For suspension cell lines, centrifugation was used to isolate cells from cell culture media prior to re-plating on new vessels. BxPC-3 cell lines with acquired resistance to bortezomib or carfilzomib were generated by culture in the continuous presence of the respective proteasome inhibitor with gradually increasing drug concentration over time. Over a period of approximately 6 months, these BxPC-3 sublines were adapted to grow in the presence of 60 nM bortezomib for BxPC-3 Btz-R and 200 nM

carfilzomib for BxPC-3 Cfz-R. Na Ra Lee and Dr. Kimberley Carmony provided assistance in the development of these cell lines.

3.4   Assaying Compounds for Cytotoxic or Antiproliferative Effects

The effects of test compounds on cell growth and survival were assayed using the MTS cell viability assays or ATP quantification-based assays in 96-well formats. Cells growing in log phase were collected via trypsinization for adherent cell lines or via centrifugation for RPMI 8226 and were then plated on 96-well cell culture-treated plates (USA Scientific) at a density of 7,000-10,000 cells per well for adherent cell lines or at 10,000 cells per well (5×10^4 cells/mL) for the RPMI 8226 cell line. Cells were plated in an initial volume of 100 µL of cell culture media and then incubated for 24 hours. Test compounds were then added via an aliquot of DMSO stock solution. The final concentration of DMSO was minimized as much as possible via the addition of compounds from high-concentration stocks. Untreated control wells were treated with DMSO alone to match the DMSO concentration of test wells. 96-well plates were then incubated for 72-hours prior to performing MTS or ATP quantification assays. For MTS assays, 20 µL of CellTiter 96® AQueous One reagent (Promega) containing MTS and PMS was added to each well as is indicated in the manufacturer's protocol. The 96-well plate was then incubated at 37°C for 1-2.5 hours (depending on the cell line in use) to allow MTS reduction to occur and the amount of reduction was quantified by reading absorbance at 490 nm using a SpectraMax M5 plate reader (Molecular Devices). Wells containing no cells were used to normalize the results. ATP-based cell viability assays were performed using the CellTiter Glo luminescent cell viability assay (Promega). As indicated in the manufacturer's protocol, 100 uL of CellTiter Glo reagent was pipetted into each well and the plate was mixed for 2 minutes on an orbital shaker and then incubated at room temperature for 10 minutes. Luminescence was then recorded using a Vertias microplate luminometer (Turner BioSystems) using a 1 second integration time. DMSO-treated control wells and wells containing no cells were included for normalization. Dr. Lin Ao provided assistance in performing cell culture cytotoxicity assays.

3.5   Resynthesis of Compound G4 and Synthesis of G4 Analogues

In order to confirm its identity and activity, hit compound G4 was re-synthesized in-house. For a detailed description of the synthesis of G4 and G4 analogues see Miller et al. 2015 [206]. The synthetic scheme for the amide-linked analogue compound G4-1 is shown in Figure 3.1. In brief, p-cresol (4-methylphenol) is treated with acetic anhydride to yield p-tolyl acetate. A Fries rearrangement catalyzed by AlCl$_3$ yields 2'-hydroxyl-5'-methylacetophenone. The phenolic hydroxyl group is then esterified with benzoyl chloride. Following reflux with potassium carbonate, this intermediate ester undergoes a Baker–Venkataraman rearrangement to yield the 1,3-diketone compound 1. Treatment with hydrazine forms the 3,5-disubstituted pyrazole compound 2. This 1H-pyrazole compound is then substituted at the 1-position nitrogen using benzyl 2-bromoacetate. The final aromatic ring is installed by reacting the free phenolic hydroxyl group with 3-trifluoromethylsulfonyl chloride. Next the benzyl protecting group is removed via hydrogenation catalyzed by palladium on carbon. Deprotection results in a free carboxylic acid which then undergoes amide bond formation with (R)-(+)-1-Boc-3-aminopyrrolidine catalyzed by TBTU. In the final step, trifluoroacetic acid is used to remove the Boc (t-butyloxycarbonyl) protecting group yielding compound G4-1 as a trifluoroacetate salt. In some cases, deprotection was performed instead with hydrogen chloride in dioxane to yield G4-1 as its hydrochloride salt.

The synthetic scheme for producing the original amine-linked compound G4 from intermediate compound 3 is shown in Figure 3.2. In this case lithium aluminum hydride is used to reduce the carboxylic acid to a primary alcohol which is then reacted with tosyl chloride before installing the final aromatic ring. The pyrrolidine ring is installed using the same Boc-protected precursor as was used for the synthesis of G4-1 before a final deprotection reaction using trifluoroacetic acid.

Analogues of G4 and G4-1 were synthesized using generally similar schemes, for example substituting modified or alternate chemical precursors in at various points such as by using alternative sulfonyl chlorides in the synthesis of compound 4 or using alternative amines in the synthesis of compound 6. For further details, see Miller et al. 2015 [206]. The synthesis of G4, G4-1, and their analogues were performed by Do Min Lee.

3.6 Jump Dilution Reversibility Assay

Jump dilution assays were performed to determine whether proteasome inhibition by G4-1 and other compounds was reversible in nature. Cell lysate containing 30 μg total protein diluted in a small volume of 20S proteasome assay buffer was treated with 10 μM G4-1 for 30 minutes in a cuvette. Suc-LLVY-AMC fluorogenic proteasome substrate was then added at a concentration of 100 μM. Proteasome activity in the presence of G4-1 inhibitor was then measured via the fluorescence of cleaved AMC. Next a large volume of proteasome assay buffer containing 100 μM Suc-LLVY-AMC was added to the cuvette while continually monitoring the AMC fluorescence signal. The volume of buffer added was sufficient to reduce the concentration of G4-1 by 25-fold from 10 μM to 0.4 μM. The increase in the slope of the fluorescence signal following dilution, if present, indicates reversible proteasome inhibition and can be quantified to estimate the speed of inhibitor dissociation from proteasome binding sites.

3.7 Statistical Analysis

Errors bars represent the standard deviation of the mean unless noted otherwise. Statistical analyses and graphing were performed in GraphPad Prism 6.01. Prism's four-variable (top, bottom, Hill slope, and IC_{50}) non-linear fit was used to obtain IC_{50} values from dose-response curves. Methods used to evaluate statistical significance are specified for individual figures.
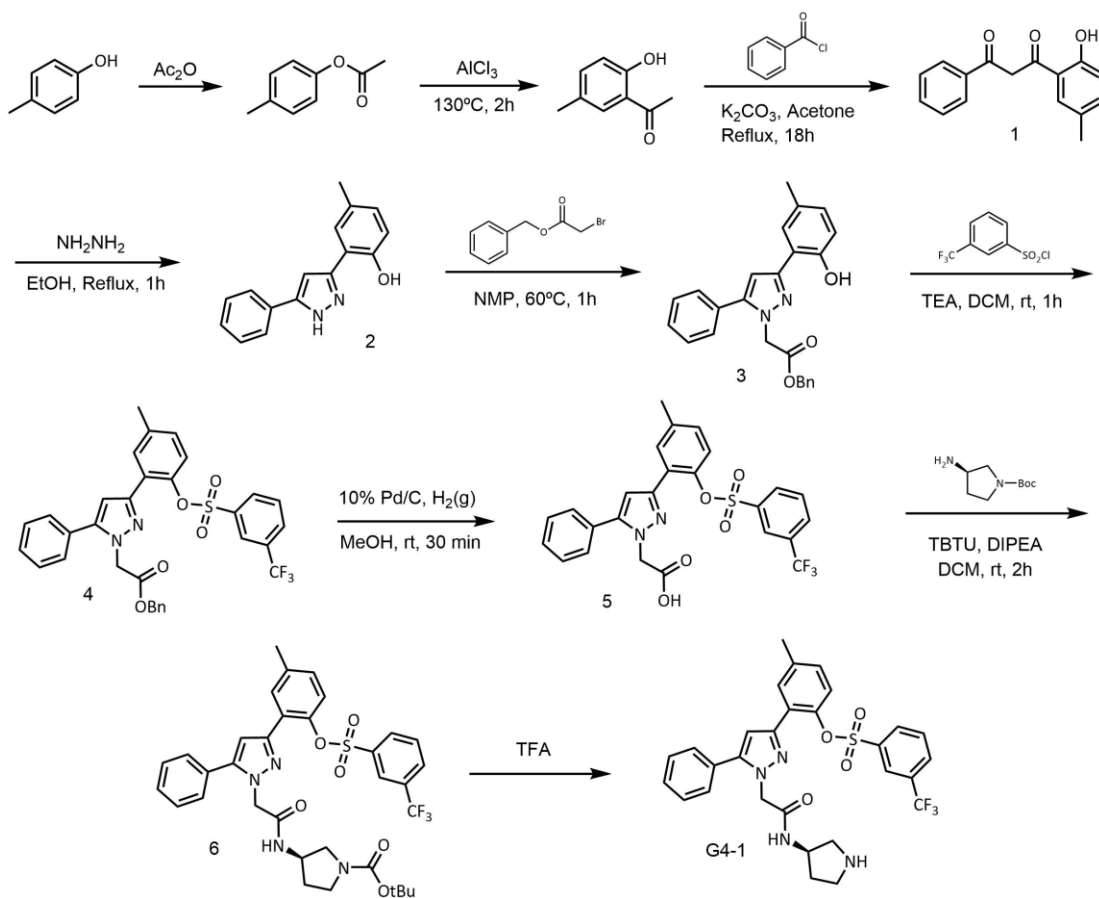
Figure 3.1   Synthetic scheme for G4-1 including intermediate compound 3
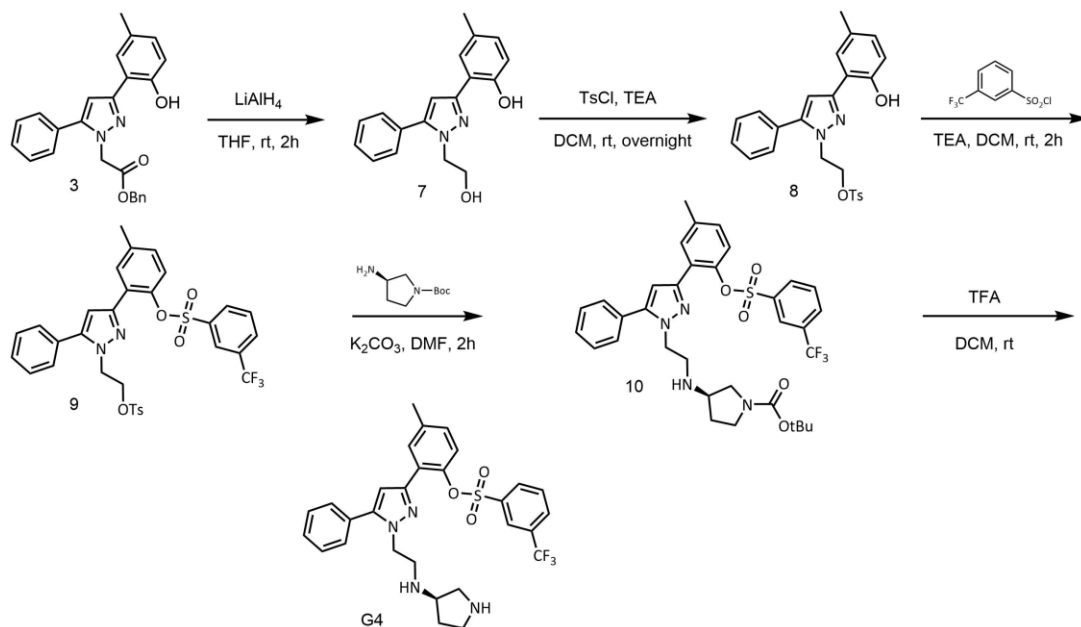
Figure 3.2 Synthetic scheme of G4 from compound 3

3.8   Microsomal Stability Assay

Pooled human liver or mouse liver microsomes were used to assess the *in vitro* metabolic stability of G4-1 relative to peptide-based inhibitors bortezomib and carfilzomib. In brief, assays were performed in 100 µL total volume containing 1 µM test compound 0.5 mg/mL microsomal protein, 100 mM Tris-Cl pH 7.4, and an NADPH-generating system (0.2 u/mL isocitric acid dehydrogenase, 5 mM isocitric acid, 5 mM magnesium chloride, 1 mM $NADP^+$). For negative controls, $NADP^+$ or liver microsomes were withheld from the reaction mixture. Pooled human liver microsomes were obtained from BD Biosciences (UltraPool) whereas mouse liver microsomes were produced in-house from BALB/c mice. Reactions were preincubated for 5 minutes at 37°C before starting reactions by the addition of NADP+. After 0, 5, 10, or 20 minutes of additional incubation time, reactions were stopped by the addition of 100 µL ice-cold acetonitrile containing 1 µM phenytoin internal standard. This mixture was held on ice for 30 minutes followed by centrifugation at 16,100g for 15 minutes. The acetonitrile supernatant was then collected and 5 µL aliquots were assayed for unmetabolized parent compound concentration using liquid chromatography–tandem mass spectrometry performed on an Agilent 1200 HPLC instrument and an Applied Biosystems Qtrap 3200 mass spectrometer equipped with an electrospray ion source. This work was performed by Dr. Yan-Yan Zhang and Dr. Hyun-Young of the University of Illinois-Chicago.

3.9   Mouse Xenograft Studies

In vivo experiments were performed using six-week-old male athymic BALB/c nude mice (Orient Bio Inc., SungNam, Republic of Korea). Animals were handled in accordance with the guidelines of the National Institute of Toxicological Research of the Korea Food and Drug Administration as well as the regulations for the care and use of laboratory animals of the animal ethics committee of the Konyang University. To generate solid tumor xenografts, a suspension of LNCaP human prostate cancer cells were subcutaneously implanted using a total of 2×10^6 cells in a 50 µL injection volume. Once xenograft tumors grew to a tumor volume of approximately 100 mm^3, mice were separated into three groups (n=5 each) to be

administered G4-1 (5 mg/kg), carfilzomib (5 mg/kg), or vehicle only (citrate buffer containing hydroxypropyl-β-cyclodextrin and 8% v/v DMSO). Injections were given intraperitoneally twice per week for a total period of 4 weeks. Tumor volumes were measured using calipers and the formula $(width)^2 \times length/2$ and body weights were measured every 4 days during the experimental period. On day 30, mice were euthanized by cervical dislocation and tumors were isolated, weighed, and photographed. This work was performed by Dr. Keun-Sik Kim of Konyang University.

Chapter 4   DISCOVERY AND OPTIMIZATION OF A NON-PEPTIDE PROTEASOME INHIBITOR

Portions of the results described below have been published previously [206].

4.1   Introduction

The clinical and commercial successes of bortezomib (Velcade®), carfilzomib (Kyprolis®), and ixazomib (Ninlaro®) have validated the proteasome as a valuable target in the treatment of cancer. While highly impactful in the treatment of multiple myeloma, these drugs have shown poor efficacy in the treatment of a variety of solid tumors, an outcome that contrasts with the broad activity of proteasome inhibitors against solid cancers in various preclinical models. While it is not yet well understood why existing proteasome inhibitors are ineffective in the treatment of solid tumors, it is our hypothesis that this discrepancy arises from suboptimal pharmacokinetic and pharmacodynamic (PK/PD) properties shared by these FDA-approved proteasome inhibitors as well as their susceptibility to a number of drug resistance mechanisms. The relative balance of activity of existing proteasome inhibitors against the six different constitutive and immunoproteasome catalytic subunits could also play a role in their efficacy. Of note, the vast majority of existing proteasome inhibitors are structurally and functionally alike, making use of a di-to-tetra-peptide backbone combined with a C-terminal reactive warhead which targets the proteasome's Thr1 catalytic site. One promising approach for the development of proteasome inhibitors with improved PK/PD properties and reduced susceptibility to known drug resistance mechanisms is to identify structurally and functionally unique drugs. To pursue this goal, we chose to utilize a two-stage strategy where potential proteasome inhibitors would be identified by structure-based virtual screening and then later confirmed via *in vitro* inhibition assays utilizing 20S purified proteasomes and fluorogenic peptide substrates of proteasome catalytic subunits. While reports of high-throughput screens to identify proteasome inhibitors can be found in literature, our two-stage approach offered the potential to identify novel proteasome inhibitors without requiring expensive and resource-intensive high-throughput screening.

4.2   Structure-Based Virtual Screening

Using the methods described in section 3.1, our collaborators in the laboratory of Dr. Chang-Guo Zhan performed structure-based virtual screening (SBVS) on a library of approximately 345,000 small molecules using a homology model of the immunoproteasome β5i binding site as a target. The β5i binding site was chosen in order to yield hits which were either non-specific inhibitors of the β5 and β5i subunits or which were specific inhibitors of the β5i subunit. While non-specific β5/β5i inhibitors are generally most active against cancer cells and were the target of this study, β5i-specific inhibitors may have other therapeutic applications such as in the treatment of inflammatory disease. As shown by tests performed in our lab (unpublished) and in the literature, β5-specific inhibitors such as CPSI generally have minimal cytotoxicity and accordingly were not sought in the design of our screening approach [118]. Any β5i-specific compounds discovered could be pursued for alternative non-oncology applications in a separate study. As described in section 3.1.7, 288 compounds were ultimately selected as having the greatest likelihood of being bona fide β5i inhibitors based on structure-based virtual screening. These selected compounds were delivered from the University of Cincinnati dissolved in DMSO at a concentration of 10 mM on four 96-well compound storage microplates.

4.3   Initial *in Vitro* Screening

All 288 compounds were then tested for their ability to inhibit proteasome activity *in vitro* using both constitutive and immunoproteasomes. Suc-LLVY-AMC was chosen as a fluorogenic substrate and was used for measuring inhibition of β5 and β5i activity as it acts as a substrate of both subunits with roughly equal activity [211]. All 288 compounds were initially tested in a single-replicate format using a compound concentration of 5 μM. This initial test revealed 18 compounds which reduced β5 or β5i activity by 30% or greater. These 18 active compounds were then re-tested for their ability to inhibit β5 or β5i activity in triplicate. For simplicity, compounds were named based on the 96-well plate they were stored in (plate A, B, C, or D) and the row and column designation on that storage plate. Compound G4 from plate D was identified as the most potent compound among those which

inhibited both β5 and β5i activities similarly. The structures of selected hit compounds are shown in Figure 4.1. The results of triplicate β5 and β5i inhibition testing are shown in Figure 4.2. Among the 18 compounds which showed inhibition exceeding our threshold of 30% at 5 μM, compound G4 from plate D (referred to simply as G4) demonstrated greater inhibition of the β5 constitutive proteasome subunit than other hit compounds and inhibited both β5 and β5i to a similar degree. Many of the other active compounds displayed a significant preference for β5i over β5, perhaps due to the choice of β5i as the target for our initial virtual screening. Based on its potency and balanced β5/β5i inhibition profile, compound G4 was chosen for more in-depth testing.

4.4   Hit Confirmation of G4 and Discovery of Compound G4-1

In order to confirm the hit, we sought a secondary source of compound G4. As it was not available commercially, our in-house chemists attempted to synthesize it. In the course of an initial unsuccessful synthesis, compound G4-1 was synthesized as a potential precursor to G4. This compound differs from G4 by having an amide functional group in place of the amine which connects the pyrrolidine ring to the pyrazole core. Although G4 was ultimately synthesized by an alternate route given in methods section 3.5, compound G4-1 as well as other synthetic intermediates were tested to determine their proteasome inhibitory potency relative to compound G4. In order to generate a dose-response curve and more accurately compare the inhibitory potency of G4 and G4-1, we tested both compound against the β5 and β5i subunits at a variety of inhibitor concentrations. The percent of β5 and β5i activity remaining following treatment of 20S constitutive or immunoproteasomes with varying concentrations of G4 and G4-1 are shown in Figure 4.4. Based on this data, compound G4 was found to be approximately two-fold more potent against the β5 subunit than against β5i, with IC_{50} values of 2.8 and 6.3 μM, respectively. Interestingly, the amide-linked G4-1 demonstrated greater potency against both subunits, while retaining mild selectivity for β5 over β5i with IC_{50} values of 1.6 and 2.4 μM, respectively. Next we attempted to determine whether G4-1 also acts similarly to G4 in living cells. Due to the difficulty of measuring proteasome inhibition in living cells, especially with regard to reversible non-covalent inhibitors, we compared their effects on cell viability. 72-hour cell viability assays were performed using three different NSCLC cell lines with G4 and G4-1. Against the H23, H358, and H460 cell lines,

G4 had an average IC$_{50}$ of 7.4 μM and only minimal differences in potency across the three cell lines. G4-1 was slightly more potent with an average IC$_{50}$ of 6.6 μM. As such we confirmed that G4-1 was more potent than the parent compound G4 in both proteasome inhibition assays and *in vitro* cytotoxicity assays. We also found that the concentrations at which G4 and G4-1 induced cell death were similar to the concentrations required to inhibit the majority of both β5 and β5i activity *in vitro*. Based on its similar or improved potency, shorter synthetic route, and easier generation of pyrrolidine ring analogues via peptide coupling reactions, we chose to use G4-1 as the lead compound for further studies of this class of compounds.

4.5   Literature and Patent Background Research

In order to determine whether G4 or closely related compounds had been previously investigated for use as proteasome inhibitors or had been investigated for other purposes, we performed a search of the chemical literature. SciFinder Scholar (Chemical Abstracts Service) was used to search for reported or patented chemicals bearing structural similarity to compound G4. Although this search revealed a total of 46 compounds with a structural similarity score (Tanimoto metric) above the threshold of 60/100, we found no evidence that any of these compounds had been previously reported as inhibitors of the proteasome. The most similar compound identified was CAS 175678-14-5, with a similarity score of 70/100. This compound was reported as an inhibitor of cyclooxygenase II, compounds which have been used medically for their anti-inflammatory and analgesic properties. The second most similar compound was CAS 1240781-81-0, with a similarity score of 69/100. This compound was reported as having a greater ability to inhibit the growth of cells which lacked the Neurofibromin 1 (NF1) gene as compared to cells which possessed NF1 in a phenotypic screen. The precise mechanism of action was not identified but EGFR (epidermal growth factor receptor) and Ras were suggested as possible candidate targets of this compound. Although these two compounds were identified has having the highest structural similarity to compound G4, their similarity scores are relatively low and close to the minimum threshold in both cases.   Likewise, by-hand comparisons reveal significant differences between the structures of these reported compounds and G4 itself. As such we cannot assume that G4 or analogues of G4 will share the same biological activities as CAS 175678-14-5 and CAS 1240781-81-0. The structures of these compounds are given in Figure 4.3. A patent for

compound G4 and a series of its analogues was filed following our discovery of their properties as proteasome inhibitors. This patent was granted in 2016 [212].

Plate: D, Compound: G4
UC DDC #751956

Plate: C, Compound: D2
UC DDC #744611

Plate: D, Compound: H1
UC DDC #799690

Plate: B, Compound: G6
UC DDC #102447

Plate: B, Compound: F2
UC DDC #115780
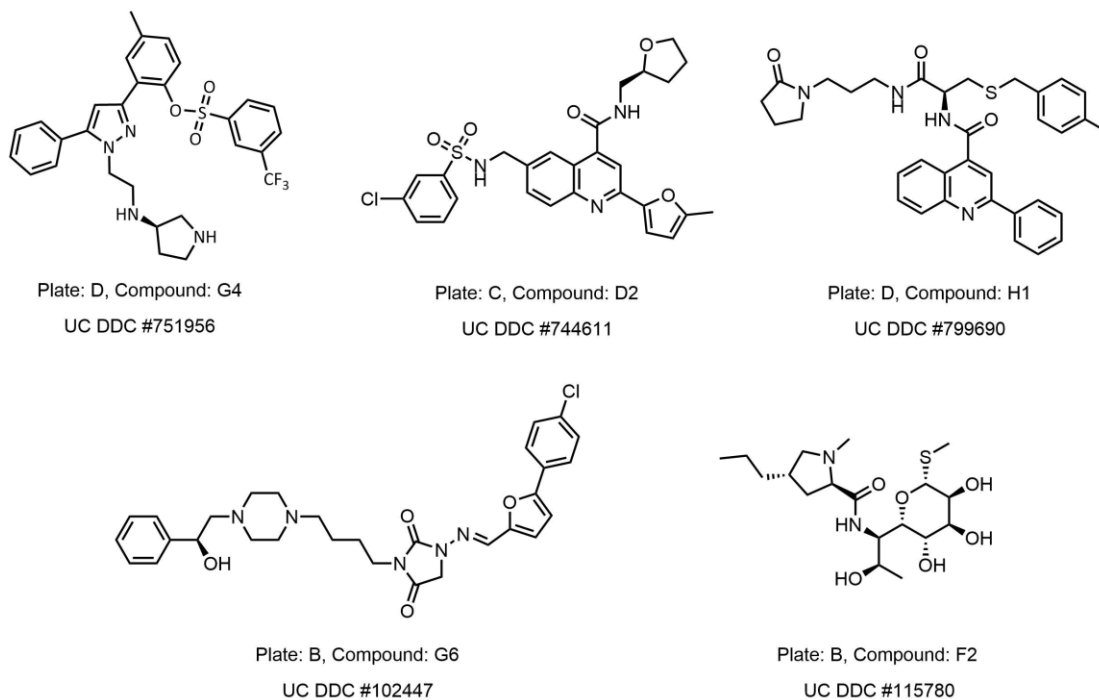
Figure 4.1   Chemical structures of selected hits from *in vitro* screening
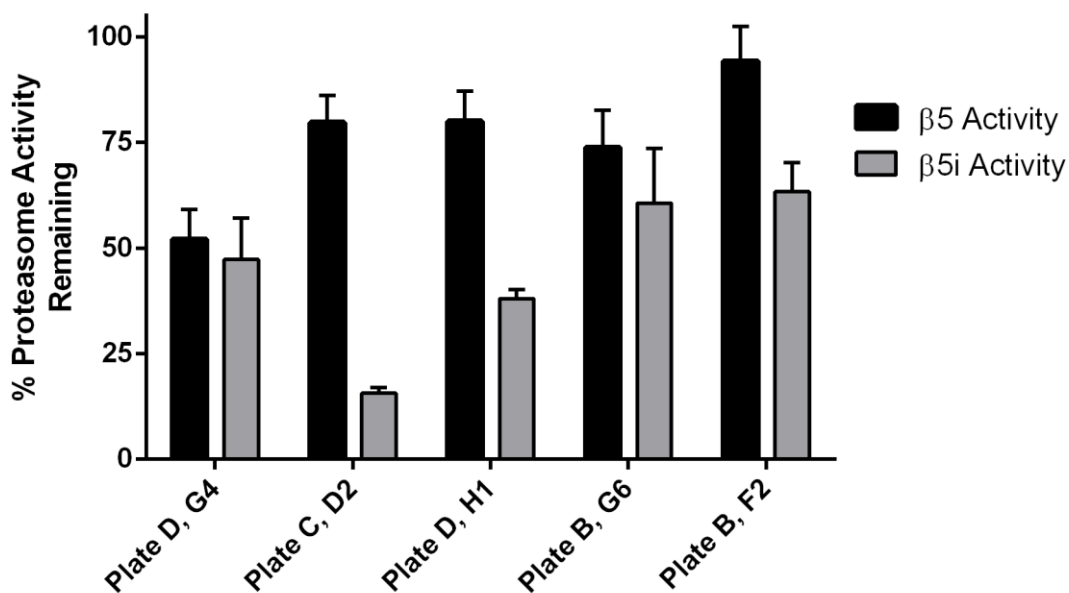
Figure 4.2   Proteasome activity remaining with 5 μM of selected hit compounds

Fluorogenic substrates were used to measure catalytic activity of 20S purified human proteasomes following inhibition. Error bars represent standard deviation (n=3).

Compound G4   CAS 175678-14-5   CAS 1240781-81-0
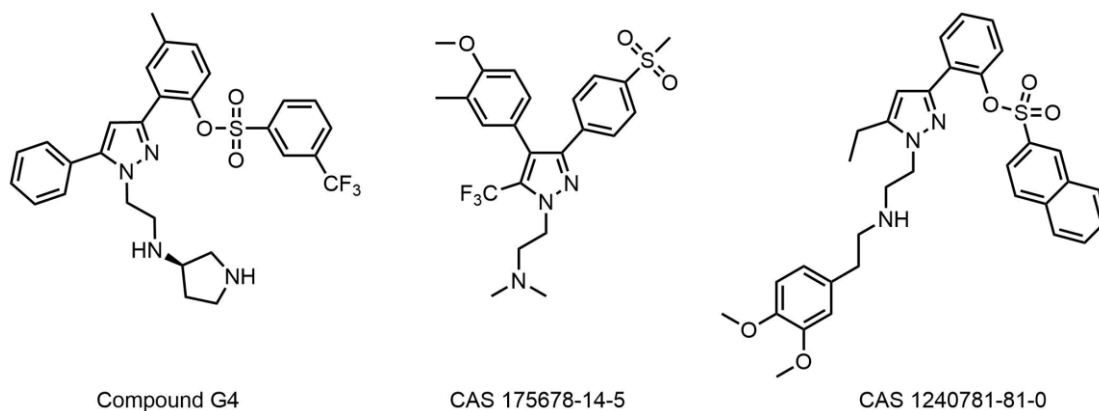
Figure 4.3   Chemical structures G4 and two structurally-similar compounds
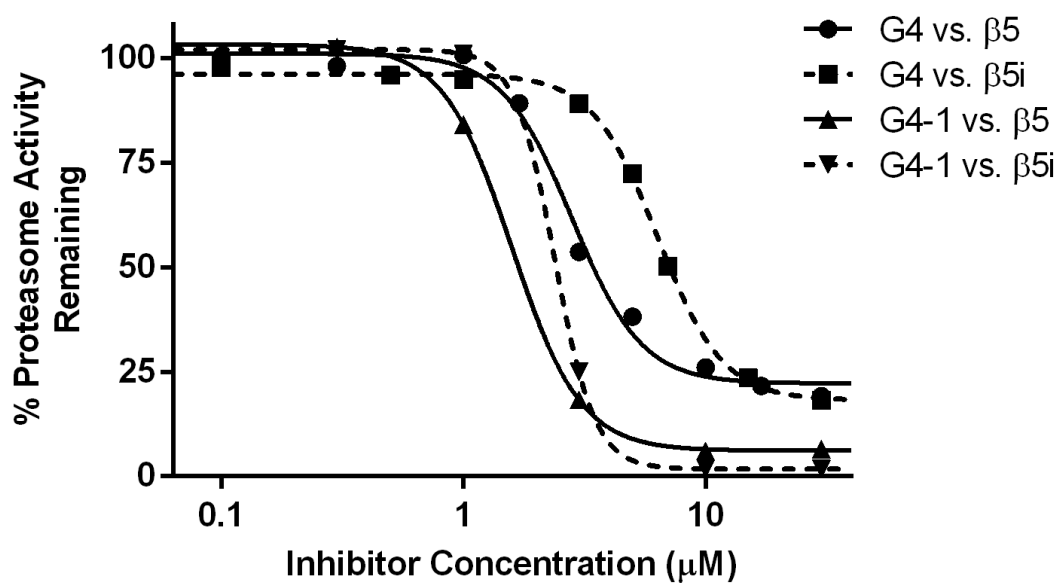
Figure 4.4   Dose-response curves for G4 and G4-1 against β5 and β5i subunits

Error bars represent standard deviation (n=3) when large enough to be visible.
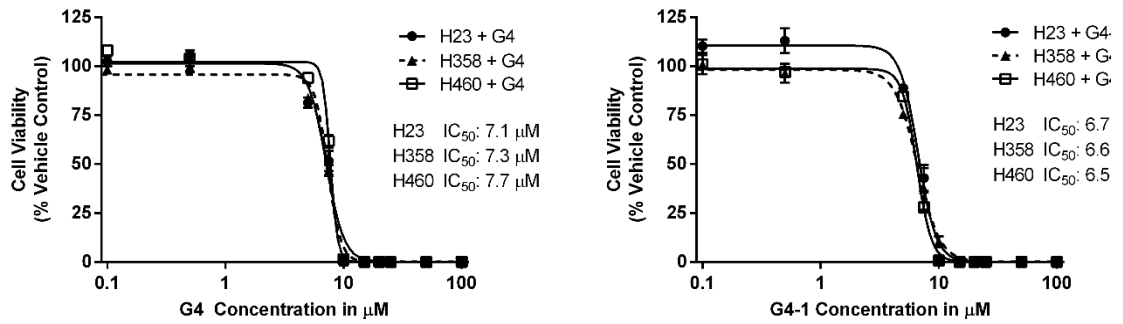
Figure 4.5   72-Hour cytotoxicity of G4 and G4-1 against three NSCLC cell lines

Error bars represent standard deviation (n=4) where large enough to be visble.

4.6   Medicinal Chemistry Efforts to Optimize G4-1

The next step in our research effort was to generate a basic structure-activity relationship (SAR) for G4-1 and related pyrazole-based compounds and, if possible, identify any analogues with greater potency as measured by proteasome activity and cytotoxicity assays. As mentioned in chapter 1, non-peptide and non-covalent inhibitors of the proteasome are at an inherent disadvantage when it comes to inhibitory potency. The greater the potency of our compound against the proteasome, the less the chance of off-target activity which could reduce the usefulness of these compounds as therapeutics. Figure 4.6 shows three locations, dubbed R^1, R^2, and R^3, which were chosen as ideal candidates for the creation of analogues of G4-1. These three locations were chosen based on relative ease of synthesis and their likely contribution towards G4-1's overall affinity for β5 and β5i binding sites.

We first synthesized a series of 17 analogues of G4-1 modified at the R^2 position. In most cases, the synthesis of these R^2-modified analogues began from the carboxylic acid intermediate compound 5 shown in Figure 3.1 and a primary or secondary amine or alcohol was used to generate a resulting amine or ester product using the coupling agent TBTU in the presence of organic base. Compounds 2-7 and 2-16 were generated from G4-1 also using TBTU and organic base in conjunction with the correct carboxylic acid to generate a second amide bond at the pyrrolidine ring nitrogen. The structures of the resulting compounds are given in Figure 4.7. These 16 analogues were then screened for their ability to inhibit proteasome β5 catalytic activity *in vitro* at an initial concentration of 10 μM. As shown in Figure 4.8, while none of the tested analogues surpassed G4-1 in inhibitory potency, there was a wide range of potencies among the compounds allowing us to draw some conclusions about the SAR for this series of compounds. The data for compound 2-14 demonstrates that there is essentially no detectable loss of potency when switching from the (R)-isomer to the (S)-isomer. Looking at compounds 2-13 and 2-15, we see that switching to an ester linkage or N-methylating the secondary amine were well tolerated and resulted in only small losses in activity. Acylating the secondary amine, effectively altering its protonation state at

physiological pH, was moderately tolerated in compounds 2-12 and 2-16. Compounds 2-5 and 2-8 are also notable due to their ability to retain much of G4-1's inhibitory activity while replacing the pyrrolidine moiety with other groups. In both cases a nitrogen atom is still present and is separated from the amide nitrogen atom by a two or three carbon linker. Replacing the pyrrolidine ring with small heteroaromatic rings as in compounds 2-9 and 2-10, or with a small aliphatic group as in compound 2-2 were resulted in a near-complete loss of activity. Notably, treating 20S proteasomes with compounds 2-2, 2-10, and 2-17 all resulted in a consistent increase in proteasome substrate hydrolysis as compared to control rather than inhibition. This effect was most pronounced for compound 2-17 which increased proteasome activity to 216% (± 8.38% SD) of the control at a concentration of 10 μM (Not shown on graph). This activating effect was found to exhibit a dose-response curve with proteasome activity increased to 302% of control at the highest tested concentration of 100 μM. Structurally and chemically compounds 2-2, 2-10, and 2-17 have a number of differences but they are all bear relatively hydrophobic substituents when compared to G4-1 and relatively active analogs such as compound 2-5. Although this activating effect is notable, it may be an artifact of *in vitro* proteasome activity assays which rely on 20S proteasomes whose gates are opened by a low concentration of detergent rather than by regulatory particles or proteasome activators as occurs *in vivo*. Ultimately we were left with the conclusion that G4-1 is the most potent proteasome inhibitor among the 18 tested compounds. While there most likely exists an R^2 analogue with greater potency, we decided to direct our efforts to the R^3 position next rather than to further refine our R^2 SAR.

Due to the fact that the synthesis of R^3-modified analogues was begun prior to our discovery that G4-1 was more potent that G4 both *in vitro* and *in cellulo*, these analogues were designed using G4's amine linkage at the R^2 position rather than G4-1's amide linkage. Accordingly, we will use G4 as the point of comparison when evaluating these analogues. The synthesis of these compounds began with the 1,3-diketone precursor compound 1. This precursor was treated with 2-hydroxyethylhydrazine in ethanol under reflux to form two pyrazole compounds bearing an N-hydroxyethyl substituent at the N1 or N2 position. The desired N1-modified pyrazole was isolated and tosylated to activate the primary alcohol. This was followed by reaction with (R)-(+)-1-Boc-3-aminopyrrolidine and subsequent protection of the newly-formed secondary amine with a second Boc protecting group. This precursor

compound was then reacted with aromatic sulfonyl chlorides and acyl chlorides followed by dual Boc deprotection to give 8 R^3-modiifed analogues of G4. The structures of these compounds are shown in Figure 4.9. These compounds were subsequently tested for their ability to inhibit 20S proteasome β5 activity at a concentration of 10 μM as shown in Figure 4.10. By examining this data, we can again draw some conclusions about the relationship between R^3-group structure and β5 inhibitory activity. As was observed at the R_2 position, all analogues tested were weaker inhibitors of β5 than the parent compound itself, G4. Compound 3-1 which exchanged the sulfonate ester for its carboxylic acid isostere resulted in the smallest reduction in potency. Compound 3-4 and 3-6 which modified the aromatic ring but maintained a substituent in the 3-position retained a moderate amount of activity. Other modifications such as the removal of the aromatic ring entirely (compound 3-3), the use of benzyl ether linker (compound 3-2), or the introduction of additional ring substituents resulted in the largest loss of inhibitory activity. Notably all tested compounds still retained measurable activity at the test concentration of 10 μM. This is in contrast to the R^2 position where some substituents resulted in a near complete loss of activity, or acted as activators of proteasome activity *in vitro*. Although alkyl sulfonates such as methyl methanesulfonate are known to act as reactive electrophiles, the finding that compound 3-1 retained strong activity against β5 suggests that sulfonate reactivity is not involved in the mechanism of action of this class of compounds [213]. Furthermore, aryl arenesulfonates are not well known as reactive electrophiles. Based on our overall findings, we came to the conclusion that original 3-trifluoromethylphenylsulfonate ester group found in G4 and G4-1 afforded the most potent β5 inhibitors and was the best choice among the tested options.

Our final attempt to optimize this class of compounds was conducted at the R^1 position (as shown in Figure 4.6). The synthesis of these R^1-modified analogues was carried out using 2-acetyl-4-methylphenol as a starting material. Analogous to the synthetic route shown in Figure 3.1, an aromatic, cyclic, or heterocyclic acyl chloride containing the desired R_1 substituent was reacted with this starting material to generate a 1,3-diketone intermediate. These compounds were then carried through the synthetic steps as shown in Figure 3.1 to form the pyrazole ring and install the R_2 and R_3 substituents to yield the final product. The structures of these R^1-modified analogues are given in Figure 4.11. Due to the presence of a basic nitrogen, compound 1-7 required additional Boc protection and deprotection of this

nitrogen during synthesis to avoid unwanted side reactions. Compounds 1-8 and 1-9 were synthesized from the Boc-protected precursor to compound 1-7. In order to investigate the effects of these structural changes, we assayed these nine compounds against 20S proteasome β5 activity *in vitro* at a compound concentration of 10 μM. The relative amount of β5 remaining following treatment with compound 1-1 through 1-9 is shown in Figure 4.12. In contrast to our previous efforts at modifying positions R^2 and R^3, R^1-modified analogues of G4-1 were found to have moderately increased potency in this assay. Using t-tests with Holm-Sidak correction for multiple comparisons, we determined that compounds 1-3 ($p<0.0005$), 1-6 ($p<0.005$), 1-7 ($p<0.0001$), 1-8 ($p<0.0001$), and 1-9 ($p<0.0001$) all inhibited β5 activity to a significantly greater degree than an equal concentration of G4-1. Although it is difficult to make SAR conclusions from a limited set of compounds, it appears that this class of compounds tolerates a variety of aromatic and non-aromatic groups at the R^1 position without major effects on potency. Likewise, the inclusion of basic nitrogen atoms in compounds 1-7, 1-8, and 1-9, which would be expected to exist primarily as charged amines under assay conditions, did not harm inhibitor potency.

In order to more accurately determine the inhibitory potency of compounds 1-3 and 1-7, a dose-response curve was obtained by measuring the degree of inhibition of β5 activity at compound concentrations ranging from 0.1 μM to 30 μM. While both compounds were found to be more potent than G4-1, the magnitude of change was relatively small. Compound 1-7 was the more potent of the two analogues, with an IC_{50} that was reduced by 1.5-fold as compared to G4-1 (Data not shown). While any improvement in potency is potentially useful, the addition of a second basic nitrogen atom complicates the synthesis of this compound. As such we chose to use the original phenyl substituent at R^1 in further investigations of this series of pyrazole-based inhibitors. Combined with the knowledge gained by studying analogues modified at the R^2 and R^3 positions, we chose to move forward with G4-1 as our lead compound.

4.7   Discussion

While we were not able to make a direct comparison between the hit rate of our combined *in silico* and *in vitro* screening approach and more conventional high-throughput screening, the identification of 18 active compounds from a pool of just 288 assayed compounds is quite remarkable in comparison to many unbiased or naïve screens. Although compound G4 demonstrated the most favorable inhibition profile for the goals of this project, other active compounds which were identified such as compound D2 from plate C and compound G6 from plate B have been studied for other purposes resulting in one additional publication to date [214]. After verifying that compound G4 inhibited both β5 and β5i activities *in vitro* with a reasonable dose-response curve, we attempted to synthesize the compound in-house. This lead to the discovery of compound G4-1, which likewise inhibits β5 and β5i activities, albeit with slightly greater potency. We also found that both compounds have cytotoxic activity against three non-small cell lung cancer cell lines with G4-1 again being slightly more potent. Although their cytotoxic activity does not directly show that these compounds are cell permeable and able to persist in cells, it does suggest it. We next attempted to explore the SAR of this 1,3,5-trisubstituted pyrazole scaffold against the β5 subunit in search of analogues with increased potency. In totality, the design, synthesis, and testing of 34 pyrazole analogues indicated that G4-1 was already acceptably optimized at the R_1, R_2, and R_3 positions. We were also able to make some initial conclusions about the structure-activity relationship for this series of compounds with respect to the proteasome's β5 subunit. While we did identify some analogues with moderately improved potency, we did not identify any analogue with greatly improved inhibitory activity. While it is likely that additional medicinal chemistry efforts could build off of our initial work to yield more significant potency improvements, we decided to move forward with G4-1 in order to investigate its effects in living cells in more detail.
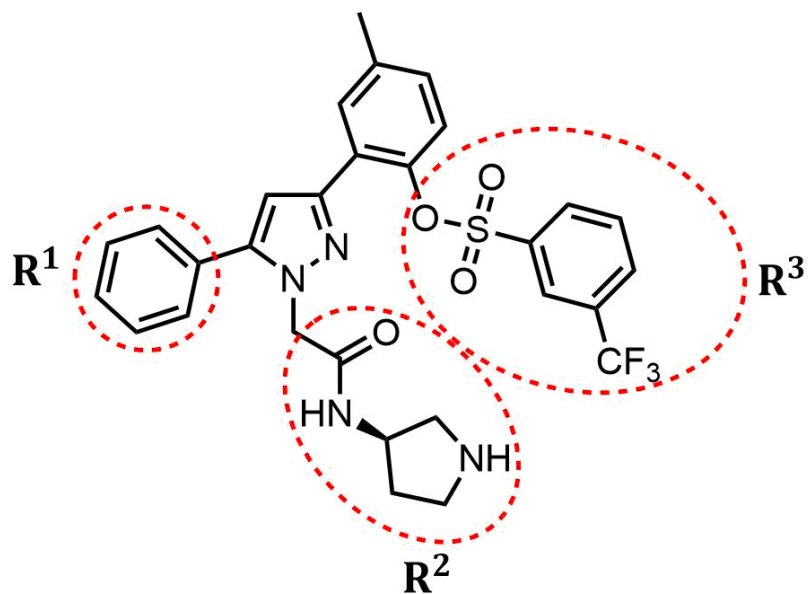
Figure 4.6 Locations targeted for the design and synthesis of G4-1 analogues
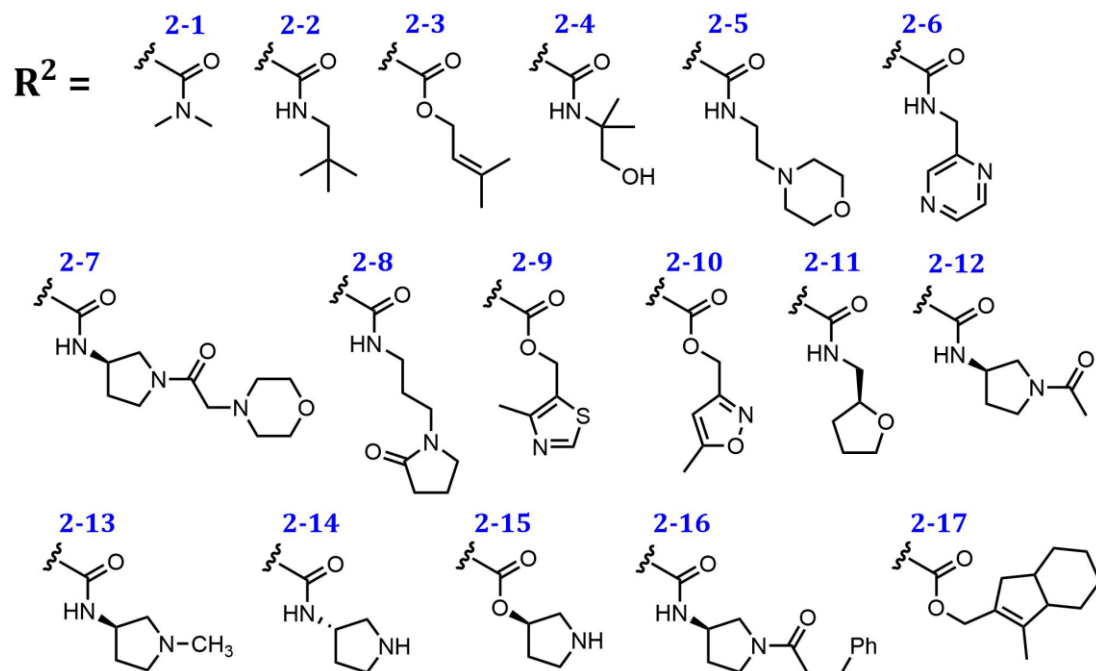
Figure 4.7 Partial structures of R_2-substituted analogues of G4-1

Where R_1 is a phenyl group and R_3 is a 3-trifluoromethylbenzenesulfonate group as in compound G4-1 shown in Figure 3.1.
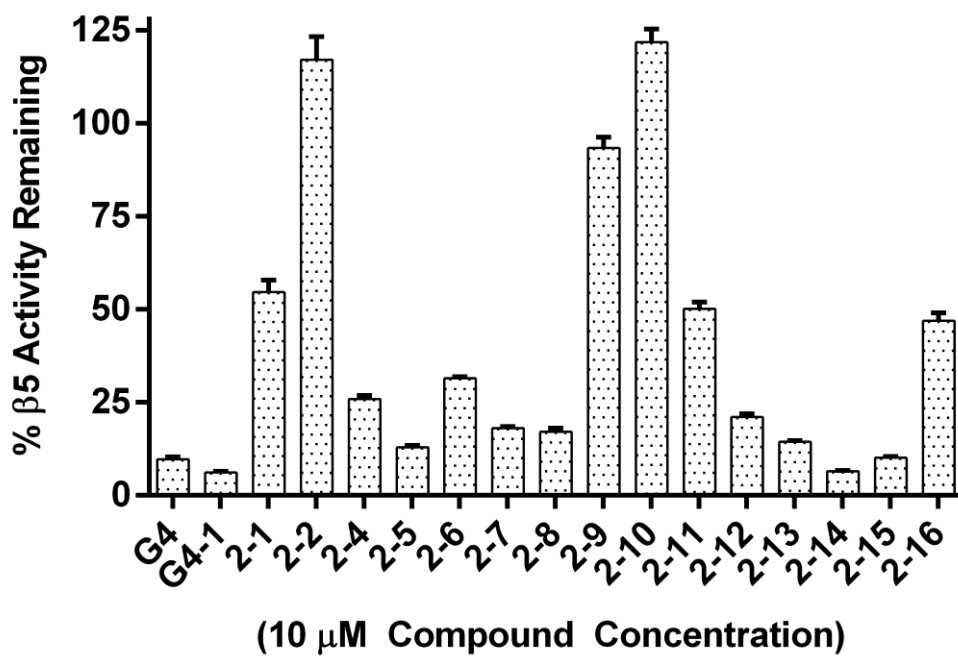
Figure 4.8 Inhibition of 20S β5 by R_2-modified analogues of G4-1 at 10 μM.

Error bars represent standard deviation (n=3-5).
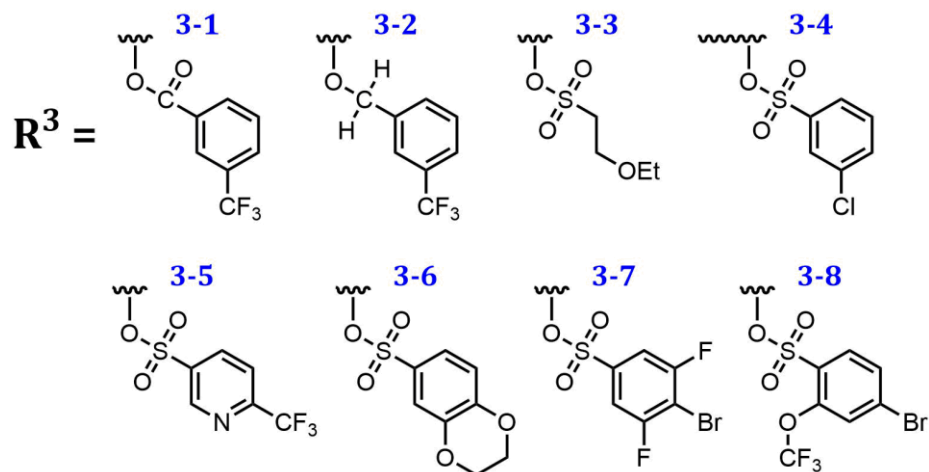
Figure 4.9 Partial structures of R_3-substituted analogues of G4

Where R_1 is a phenyl group and R_2 is an amine-linked pyrrolidine group as in compound G4, shown in Figure 3.2.

93
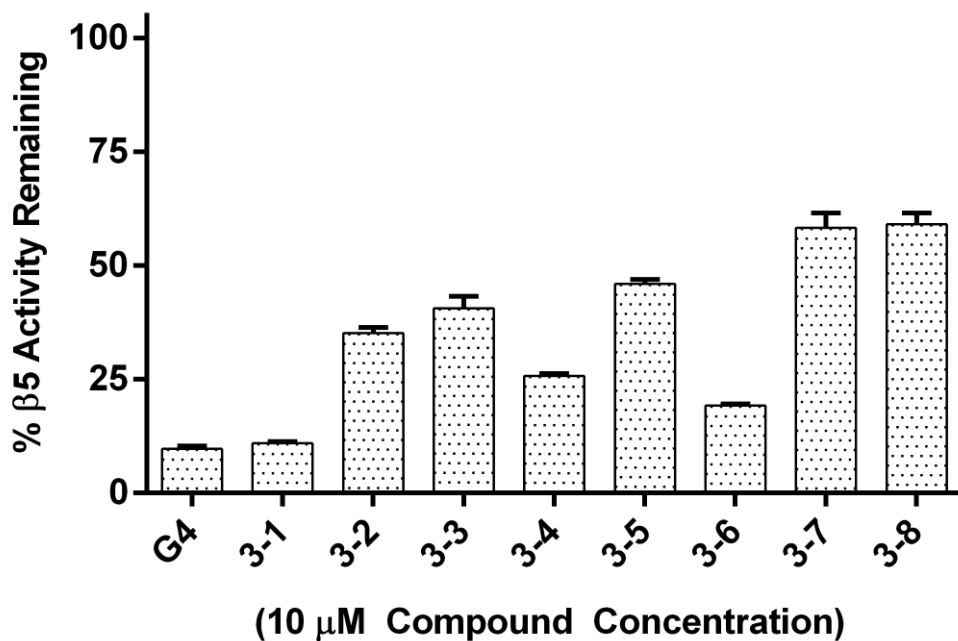
Figure 4.10 Inhibition of 20S β5 by R$_3$-modified analogues of G4 at 10 μM

Error bars represent standard deviation (n=3).
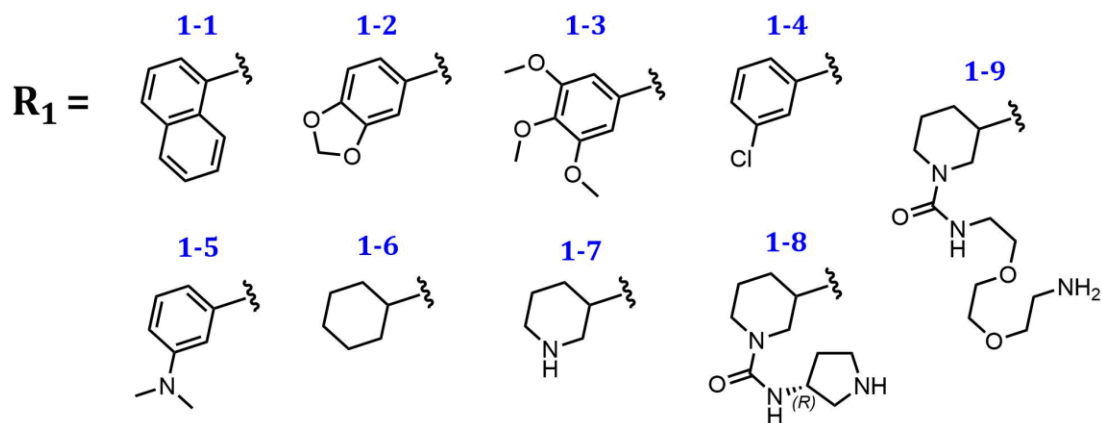
Figure 4.11 Partial structures of R$_1$-substituted analogues of G4

Where R$_2$ is an amide-linked pyrrolidine group and R$_3$ is a 3-trifluoromethyl-benzenesulfonate group as in compound G4-1, shown in Figure 3.2.
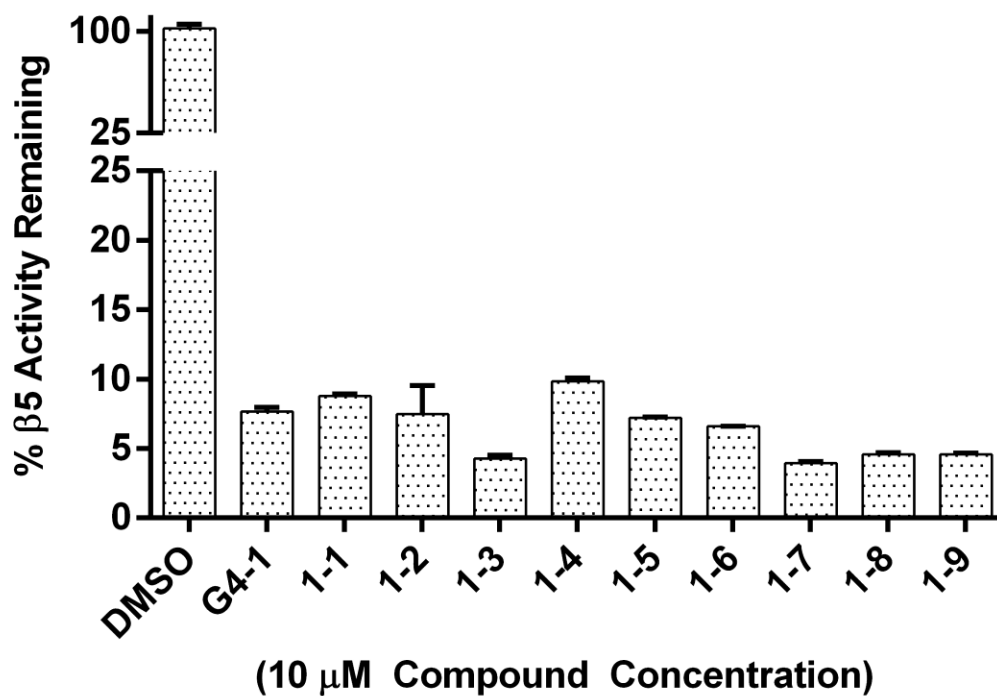
Figure 4.11   Inhibition of 20S β5 by R_1-modified analogues of G4-1 at 10 μM

A control reaction containing no inhibitor but an equivalent amount of DMSO solvent in addition to purified 20S proteasome and fluorogenic peptide substrate is shown for reference. Error bars represent standard deviation (n=3-6).

Chapter 5   CHARACTERIZATION OF THE PYRZOLE-BASED NON-PEPTIDE PROTEASOME INHIBITOR G4-1

Portions of the results described below have been published previously [206].

5.1   Introduction

Our medicinal chemistry efforts to optimize G4 concluded that compound G4-1 was the most suitable candidate for further investigation. In order to evaluate G4-1's potential as an anti-cancer therapeutic, we planned to gather more detailed information about its activities *in vitro* and in cell culture, and ideally to test the compound in live animals should no development road blocks arise. In our previous work we showed that G4-1 was an inhibitor of β5 and β5i sites in *in vitro* assays of purified 20S proteasomes, and that it exhibited cytotoxic activity in a limited set of cancer cell lines. In order to move forward we needed to examine G4-1's activity against other proteasome catalytic subunits, to measure its ability to inhibit the proteasome in complex cell-derived mixtures, and to test the reversibility of its inhibitory effect. Following this we would test G4-1's cytotoxicity against a wider range of cancer cell lines, including those bearing acquired resistance to conventional proteasome inhibitors. Lastly we sought a method to estimate G4-1's metabolic stability before moving to animal models.

5.2   *In vitro* Proteasome Activity Profiling

We had previously established that G4-1 inhibited both the β5 and β5i catalytic subunits *in vitro* with a 1.5-fold greater potency against the constitutive β5 subunit. We next examined G4-1's ability to inhibit other 20S proteasome catalytic subunits. This data is shown in Figure 5.1. Both the constitutive 20S β1 subunit and the homologous immunoproteasome subunit β1i were inhibited relatively potently by G4-1 with IC_{50} values of 2.90 and 2.89 μM, respectively. This selectivity profile is in contrast to the FDA-approved peptide-based

inhibitors bortezomib and carfilzomib. In this case of carfilzomib, it demonstrates high selectivity for β5 and β5i over β1 and β1i, with selectivity ratios of >72-fold [215]. Bortezomib has been reported to have at least 9-fold selectivity for β5 over β1, but potently inhibits the immunoproteasome β1i subunit without any appreciable selectivity [215]. While the roles of different proteasome subunits in the cytotoxic activities of proteasome inhibitors is fully well understood, there is published evidence that an inhibitor which targets β1 and β1i can potentiate the cytotoxic effects of a β5/β5i-targeting inhibitor [216]. We have also observed similar effects in our own research with peptide epoxyketones which specifically inhibit β1i only with >10-fold specificity. The addition of a non-cytotoxic concentration of the β1i inhibitor was shown to significantly increase cell death in combination with bortezomib or carfilzomib in two human myeloma cell lines (unpublished data). It is plausible that G4-1's ability to inhibit β1 and β1i in addition to the two chymotrypsin-like subunits could increase its effectiveness against cancer cells. We also examined G4-1's activity against the immunoproteasome's trypsin-like catalytic subunit β2i. In this case we observed only partial subunit inhibition at a concentration of 100 μM and little to no inhibition at lower concentrations. Due to the high degree of similarity in the binding pockets of β2i and the constitutive subunit β2, we expect that G4-1 is a poor inhibitor of both subunits.

5.3   Confirmation of Activity in Cell Lysates

While purified 20S constitutive and immunoproteasomes are convenient for examining the *in vitro* activity of proteasome inhibitors, proteasomes in living cells tend to be singly- or doubly-capped with regulatory complexes such as the 19S regulatory particle or PA28αβ [217]. An *in vitro* cell lysate assay was used to observe the effects of G4-1 on proteasomes from a heterogeneous cellular source. Cell lysates were obtained from RPMI-8226 cells which are known to express all six catalytic subunits (Western blot, unpublished data) and using a permeabilzation method believed to preserve proteasomes in their intact and capped states. The addition of Mg-ATP during permeabilzation also acts to stabilize proteasomes capped by the ATP-dependent 19S regulatory particle proteasomes [218]. Assays were performed in the presence of 0.035% SDS to activate 20S proteasome particles present in the lysate. Figure 5.2 shows dose-response curves for G4-1 against the CT-L, C-L, and T-L activities of

RPMI-8226 lysate. CT-L activity (β5 and β5i) was inhibited potently with a calculated IC_{50} value of 3.60 μM. As was observed using purified 20S proteasomes, C-L activity (β1 and β1i) was inhibited less potently with an IC_{50} value of 8.13 μM. Even at the highest tested concentration of G4-1, substrate hydrolysis at approximately 15% of control was observed. Whether this is due to G4-1 not fully inhibiting the β1 and β1i subunits, or due to a non-proteasomal enzyme hydrolyzing the Z-LLE-AMC peptide is unknown. Trypsin-like activity was not inhibited by G4-1, with >90% activity remaining at all tested concentrations. Overall these results roughly mirror those observed using purified 20S proteasomes, with acceptable difference which may be explained by factors such as altered enzyme and substrate concentration. This data also confirms that G4-1's inhibitory activity is not limited to assays which rely on purified 20S proteasomes.

5.4   Jump Dilution Assay

We next used a jump dilution assay to measure the ability of G4-1 to dissociate from its proteasome binding sites. In this assay, a concentrated solution of cell lysate is treated with an inhibitory concentration of G4-1 in a microcuvette. As described in the methods section, RPMI-8226 cell lysate was used as a concentrated source of proteasomes. In the case of covalent irreversible inhibitor such as the epoxyketone carfilzomib, reducing the free inhibitor concentration (via dilution or methods such as membrane dialysis) does not result in an increase in proteasome substrate hydrolysis. In contrast, substrate hydrolysis is expected to increase in the case of a reversible inhibitor as the shift in equilibrium favors the dissociation of the inhibitor from its binding sites. The rate at which this increase occurs may differ based on the residence time of the inhibitor [219]. Figure 5.3 shows the results upon diluting a solution of cell lysate pre-treated with 10 μM G4-1 by 25-fold with buffer giving a final inhibitor concentration of 0.25 μM. Suc-LLVY-AMC was present as substrate of β5 and β5i at a concentration of 100 μM. Data collection was begun within 15 seconds after dilution, with AMC fluorescence being measured every 10 seconds for a total of 30 minutes. A non-linear regression was used to calculate the observed rate constant which represents the rate at which enzyme activity returns to steady-state following dilution. The rate constant, k_{obs}, was found to be 0.00356 s^{-1} which translates to a half-life of 195 seconds. The R^2 value for

this regression was greater than 0.999. Ultimately the key finding from this experiment is that dilution of a mixture containing compound G4-1 and proteasomes does result in a restoration of proteasome substrate hydrolysis. Additional data about the rate of G4-1's association and dissociation from proteasome binding sites would be better obtained using more advanced techniques such surface plasmon resonance spectroscopy [220].

5.5   Comparisons of Cytotoxicity Across Multiple Cancer Cell Lines

Having previously established that G4-1 was cytotoxic against three NSCLC cell lines (H23, H358, and H460), we tested G4-1's activity in a variety of other cell lines, including both solid cancer cell lines and multiple myeloma cell lines. As described in chapter 1, both bortezomib and carfilzomib are active in a wide variety of cancer cell lines with relatively few exceptions. The NCI's 60 cell line panel (NCI-60) assays of bortezomib and carfilzomib highlight this. Averaging data from bortezomib's multiple submissions to the NCI-60 screening program, the difference between the lowest GI_{50} for any one cell line and the highest GI_{50} for any cell line was only 20-fold (GI_{50} 2.2 nM vs. 44 nM). This is in contrast to the higher values obtained for targeted therapies such as the kinase inhibitors erlotinib, imatinib, ibrutinib, and gefitinib which had ratios of 1880-fold, 1770-fold, 960-fold, and 250-fold, respectively. In order to examine G4-1's cytotoxic potency in other cell lines, we performed 72-hour viability assays with the MM cell line RPMI-8826, the prostate cancer cell line LNCaP, and the pancreatic cancer cell lines Panc-1, BxPC-3, and AsPC-1. The results of these viability assays, along with previous data from NSCLC cell lines is shown in Figure 5.4. IC_{50} values as calculated using a four-parameter variable slope model are shown inset. Note that in the case of LNCaP, the dose-response curve appeared to demonstrate two slopes, a shallower slope at low doses and a steeper slope at higher doses. Accordingly, the R^2 value for the regression was lower than typical at 0.974. Across the eight cell lines we tested, G4-1's IC_{50} ranged from 6.5 to 16.9 µM. At G4-1 concentrations of 50 µM or higher, ≥95% loss of viability was observed in all cell lines. These results indicate that G4-1 retains its efficacy across this sampling of cancer cell lines.

5.6 Evaluating G4-1 in Proteasome Inhibitor-Resistance Cell Lines

Considering the potential role of resistance mechanisms in the response to proteasome inhibitor therapy as discussed in chapter 1, we next sought to examine whether G4-1 could retain activity in cell line models of proteasome inhibitor resistance. In order to do so we utilized a pair of BxPC-3 pancreatic adenocarcinoma cell lines which had developed resistance to the conventional peptide-based proteasome inhibitors bortezomib and carfilzomib. These two cell lines were established by incubating parental BxPC-3 cells in a continuous sub-lethal concentration of drug, gradually increasing stepwise over a period of approximately 6 months. Thereafter, these cell lines were maintained in a stable level of proteasome inhibitor; 60 nM of bortezomib for the BxPC-3 Btz-R cell line and 200 nM of carfilzomib for the BxPC-3 Cfz-R cell line. In both cases the overall appearance and rate of growth of both cell lines appeared to be similar to that of the parental cell line. These cell lines were cultured in the absence of drug for one week prior to performing a viability assay to allow for a complete washout of bortezomib or carfilzomib. In order to confirm the degree of drug resistance exhibited these cell lines, we performed 72-hour cell viability assays with bortezomib or carfilzomib. Analysis of this data showed that BxPC-3 Btz-R was 5.1-fold (IC_{50} 53.6 vs. 10.6 nM) less sensitive to bortezomib than the parental cell line. The BxPC-3 Cfz-R was 4.5-fold (IC_{50} 97.2 vs. 21.6 nM) less sensitive to carfilzomib than the parental cell line. We also identified that the BxPC-3 Cfz-R cell line exhibited significant cross-resistance to bortezomib with 4.6-fold (IC_{50} 48.0 vs. 10.4 nM) decrease in drug sensitivity relative to BxPC-3 cells. Next a 72-hour viability assay was performed using variable concentrations of G4-1, again following a one-week washout period. As shown in Figure 5.5, the G4-1 IC_{50} for bortezomib-resistant cells was slightly lower than for parental cells and the G4-1 IC_{50} carfilzomib-resistant cells was slightly higher than for parental cells. A two-tailed unpaired t-test was used to compare the $\log(IC_{50})$ of the regression curve of the Cfz-R cells with that of parental BxPC-3. No statistically significant difference was found between them (p=0.288). These results indicate that the resistance mechanisms in play in these cell lines with acquired resistance to conventional proteasome inhibitors do not afford them protection from the cytotoxic effects of G4-1. Unfortunately, our group and collaborators have done a significant amount of work to characterize the resistance mechanisms of these cell lines, their degree of relevance to the clinical use of bortezomib and carfilzomib is still unclear.

5.7   *In vitro* Metabolic Stability of G4-1

Due to the presence of peptidase and epoxide hydrolase enzymes throughout many of the body's tissues, the peptide epoxyketone inhibitor carfilzomib is metabolized extremely rapidly as described in section 1.7.8. It is only via the covalent effect of its reactive warhead that carfilzomib achieves the duration of proteasome inhibition required to effectively cause cytotoxicity. Although short-duration exposure to proteasome inhibitors can be cytotoxic, the required doses are much higher [221]. Due to their reversible mode of inhibition, non-peptide non-covalent proteasome inhibitors must exhibit good metabolic stability to achieve an appropriate duration of effect. In order to estimate the metabolic stability of G4-1, our collaborators exposed pooled human or mouse liver microsomes to a dose of 1 μM G4-1 for 5, 10, or 20 minutes before halting the reaction and analyzing the concentration of G4-1 remaining via LC-MS/MS. The *in vitro* metabolic stability of bortezomib and carfilzomib were also tested under the same conditions. Assays were performed using two replicates per experimental condition. In tests using pooled mouse (BALB/c) liver microsomes, experiments were performed both with and without the addition of an NAPDH regenerating system to examine the contribution of non-NADPH-dependent degradation to the overall loss of parent compound. In tests using pooled human liver microsomes, G4-1 was tested with and without NADPH regenerating system whereas bortezomib and carfilzomib were tested only with NADPH regenerating system. The results of these experiments are shown in Figure 5.6. In the presence of mouse liver microsomes, G4-1 was metabolized more slowly than epoxomicin or bortezomib. In the presence of NADPH, >95% of carfilzomib was metabolized within 5 minutes and >70% of bortezomib was metabolized after 20 minutes. In contrast, over 80% of G4-1 remained unchanged after 20 minutes of incubation. Although the apparent rate of metabolism of each drug was slower when using human liver microsomes, the overall trend was the same. In this case 95% of G4-1 remained unmetabolized at 20 minutes as compared to 74% of bortezomib and just 1% of carfilzomib. While *in vitro* assays using liver microsomes are not a substitute for the measurement of pharmacokinetic parameters in living animals, they are a useful tool for the early identification of drug candidates likely to suffer from rapid clearance [222]. Based on these preliminary results we found no reason to suspect that G4-1 is susceptible to rapid metabolism and we began planning to test the effects of G4-1 *in vivo*.

5.8   Mouse Xenograft Assay

Considering our stated goal to develop novel proteasome inhibitors with improved efficacy against solid cancers, we designed a solid tumor xenograft experiment using BALB/c athymic nude mice. We utilized the LNCaP cell line, originally isolated from a patient with metastatic prostate adenocarcinoma. LNCaP cells were injected into nude mice and allowed to grow to a size of approximately 100 mm^3 before beginning the drug treatment regimen. Tumor-bearing mice, organized into three groups of five subjects each, were treated with G4-1, carfilzomib, or vehicle alone twice per week for a period of four weeks. G4-1 and carfilzomib were both dosed at 5 mg/kg. Examples of carfilzomib mouse xenograft experiments in the scientific literature suggest that a twice-weekly dose of 5 mg/kg is sufficient to achieve a tumor growth reduction effect in many cases [133, 152, 223]. Lacking *in vivo* data on the pharmacodynamics of G4-1, we chose to match the carfilzomib dose by weight. During the treatment period, tumor volume and body weight were monitored prior to each dose. After the four-week treatment period, mice were sacrificed by cervical dislocation and tumors were excised and weighed. Tumor volume data is shown in Figure 5.7. Statistical analysis was performed first using two-way repeated measures ANOVA across the three treatment groups which indicated a highly significant ($p<0.001$) main effect of treatment. Post-hoc testing was performed pairwise on the treatment groups using Student-Newmann-Keuls testing for each treatment day for a total of 27 comparisons. Annotations in Figure 5.7 indicate when tumor volume in G4-1- or carfilzomib-treated animals was significant reduced as compared to the control group. The difference in tumor volume between the G4-1 and carfilzomib treatment groups did not reach statistical significance except for day 27 ($p<0.001$).

Figure 5.8 shows changes in the body weight of xenograft-bearing mice over the four-week treatment period. Following an initial two-way repeated measures ANOVA which demonstrated a significant effect of treatment, Bonferroni post-hoc testing was used to examine whether animal body weight in the carfilzomib-treated or the G4-1-treated group differed significantly from the vehicle-treated group. While G4-1 did not have a significant effect on body weight for any measurement day, the body weight of carfilzomib-treated mice was significantly lower ($p<0.01$) than vehicle-treated mice on the last four measurement days. Body weight can be useful as a basic non-invasive measure of animal health. Despite

the equal or greater reductions in tumor volume effected by G4-1 as compared to carfilzomib, G4-1 did not cause the same reduction in body weight observed in carfilzomib treated animals. In an attempt to remove the influence of tumor weight from body weight measurements, an average tumor density of 0.96 g/mL was calculated based on the average size and mass of the excised tumors. Body weight was then corrected by subtracting the tumor volume times 0.96 g/mL for each measurement. After performing this correction, the final non-tumor body weight of G4-1 treated animals was significantly higher ($p < 0.005$) than that of animals in the vehicle-control group (22.9 ± 0.69 vs. 20.7 ± 0.66 grams, mean $\pm$ SD).

The weight of the excised tumors also provides additional confirmation that G4-1 had a statistically-significant impact on tumor growth as compared to vehicle-treated animals. Figure 5.9 shows the average weight of excised xenograft tumors following sacrifice on day 30. Both G4-1-treated and carfilzomib-treated groups had significantly lower ($p < 0.001$) tumor weights as compared to tumors from the vehicle control group.

In conclusion, a 5 mg/kg twice-weekly dose of G4-1 caused a significant reduction in both tumor volume and final tumor weight in nude mice bearing LNCaP xenografts. G4-1 treatment did not significantly reduce overall body weight as compared to control. A mass-equivalent dose of carfilzomib also significantly reduced tumor volume and tumor weight, however the magnitude of these effects was smaller than observed with G4-1. Carfilzomib treatment also caused a significant reduction in overall body weight as compared to control during the final two weeks of drug treatment. These findings indicate that G4-1 is acts as an anticancer agent in mice without generating any signs of overt toxicity.

5.9   Discussion

The experiments described in this chapter revealed a number of promising features of G4-1 as an early therapeutic candidate including activity against multiple distinct proteasome subunits, cytotoxicity across a range of different cancer cell lines, both of hematologic and nonhematologic origin, a reversible mode of action, and high *in vitro* metabolic stability. Ultimately *in vitro* and *in cellulo* methods are significantly limited in their ability to predict the success of new therapeutic agents as compared to animal models of disease. Having

demonstrated that G4-1 reduces xenograft tumor volumes at the relatively modest dose of 5 mg/kg twice per week, we feel that this series of compounds warrants additional research in order to make progress towards the development of novel anticancer agents. Further investigations of G4-1 (or an improved analogue thereof) are needed to confirm our results and to more thoroughly evaluate the preclinical properties of G4-1 before considering any potential use in the treatment of human disease. Potential avenues of future research will be discussed in chapter 6.
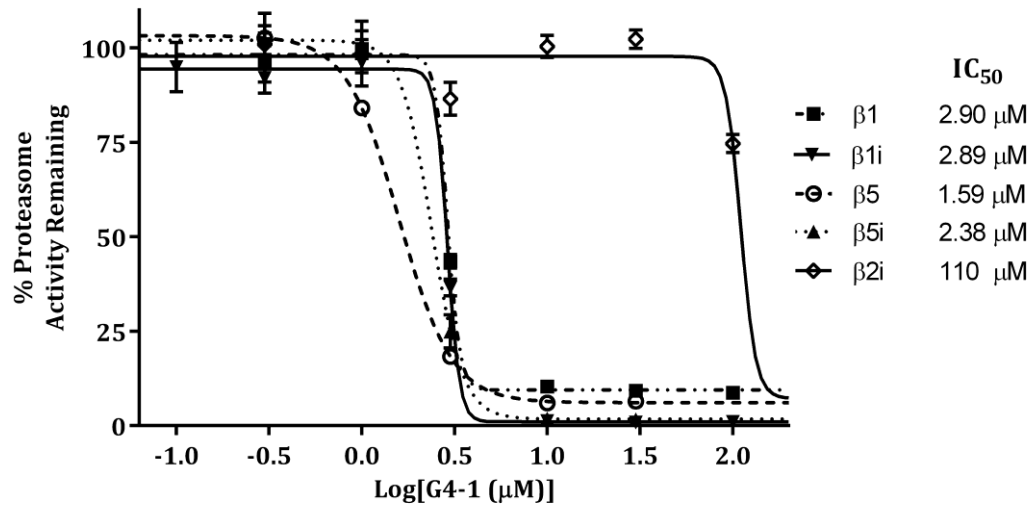
Figure 5.1   Inhibition of specific 20S subunits by G4-1

Inhibition of specific proteasome subunits by G4-1 measured using purified 20S constitutive or immunoproteasome and subunit-specific fluorogenic peptide substrates as required. Error bars represent standard deviation (n=3).
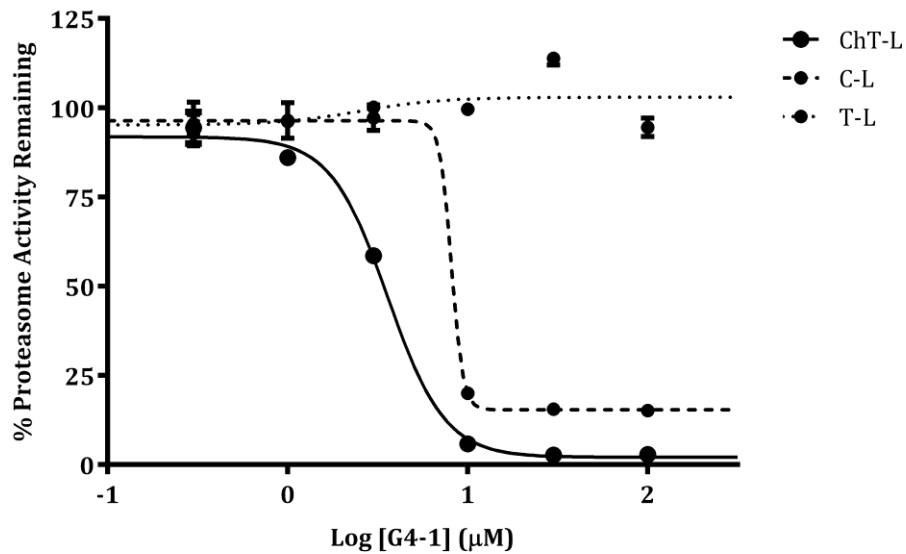
Figure 5.2   Inhibition of cell lysate proteasome activities by G4-1

Chymotrypsin-like, caspase-like, and trypsin-like activities were measured in RPMI-8226 lysate using appropriate fluorogenic substrates. Error bars show SD (n=3).
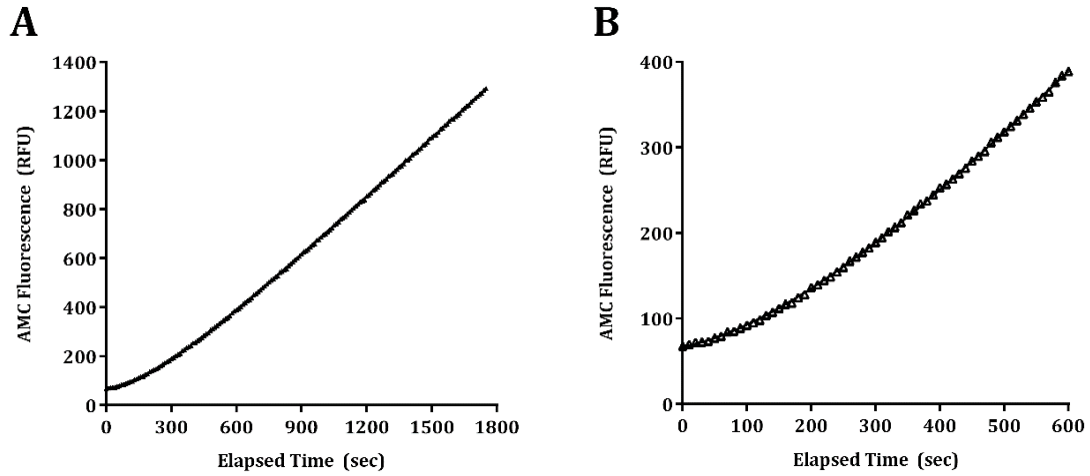
Figure 5.3 Jump dilution assay of G4-1 in RPMI-8226 cell lysate

A.) Full 30-minute data set, 10 second data collection interval. B.) First 10 minutes of data overlaid with a non-linear regression calculated from the full data set shown in A. The data shown represents only a single experiment.
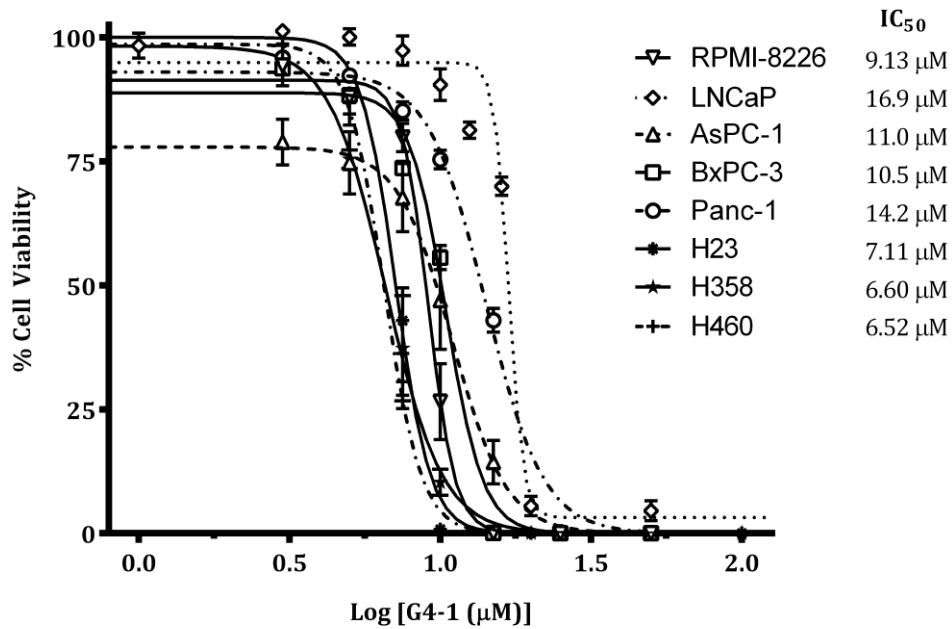
Figure 5.4 Evaluation of G4-1 in multiple 72-hour cell viability assays

Error bars represent standard deviation (n=3-4).

106
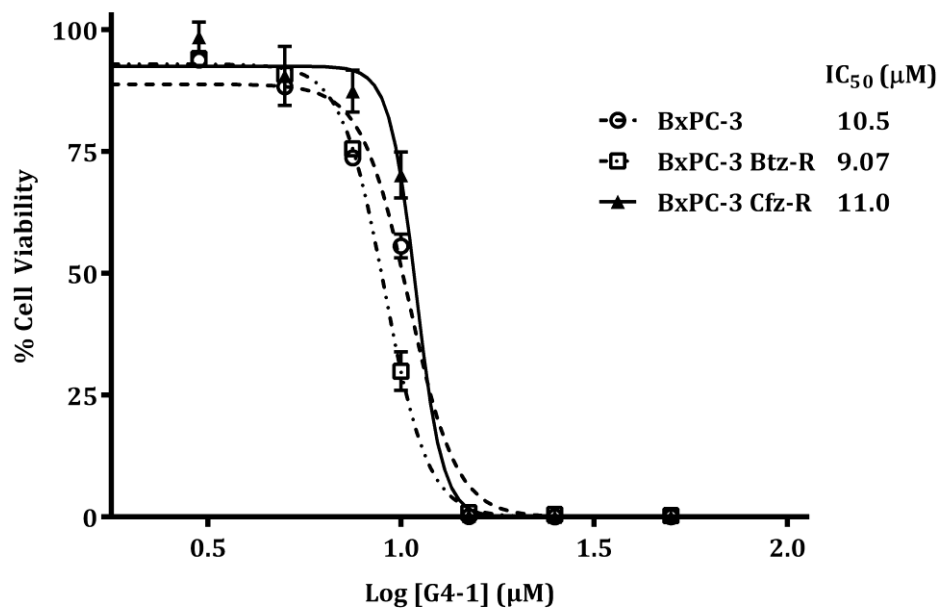
Figure 5.5   Evaluation of G4-1 in cell viability assay PI-resistant BxPC-3 cell lines

Error bars represent standard deviation (n=4).
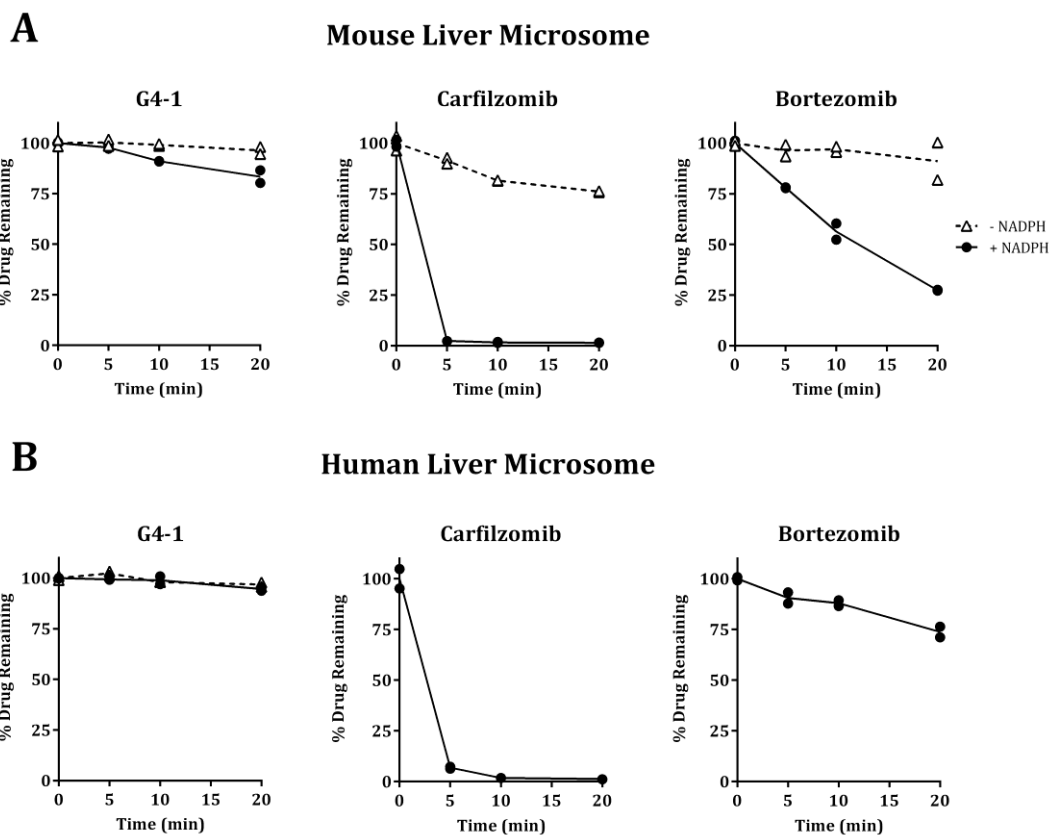
Figure 5.6   *In vitro* metabolic stability assay of G4-1, carfilzomib, and bortezomib

Experiments were performed both with and without the addition of NADPH, with the exception of the tests of carfilzomib and bortezomib using human liver microsomes. Filled circles with a solid line indicates with NADPH, open triangles with a dashed line indicates without NAPDH. Only two replicates were performed, both data points are plotted individually. Connecting lines between their means are shown.
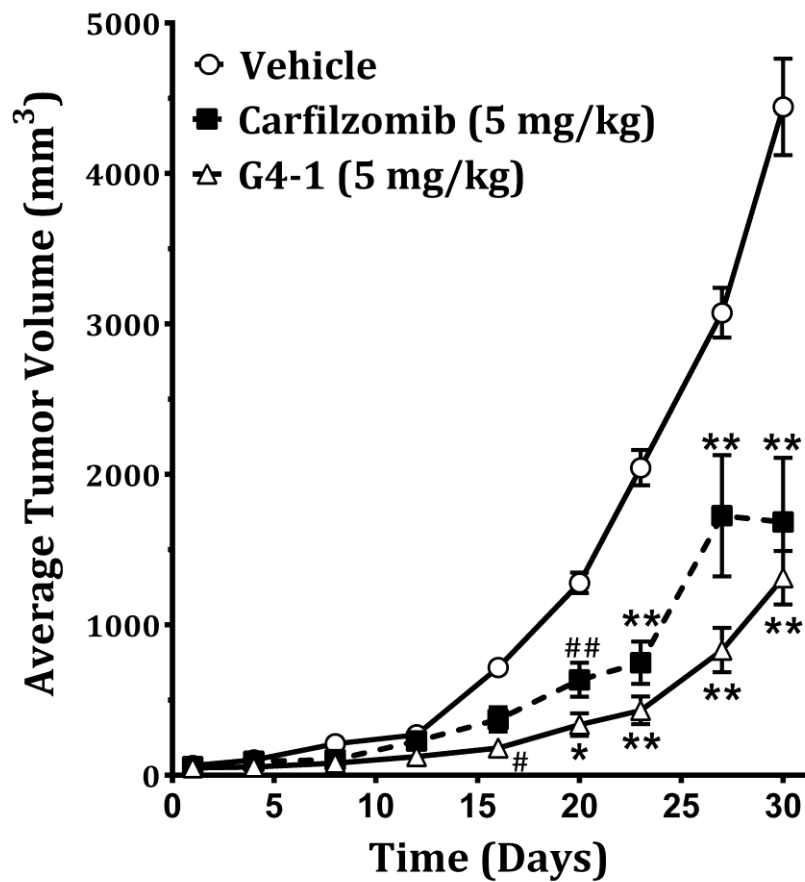
Figure 5.7   Effect of G4-1 versus carfilzomib on mouse xenograft tumor volume

Effect of twice-weekly 5 mg/kg carfilzomib or G4-1 on the growth of LNCap xenograft tumors in nude mice. Following initial two-way ANOVA analysis, two-way repeated measures Student-Newmann-Keuls (SNK) post-hoc tests were used to assess differences in tumor volume between treatment groups. Annotations indicate statistically-significant differences from the vehicle-treated group: #: $p<0.05$, ##: $p<0.01$, *: $p<0.005$, **: $p<0.001$. Data is shown as mean ± standard error.
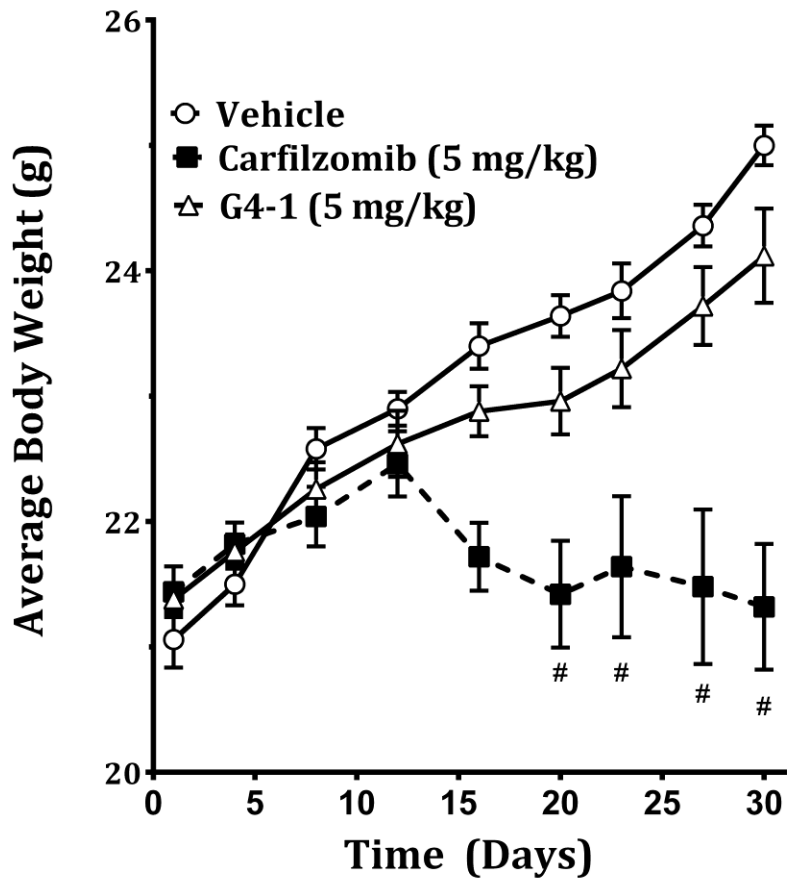
Figure 5.8   Effect of G4-1 versus carfilzomib on mouse body weight

Effect of twice-weekly 5 mg/kg carfilzomib or G4-1 on overall body weight of mice bearing LNCaP xenograft tumors. Following two-way ANOVA, Bonferroni post-hoc testing was used to examine differences in body weights between treatment groups on each day. Annotations indicate statistically-significant differences from the vehicle-treated group: #: $p<0.01$. Data is shown as mean ± standard error.
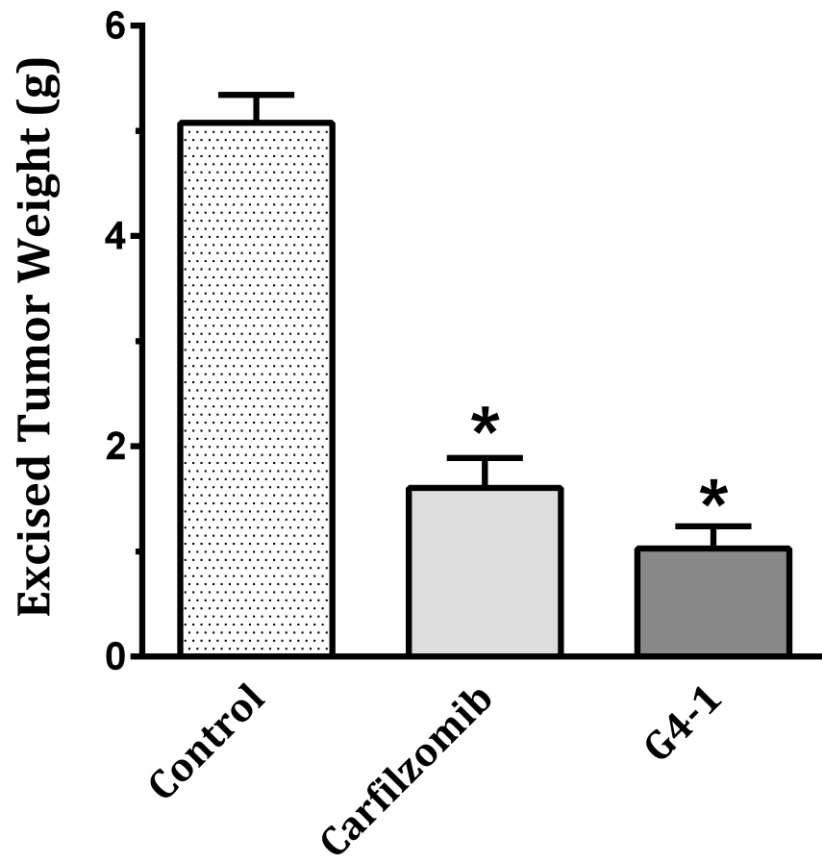
Figure 5.9   Effect of G4-1 versus carfilzomib on final tumor weight

Effect of twice-weekly 5 mg/kg carfilzomib or G4-1 on excised tumor weight after four weeks of treatment. Data was analyzed using one-way ANOVA followed by SNK post-hoc testing. Annotations indicate statistically-significant differences from the vehicle-treated group: *: $p < 0.001$. Data is shown as mean ± standard error.

Chapter 6   SUMMARY AND FUTURE DIRECTIONS

While it is our goal and our hope that the work described here could lead to an approved human therapeutic based on the recently-identified G4/G4-1 pyrazole scaffold, drug development is a costly and laborious process, with only a tiny fraction of drug candidates reaching the market [224-226]. In order to evaluate the prospects of G4-1 or a related compound, a number of additional studies should be performed to better characterize G4-1 as an anticancer agent. One first step could be additional medicinal chemistry efforts which aim to identify related compounds with greater inhibitory potency. With sufficient resources, a number of tools are available to aid in the optimization of drug potency. For example, X-ray crystallography has been successfully used to identify the binding mode of bortezomib, carfilzomib, and other proteasome inhibitors as well as their specific molecular interactions with catalytic subunits [227]. Identifying G4-1's precise orientation, location, and interactions when bound to proteasome catalytic subunits could significantly aid in the rational design G4-1 analogues with improved binding affinity and hence improved potency. NMR (nuclear magnetic resonance) spectroscopy is likewise useful in the determination of ligand binding sites and poses, but protein size is a major limitation in these types of techniques [228]. As such, applying NMR spectroscopy to proteasome-ligand interactions requires specialized techniques as well as costly high field NMR instruments [229, 230]. G4 analogues with increased potency against the proteasome are likely to require lower drug exposure *in vivo* which often results in less undesirable off-target activity. Ultimately, due to the proteasome's inherent affinity for peptides, achieving high-potency non-peptide-based inhibitors is likely to require a significant research effort.

Returning to G4-1 itself, this compound in many ways still remains uncharacterized, for example we lack an understanding of its pharmacokinetics in animal models. Acquiring pharmacokinetic data in mice, dogs, primates, or other species is an important step towards identifying a new compound's suitability for use in humans. We have also not yet investigated the oral bioavailability of G4-1 or any of its analogues. Even in the unique area of oncology, orally-administered drugs have significant advantages over parenterally-administered drugs

in terms of ease of administration and convenience for patients. It would also be prudent to examine the pharmacodynamics of G4-1 in live animals. Understanding the duration and degree of proteasome inhibition generated by agents such as bortezomib, carfilzomib, and ixazomib has aided in optimizing the dosing schedules of these drugs for maximum efficacy. Although measurements of proteasome activity in red blood cells, PBMCs, or even tumor cells from patients or animals are now frequently performed, these assays are often incompatible with reversible inhibitors (excepting the case of slowly-reversible compounds such as bortezomib) due to their ability to dissociate from their binding site after collecting and lysing cells [231, 232]. Move advanced techniques which do not rely on long-term occupancy of the catalytic subunit binding site are required to investigate the *in vivo* pharmacodynamics of reversible proteasome inhibitors. One such technique suitable for use in mice is to create a xenograft composed of human cancer cells which express a fluorescent or luminescent protein which acts as a biosensor for proteasome activity [233, 234]. Proteasome activity in these xenografted cells can then be measured using non-destructive bioimaging techniques. It should also be noted that G4-1 has only been tested in a single animal model to date. A better understanding of G4-1's profile of anticancer activity could be obtained using additional mouse xenograft models generated with human cancer cell lines originating from other (non-prostate) cancers. It would also be useful to examine G4-1's activity in other types of animal models which more closely recapitulate the biology of human solid tumors. These include patient-derived xenograft (PDX) models as well as genetically-engineered mouse models (GEMMs) of cancer in immunocompetent mice [235].

Preclinical screening of off-target activities could also be performed to gauge G4-1's selectivity for the proteasome over other targets, and to identify potential liabilities. Such screens could include a variety of non-proteasomal proteases as well as a panel of common drug targets which may include various GCPRs, ion channels, enzymes, and nuclear receptors [236]. Gene expression profiling in cells treated with G4-1 could also be used to compare its effects on cellular mRNA levels to those of validated proteasome inhibitors such as bortezomib making it possible to characterize their similarities and differences [237, 238]. Additionally a large database of gene expression signatures of various other drugs are available for comparison [239, 240]. Other preclinical data of interest could include the identification G4-1's metabolites in various species, the enzymes involved in G4-1

metabolism, whether G4-1 or its metabolites significantly inhibit any CYP P450 enzymes, and *in vitro* measurements of drug permeability and susceptibility to transporter-mediated efflux [241-243]. Preclinical data can also identify unwanted sources of toxicity, such as via assays for genotoxic activity. Moving back into animal models, acute and chronic toxicology studies are a prerequisite which must be filled before any attempt to examine a new compound's effects on humans. To date we know very little by G4-1's toxiological profile.

Ultimately I feel that the discovery and development of G4-1 reported in this dissertation is a significant advancement towards the potential application of non-peptide non-covalent proteasome inhibitors in human patients. While non-peptide non-covalent inhibitors suffer from some disadvantages, such as lower potency, we believe that they could offer major advantages over existing peptide-based covalent proteasome inhibitors. These potential advantages include improved pharmacokinetics, broader subunit inhibition profiles, reduced susceptibility to drug resistance mechanisms, and greater drug tissue penetration. It is our hypothesis that these properties, while potentially beneficial in the treatment of multiple myeloma, may prove to be critical factors in identifying proteasome inhibitors which are efficacious in patients with solid tumors. Considering the massive success of existing proteasome inhibitors in improving the treatment of multiple myeloma, we believe that any effort to expand the use of PIs to solid cancers is worth pursuing. This holds true especially for those solid cancers which are relatively lacking in safe and effective treatment options such as pancreatic cancer, ovarian cancer, and glioblastoma. While there is a tremendous amount of work still required to progress G4-1 towards any potential use in humans, we have successfully identified a non-peptide non-covalent compound which inhibits multiple proteasome catalytic subunits at low micromolar concentrations. G4-1 furthermore induces cell death in a variety of human cancer cell lines at concentration of 5-15 μM. In mice bearing human prostate cancer xenografts, G4-1 was found to significantly reduce tumor growth without producing overt signs of toxicity. Regardless of the future prospects of G4-1 or its analogues as therapeutic agents, it is our belief that the documentation and publication of our methodology can contribute to the future discovery and development of novel proteasome inhibitors. There is still much to be learned about the proteasome and the potential for proteasome inhibitors to treat human disease. Our ultimate goal is to improve the lives of those affected by cancer. Over the past decade and a half, bortezomib, carfilzomib, and

ixazomib have collectively made a tremendous positive impact on the lives of multiple myeloma patients. We can only hope that continuing research into the development of novel proteasome inhibitors will lead to an even greater impact for patients suffering from cancer of all types.

REFERENCES

1. Schoenheimer, R. and H.T. Clarke, *The dynamic state of body constituents*. Harvard University monographs in medicine and public health. 1942, Cambridge, Mass.,: Harvard university press. 3 p., 3 l., 3 -78 p., 2 l.

2. Ciechanover, A., *Intracellular protein degradation: from a vague idea thru the lysosome and the ubiquitin-proteasome system and onto human diseases and drug targeting.* Cell Death Differ, 2005. **12**(9): p. 1178-90.

3. De Duve, C., et al., *Tissue fractionation studies. 6. Intracellular distribution patterns of enzymes in rat-liver tissue.* Biochem J, 1955. **60**(4): p. 604-17.

4. Etlinger, J.D. and A.L. Goldberg, *A soluble ATP-dependent proteolytic system responsible for the degradation of abnormal proteins in reticulocytes.* Proc Natl Acad Sci U S A, 1977. **74**(1): p. 54-8.

5. Ciechanover, A., et al., *ATP-dependent conjugation of reticulocyte proteins with the polypeptide required for protein degradation.* Proc Natl Acad Sci U S A, 1980. **77**(3): p. 1365-8.

6. Hershko, A., et al., *Proposed role of ATP in protein breakdown: conjugation of protein with multiple chains of the polypeptide of ATP-dependent proteolysis.* Proc Natl Acad Sci U S A, 1980. **77**(4): p. 1783-6.

7. Wilkinson, K.D., M.K. Urban, and A.L. Haas, *Ubiquitin is the ATP-dependent proteolysis factor I of rabbit reticulocytes.* J Biol Chem, 1980. **255**(16): p. 7529-32.

8. Hershko, A., et al., *Components of ubiquitin-protein ligase system. Resolution, affinity purification, and role in protein breakdown.* J Biol Chem, 1983. **258**(13): p. 8206-14.

9. Ciechanover, A., D. Finley, and A. Varshavsky, *Ubiquitin dependence of selective protein degradation demonstrated in the mammalian cell cycle mutant ts85.* Cell, 1984. **37**(1): p. 57-66.

10. Wilk, S., S. Pearce, and M. Orlowski, *Identification and partial purification of a cation-sensitive neutral endopeptidase from bovine pituitaries.* Life Sci, 1979. **24**(5): p. 457-64.

11. Wilk, S. and M. Orlowski, *Cation-sensitive neutral endopeptidase: isolation and specificity of the bovine pituitary enzyme.* J Neurochem, 1980. **35**(5): p. 1172-82.

12. Hough, R., G. Pratt, and M. Rechsteiner, *Ubiquitin-lysozyme conjugates. Identification and characterization of an ATP-dependent protease from rabbit reticulocyte lysates.* J Biol Chem, 1986. **261**(5): p. 2400-8.

13. Arrigo, A.P., et al., *Identity of the 19S 'prosome' particle with the large multifunctional protease complex of mammalian cells (the proteasome).* Nature, 1988. **331**(6152): p. 192-4.

14. Eytan, E., et al., *ATP-dependent incorporation of 20S protease into the 26S complex that degrades proteins conjugated to ubiquitin.* Proc Natl Acad Sci U S A, 1989. **86**(20): p. 7751-5.

15. Tanahashi, N., et al., *Molecular structure of 20S and 26S proteasomes.* Enzyme Protein, 1993. **47**(4-6): p. 241-51.

16. Orlowski, M., *The multicatalytic proteinase complex, a major extralysosomal proteolytic system.* Biochemistry, 1990. **29**(45): p. 10289-97.

17. Jackson, S.P. and D. Durocher, *Regulation of DNA damage responses by ubiquitin and SUMO.* Mol Cell, 2013. **49**(5): p. 795-807.

18.   Schwarz, L.A. and G.N. Patrick, *Ubiquitin-dependent endocytosis, trafficking and turnover of neuronal membrane proteins.* Mol Cell Neurosci, 2012. **49**(3): p. 387-93.

19.   Wang, Y., et al., *PolyUbiquitin chain linkage topology selects the functions from the underlying binding landscape.* PLoS Comput Biol, 2014. **10**(7): p. e1003691.

20.   Sadowski, M., et al., *Protein monoubiquitination and polyubiquitination generate structural diversity to control distinct biological processes.* IUBMB Life, 2012. **64**(2): p. 136-42.

21.   Husnjak, K. and I. Dikic, *Ubiquitin-binding proteins: decoders of ubiquitin-mediated cellular functions.* Annu Rev Biochem, 2012. **81**: p. 291-322.

22.   Li, W., et al., *Genome-wide and functional annotation of human E3 ubiquitin ligases identifies MULAN, a mitochondrial E3 that regulates the organelle's dynamics and signaling.* PLoS One, 2008. **3**(1): p. e1487.

23.   Jackson, P.K., et al., *The lore of the RINGs: substrate recognition and catalysis by ubiquitin ligases.* Trends Cell Biol, 2000. **10**(10): p. 429-39.

24.   Deshaies, R.J. and C.A. Joazeiro, *RING domain E3 ubiquitin ligases.* Annu Rev Biochem, 2009. **78**: p. 399-434.

25.   Li, W., et al., *A ubiquitin ligase transfers preformed polyubiquitin chains from a conjugating enzyme to a substrate.* Nature, 2007. **446**(7133): p. 333-7.

26.   Hurley, J.H., S. Lee, and G. Prag, *Ubiquitin-binding domains.* Biochem J, 2006. **399**(3): p. 361-72.

27.   Unno, M., et al., *The structure of the mammalian 20S proteasome at 2.75 A resolution.* Structure, 2002. **10**(5): p. 609-18.

28.   Tanaka, K., *The proteasome: overview of structure and functions.* Proc Jpn Acad Ser B Phys Biol Sci, 2009. **85**(1): p. 12-36.

29.   Dick, T.P., et al., *Contribution of proteasomal beta-subunits to the cleavage of peptide substrates analyzed with yeast mutants.* J Biol Chem, 1998. **273**(40): p. 25637-46.

30.   Rabl, J., et al., *Mechanism of gate opening in the 20S proteasome by the proteasomal ATPases.* Mol Cell, 2008. **30**(3): p. 360-8.

31.   Arendt, C.S. and M. Hochstrasser, *Eukaryotic 20S proteasome catalytic subunit propeptides prevent active site inactivation by N-terminal acetylation and promote particle assembly.* Embo J, 1999. **18**(13): p. 3575-85.

32.   Huber, E.M., et al., *Systematic Analyses of Substrate Preferences of 20S Proteasomes Using Peptidic Epoxyketone Inhibitors.* J Am Chem Soc, 2015. **137**(24): p. 7835-42.

33.   Groll, M., et al., *Structure of 20S proteasome from yeast at 2.4 A resolution.* Nature, 1997. **386**(6624): p. 463-71.

34.   Huber, E.M., et al., *Immuno- and constitutive proteasome crystal structures reveal differences in substrate and inhibitor specificity.* Cell, 2012. **148**(4): p. 727-38.

35.   Schechter, I. and A. Berger, *On the size of the active site in proteases. I. Papain.* Biochem Biophys Res Commun, 1967. **27**(2): p. 157-62.

36.   Borissenko, L. and M. Groll, *20S proteasome and its inhibitors: crystallographic knowledge for drug development.* Chem Rev, 2007. **107**(3): p. 687-717.

37.   Wei, D., et al., *Fundamental reaction pathway for peptide metabolism by proteasome: insights from first-principles quantum mechanical/molecular mechanical free energy calculations.* J Phys Chem B, 2013. **117**(43): p. 13418-34.

38. Kisselev, A.F., et al., *The sizes of peptides generated from protein by mammalian 26 and 20 S proteasomes. Implications for understanding the degradative mechanism and antigen presentation.* J Biol Chem, 1999. **274**(6): p. 3363-71.

39. Bedford, L., et al., *Assembly, structure, and function of the 26S proteasome.* Trends Cell Biol, 2010. **20**(7): p. 391-401.

40. Jung, T. and T. Grune, *The proteasome and its role in the degradation of oxidized proteins.* IUBMB Life, 2008. **60**(11): p. 743-52.

41. Gillette, T.G., et al., *Differential roles of the COOH termini of AAA subunits of PA700 (19 S regulator) in asymmetric assembly and activation of the 26 S proteasome.* J Biol Chem, 2008. **283**(46): p. 31813-22.

42. Tanahashi, N., et al., *Hybrid proteasomes. Induction by interferon-gamma and contribution to ATP-dependent proteolysis.* J Biol Chem, 2000. **275**(19): p. 14336-45.

43. Hiyama, H., et al., *Interaction of hHR23 with S5a. The ubiquitin-like domain of hHR23 mediates interaction with S5a subunit of 26 S proteasome.* J Biol Chem, 1999. **274**(39): p. 28019-25.

44. Husnjak, K., et al., *Proteasome subunit Rpn13 is a novel ubiquitin receptor.* Nature, 2008. **453**(7194): p. 481-8.

45. Elsasser, S., et al., *Proteasome subunit Rpn1 binds ubiquitin-like protein domains.* Nat Cell Biol, 2002. **4**(9): p. 725-30.

46. Worden, E.J., C. Padovani, and A. Martin, *Structure of the Rpn11-Rpn8 dimer reveals mechanisms of substrate deubiquitination during proteasomal degradation.* Nat Struct Mol Biol, 2014. **21**(3): p. 220-7.

47. Sutoh, Y., et al., *Comparative genomic analysis of the proteasome beta5t subunit gene: implications for the origin and evolution of thymoproteasomes.* Immunogenetics, 2012. **64**(1): p. 49-58.

48. Ferrington, D.A. and D.S. Gregerson, *Immunoproteasomes: structure, function, and antigen presentation.* Prog Mol Biol Transl Sci, 2012. **109**: p. 75-112.

49. Aki, M., et al., *Interferon-gamma induces different subunit organizations and functional diversity of proteasomes.* J Biochem (Tokyo), 1994. **115**(2): p. 257-69.

50. Toes, R.E., et al., *Discrete cleavage motifs of constitutive and immunoproteasomes revealed by quantitative analysis of cleavage products.* J Exp Med, 2001. **194**(1): p. 1-12.

51. Basler, M., et al., *Why the structure but not the activity of the immunoproteasome subunit low molecular mass polypeptide 2 rescues antigen presentation.* J Immunol, 2012. **189**(4): p. 1868-77.

52. Cascio, P., et al., *26S proteasomes and immunoproteasomes produce mainly N-extended versions of an antigenic peptide.* Embo J, 2001. **20**(10): p. 2357-66.

53. Chang, S.C., et al., *The ER aminopeptidase, ERAP1, trims precursors to lengths of MHC class I peptides by a "molecular ruler" mechanism.* Proc Natl Acad Sci U S A, 2005. **102**(47): p. 17107-12.

54. McCarthy, M.K. and J.B. Weinberg, *The immunoproteasome and viral infection: a complex regulator of inflammation.* Front Microbiol, 2015. **6**: p. 21.

55. Engelhard, V.H., *Structure of peptides associated with MHC class I molecules.* Curr Opin Immunol, 1994. **6**(1): p. 13-23.

56. Basler, M., C.J. Kirk, and M. Groettrup, *The immunoproteasome in antigen processing and other immunological functions.* Curr Opin Immunol, 2013. **25**(1): p. 74-80.

57.	Pang, K.C., et al., *Immunoproteasome subunit deficiencies impact differentially on two immunodominant influenza virus-specific CD8+ T cell responses.* J Immunol, 2006. **177**(11): p. 7680-8.

58.	Hensley, S.E., et al., *Unexpected role for the immunoproteasome subunit LMP2 in antiviral humoral and innate immune responses.* J Immunol, 2010. **184**(8): p. 4115-22.

59.	Moebius, J., et al., *Immunoproteasomes are essential for survival and expansion of T cells in virus-infected mice.* Eur J Immunol, 2010. **40**(12): p. 3439-49.

60.	Mishto, M., et al., *Immunoproteasome and LMP2 polymorphism in aged and Alzheimer's disease brains.* Neurobiol Aging, 2006. **27**(1): p. 54-66.

61.	Ethen, C.M., et al., *Transformation of the proteasome with age-related macular degeneration.* FEBS letters, 2007. **581**(5): p. 885-90.

62.	Diaz-Hernandez, M., et al., *Neuronal induction of the immunoproteasome in Huntington's disease.* J Neurosci, 2003. **23**(37): p. 11653-61.

63.	Basler, M., et al., *The immunoproteasome: a novel drug target for autoimmune diseases.* Clin Exp Rheumatol, 2015. **33**(4 Suppl 92): p. S74-9.

64.	Xing, Y., S.C. Jameson, and K.A. Hogquist, *Thymoproteasome subunit-beta5T generates peptide-MHC complexes specialized for positive selection.* Proc Natl Acad Sci U S A, 2013. **110**(17): p. 6979-84.

65.	Nitta, T., et al., *Thymoproteasome shapes immunocompetent repertoire of CD8+ T cells.* Immunity, 2010. **32**(1): p. 29-40.

66.	Komander, D., M.J. Clague, and S. Urbe, *Breaking the chains: structure and function of the deubiquitinases.* Nat Rev Mol Cell Biol, 2009. **10**(8): p. 550-63.

67.	He, M., et al., *The emerging role of deubiquitinating enzymes in genomic integrity, diseases, and therapeutics.* Cell Biosci, 2016. **6**: p. 62.

68.	Alonso, V. and P.A. Friedman, *Minireview: ubiquitination-regulated G protein-coupled receptor signaling and trafficking.* Mol Endocrinol, 2013. **27**(4): p. 558-72.

69.	Sun, X.X. and M.S. Dai, *Deubiquitinating enzyme regulation of the p53 pathway: A lesson from Otub1.* World J Biol Chem, 2014. **5**(2): p. 75-84.

70.	Harhaj, E.W. and V.M. Dixit, *Deubiquitinases in the regulation of NF-kappaB signaling.* Cell Res, 2011. **21**(1): p. 22-39.

71.	Sun, X.X., R.C. Sears, and M.S. Dai, *Deubiquitinating c-Myc: USP36 steps up in the nucleolus.* Cell Cycle, 2015. **14**(24): p. 3786-93.

72.	Schwartz, A.L. and A. Ciechanover, *The ubiquitin-proteasome pathway and pathogenesis of human diseases.* Annu Rev Med, 1999. **50**: p. 57-74.

73.	Vinitsky, A., et al., *Inhibition of the chymotrypsin-like activity of the pituitary multicatalytic proteinase complex.* Biochemistry, 1992. **31**(39): p. 9421-8.

74.	Rock, K.L., et al., *Inhibitors of the proteasome block the degradation of most cell proteins and the generation of peptides presented on MHC class I molecules.* Cell, 1994. **78**(5): p. 761-71.

75.	Thompson, R.C., *Peptide aldehydes: potent inhibitors of serine and cysteine proteases.* Methods Enzymol, 1977. **46**: p. 220-5.

76.	Schramm, V.L., *Transition States, analogues, and drug development.* ACS Chem Biol, 2013. **8**(1): p. 71-81.

77.	de Bettignies, G. and O. Coux, *Proteasome inhibitors: Dozens of molecules and still counting.* Biochimie, 2010. **92**(11): p. 1530-45.

78. Adams, J., et al., *Potent and selective inhibitors of the proteasome: dipeptidyl boronic acids.* Bioorg Med Chem Lett, 1998. **8**(4): p. 333-8.

79. Smoum, R., et al., *Boron containing compounds as protease inhibitors.* Chem Rev, 2012. **112**(7): p. 4156-220.

80. Groll, M., et al., *Crystal structure of the boronic acid-based proteasome inhibitor bortezomib in complex with the yeast 20S proteasome.* Structure, 2006. **14**(3): p. 451-6.

81. Kupperman, E., et al., *Evaluation of the proteasome inhibitor MLN9708 in preclinical models of human cancer.* Cancer Res. **70**(5): p. 1970-80.

82. Vogl, D.T., et al., *Phase I/II study of the novel proteasome inhibitor delanzomib (CEP-18770) for relapsed and refractory multiple myeloma.* Leuk Lymphoma, 2017. **58**(8): p. 1872-1879.

83. Fenteany, G., et al., *A beta-lactone related to lactacystin induces neurite outgrowth in a neuroblastoma cell line and inhibits cell cycle progression in an osteosarcoma cell line.* Proc Natl Acad Sci U S A, 1994. **91**(8): p. 3358-62.

84. Fenteany, G. and S.L. Schreiber, *Lactacystin, proteasome function, and cell fate.* J Biol Chem, 1998. **273**(15): p. 8545-8.

85. Craiu, A., et al., *Lactacystin and clasto-lactacystin beta-lactone modify multiple proteasome beta-subunits and inhibit intracellular protein degradation and major histocompatibility complex class I antigen presentation.* J Biol Chem, 1997. **272**(20): p. 13437-45.

86. Shah, I.M., et al., *Early clinical experience with the novel proteasome inhibitor PS-519.* Br J Clin Pharmacol, 2002. **54**(3): p. 269-76.

87. Feling, R.H., et al., *Salinosporamide A: a highly cytotoxic proteasome inhibitor from a novel microbial source, a marine bacterium of the new genus salinospora.* Angew Chem Int Ed Engl, 2003. **42**(3): p. 355-7.

88. Chauhan, D., et al., *A novel orally active proteasome inhibitor induces apoptosis in multiple myeloma cells with mechanisms distinct from Bortezomib.* Cancer Cell, 2005. **8**(5): p. 407-19.

89. Macherla, V.R., et al., *Structure-activity relationship studies of salinosporamide A (NPI-0052), a novel marine derived proteasome inhibitor.* J Med Chem, 2005. **48**(11): p. 3684-7.

90. Hamlin, P.A., et al., *First-in-human phase I study of the novel structure proteasome inhibitor NPI-0052.* J Clin Oncol, 2009. **27**(15_suppl): p. 3516.

91. Spencer, A., et al., *A phase 1 clinical trial evaluating marizomib, pomalidomide and low-dose dexamethasone in relapsed and refractory multiple myeloma (NPI-0052-107): final study results.* Br J Haematol, 2018. **180**(1): p. 41-51.

92. Di, K., et al., *Marizomib activity as a single agent in malignant gliomas: ability to cross the blood-brain barrier.* Neuro Oncol, 2016. **18**(6): p. 840-8.

93. NCT03345095, http://clinicaltrials.gov

94. Palmer, J.T., et al., *Vinyl Sulfones as Mechanism-Based Cysteine Protease Inhibitors.* J. Med. Chem., 1995. **38**(17): p. 3193-3196.

95. Bogyo, M., et al., *Covalent modification of the active site threonine of proteasomal beta subunits and the Escherichia coli homolog HslV by a new class of inhibitors.* Proc Natl Acad Sci U S A, 1997. **94**(13): p. 6629-34.

96.   Nazif, T. and M. Bogyo, *Global analysis of proteasomal substrate specificity using positional-scanning libraries of covalent inhibitors.* Proc Natl Acad Sci U S A, 2001. **98**(6): p. 2967-72.

97.   Verdoes, M., et al., *A fluorescent broad-spectrum proteasome inhibitor for labeling proteasomes in vitro and in vivo.* Chem Biol, 2006. **13**(11): p. 1217-26.

98.   Sugawara, K., et al., *Eponemycin, a new antibiotic active against B16 melanoma. I. Production, isolation, structure and biological activity.* J Antibiot (Tokyo), 1990. **43**: p. 8-18.

99.   Hanada, M., et al., *Epoxomicin, a new antitumor agent of microbial origin.* J Antibiot (Tokyo), 1992. **45**: p. 1746-1752.

100.   Sin, N., et al., *Eponemycin analogues: syntheses and use as probes of angiogenesis.* Bioorg Med Chem, 1998. **6**(8): p. 1209-17.

101.   Meng, L., et al., *Eponemycin exerts its antitumor effect through the inhibition of proteasome function.* Cancer Res, 1999. **59**(12): p. 2798-801.

102.   Meng, L., et al., *Epoxomicin, a potent and selective proteasome inhibitor, exhibits in vivo antiinflammatory activity.* Proc Natl Acad Sci U S A, 1999. **96**(18): p. 10403-8.

103.   Groll, M., et al., *Crystal Structure of Epoxomicin:20S Proteasome Reveals a Molecular Basis for Selectivity of α',β'-Epoxyketone Proteasome Inhibitors.* J. Am. Chem. Soc., 2000. **122**(6): p. 1237-1238.

104.   Schrader, J., et al., *The inhibition mechanism of human 20S proteasomes enables next-generation inhibitor design.* Science, 2016. **353**(6299): p. 594-8.

105.   Carmony, K., W. Lee, and K.B. Kim, *High-Resolution Snapshots of Proteasome Inhibitors in Action Revise Inhibition Paradigms and Inspire Next-Generation Inhibitor Design.* Chembiochem, 2016. **17**(22): p. 2115-2117.

106.   Carmony, K.C., et al., *A bright approach to the immunoproteasome: Development of LMP2/beta1i-specific imaging probes.* Bioorganic & medicinal chemistry, 2011.

107.   Park, J.E., et al., *A FRET-based approach for identification of proteasome catalytic subunit composition.* Mol Biosyst, 2013. **10**(2): p. 196-200.

108.   Herndon, T.M., et al., *U.s. Food and Drug Administration approval: carfilzomib for the treatment of multiple myeloma.* Clin Cancer Res, 2013. **19**(17): p. 4559-63.

109.   Goodwin, J.T., et al., *Strategies toward predicting peptide cellular permeability from computed molecular descriptors.* J Pept Res, 1999. **53**(4): p. 355-69.

110.   Mirabella, A.C., et al., *Specific cell-permeable inhibitor of proteasome trypsin-like sites selectively sensitizes myeloma cells to bortezomib and carfilzomib.* Chemistry & biology, 2011. **18**(5): p. 608-18.

111.   Geurink, P.P., et al., *Incorporation of non-natural amino acids improves cell permeability and potency of specific inhibitors of proteasome trypsin-like sites.* J Med Chem, 2013. **56**(3): p. 1262-75.

112.   de Bruin, G., et al., *A Set of Activity-Based Probes to Visualize Human (Immuno)proteasome Activities.* Angew Chem Int Ed Engl, 2016. **55**(13): p. 4199-203.

113.   Blackburn, C., et al., *Characterization of a new series of non-covalent proteasome inhibitors with exquisite potency and selectivity for the 20S beta5-subunit.* The Biochemical journal, 2010. **430**(3): p. 461-76.

114.   Kisselev, A.F., et al., *The caspase-like sites of proteasomes, their substrate specificity, new inhibitors and substrates, and allosteric interactions with the trypsin-like sites.* J Biol Chem, 2003. **278**(38): p. 35869-77.

115. Ho, Y.K., et al., *LMP2-specific inhibitors: chemical genetic tools for proteasome biology.* Chem Biol, 2007. **14**(4): p. 419-30.

116. de Bruin, G., et al., *Structure-based design of beta1i or beta5i specific inhibitors of human immunoproteasomes.* J Med Chem, 2014. **57**(14): p. 6197-209.

117. Myung, J., et al., *Lack of proteasome active site allostery as revealed by subunit- specific inhibitors.* Mol Cell, 2001. **7**(2): p. 411-20.

118. Parlati, F., et al., *Carfilzomib can induce tumor cell death through selective inhibition of the chymotrypsin-like activity of the proteasome.* Blood, 2009. **114**(16): p. 3439-47.

119. Muchamuel, T., et al., *A selective inhibitor of the immunoproteasome subunit LMP7 blocks cytokine production and attenuates progression of experimental arthritis.* Nat Med, 2009. **15**(7): p. 781-7.

120. Zhou, H.J., et al., *Design and Synthesis of an Orally Bioavailable and Selective Peptide Epoxyketone Proteasome Inhibitor (PR-047).* J Med Chem, 2009.

121. Mitch, W.E. and A.L. Goldberg, *Mechanisms of muscle wasting. The role of the ubiquitin-proteasome pathway.* N Engl J Med, 1996. **335**(25): p. 1897-905.

122. Sanchez-Serrano, I., *Success in translational research: lessons from the development of bortezomib.* Nat Rev Drug Discov, 2006. **5**(2): p. 107-14.

123. Palombella, V.J., et al., *The ubiquitin-proteasome pathway is required for processing the NF- kappa B1 precursor protein and the activation of NF-kappa B.* Cell, 1994. **78**(5): p. 773-85.

124. Christman, J.W., L.H. Lancaster, and T.S. Blackwell, *Nuclear factor kappa B: a pivotal role in the systemic inflammatory response syndrome and new target for therapy.* Intensive Care Med, 1998. **24**(11): p. 1131-8.

125. Adams, J., et al., *Proteasome inhibitors: a novel class of potent and effective antitumor agents.* Cancer Res, 1999. **59**(11): p. 2615-22.

126. Teicher, B.A., et al., *The proteasome inhibitor PS-341 in cancer therapy.* Clin Cancer Res, 1999. **5**(9): p. 2638-45.

127. Adams, J., *Development of the Proteasome Inhibitor PS-341.* Oncologist, 2002. **7**(1): p. 9-16.

128. Orlowski, R.Z., et al., *Phase I trial of the proteasome inhibitor PS-341 in patients with refractory hematologic malignancies.* J Clin Oncol, 2002. **20**(22): p. 4420-7.

129. Richardson, P.G., et al., *Extended follow-up of a phase II trial in relapsed, refractory multiple myeloma:: final time-to-event results from the SUMMIT trial.* Cancer, 2006. **106**(6): p. 1316-9.

130. Blade, J., M.T. Cibeira, and L. Rosinol, *Bortezomib: a valuable new antineoplastic strategy in multiple myeloma.* Acta Oncol, 2005. **44**(5): p. 440-8.

131. Elofsson, M., et al., *Towards subunit-specific proteasome inhibitors: synthesis and evaluation of peptide alpha',beta'-epoxyketones.* Chem Biol, 1999. **6**(11): p. 811-22.

132. Kim, K.B. and C.M. Crews, *From epoxomicin to carfilzomib: chemistry, biology, and medical outcomes.* Nat Prod Rep, 2013. **30**(5): p. 600-4.

133. Demo, S.D., et al., *Antitumor activity of PR-171, a novel irreversible inhibitor of the proteasome.* Cancer research, 2007. **67**(13): p. 6383-91.

134. Alsina, M., et al., *A phase I single-agent study of twice-weekly consecutive-day dosing of the proteasome inhibitor carfilzomib in patients with relapsed or refractory multiple myeloma or lymphoma.* Clin Cancer Res, 2012. **18**(17): p. 4830-40.

135. Jagannath, S., et al., *An open-label single-arm pilot phase II study (PX-171-003-A0) of low-dose, single-agent carfilzomib in patients with relapsed and refractory multiple myeloma.* Clin Lymphoma Myeloma Leuk, 2012. **12**(5): p. 310-8.

136. diCapua Siegel, D.S., et al., *Results of PX-171-003-A1, An Open-Label, Single-Arm, Phase 2 (Ph 2) Study of Carfilzomib (CFZ) In Patients (pts) with Relapsed and Refractory Multiple Myeloma (MM).* Blood, 2010. **116**(21): p. 985-985.

137. Richardson, P.G., et al., *Extended follow-up of a phase 3 trial in relapsed multiple myeloma: final time-to-event results of the APEX trial.* Blood, 2007. **110**(10): p. 3557-60.

138. Stewart, A.K., et al., *Carfilzomib, lenalidomide, and dexamethasone for relapsed multiple myeloma.* N Engl J Med, 2015. **372**(2): p. 142-52.

139. Dimopoulos, M.A., et al., *Carfilzomib and dexamethasone versus bortezomib and dexamethasone for patients with relapsed or refractory multiple myeloma (ENDEAVOR): a randomised, phase 3, open-label, multicentre study.* Lancet Oncol, 2016. **17**(1): p. 27-38.

140. Dimopoulos, M.A., et al., *Carfilzomib or bortezomib in relapsed or refractory multiple myeloma (ENDEAVOR): an interim overall survival analysis of an open-label, randomised, phase 3 trial.* Lancet Oncol, 2017. **18**(10): p. 1327-1337.

141. Moreau, P., et al., *Oral Ixazomib, Lenalidomide, and Dexamethasone for Multiple Myeloma.* N Engl J Med, 2016. **374**(17): p. 1621-34.

142. Teras, L.R., et al., *2016 US lymphoid malignancy statistics by World Health Organization subtypes.* CA Cancer J Clin, 2016.

143. Alexander, D.D., et al., *Multiple myeloma: a review of the epidemiologic literature.* Int J Cancer, 2007. **120 Suppl 12**: p. 40-61.

144. Cusack, J.C., Jr., et al., *Enhanced chemosensitivity to CPT-11 with proteasome inhibitor PS-341: implications for systemic nuclear factor-kappaB inhibition.* Cancer Res, 2001. **61**(9): p. 3535-40.

145. Amiri, K.I., et al., *Augmenting chemosensitivity of malignant melanoma tumors via proteasome inhibition: implication for bortezomib (VELCADE, PS-341) as a therapeutic agent for malignant melanoma.* Cancer Res, 2004. **64**(14): p. 4912-8.

146. Satou, Y., et al., *Proteasome inhibitor, bortezomib, potently inhibits the growth of adult T-cell leukemia cells both in vivo and in vitro.* Leukemia, 2004. **18**(8): p. 1357-63.

147. Ryan, D.P., et al., *Phase I clinical trial of bortezomib in combination with gemcitabine in patients with advanced solid tumors.* Cancer, 2006. **107**(10): p. 2482-9.

148. Dreicer, R., et al., *Phase I/II study of bortezomib plus docetaxel in patients with advanced androgen-independent prostate cancer.* Clin Cancer Res, 2007. **13**(4): p. 1208-15.

149. Rosenberg, J.E., et al., *Phase II study of bortezomib in patients with previously treated advanced urothelial tract transitional cell carcinoma: CALGB 90207.* Ann Oncol, 2008. **19**(5): p. 946-50.

150. Denlinger, C.S., et al., *A phase II trial of the proteasome inhibitor bortezomib in patients with advanced biliary tract cancers.* Clin Colorectal Cancer, 2014. **13**(2): p. 81-6.

151. Ishitsuka, K., et al., *A phase II study of bortezomib in patients with relapsed or refractory aggressive adult T-cell leukemia/lymphoma.* Cancer Sci, 2015. **106**(9): p. 1219-23.

152. Baker, A.F., et al., *Carfilzomib demonstrates broad anti-tumor activity in pre-clinical non-small cell and small cell lung cancer models.* J Exp Clin Cancer Res, 2014. **33**: p. 111.

153. Tang, W., et al., *Enhanced anti-colorectal cancer effects of carfilzomib combined with CPT-11 via downregulation of nuclear factor-kappaB in vitro and in vivo.* Int J Oncol, 2014. **45**(3): p. 995-1010.

154. Papadopoulos, K.P., et al., *A phase I/II study of carfilzomib 2-10-min infusion in patients with advanced solid tumors.* Cancer Chemother Pharmacol, 2013. **72**(4): p. 861-8.

155. Smith, D.C., et al., *Phase 1 study of ixazomib, an investigational proteasome inhibitor, in advanced non-hematologic malignancies.* Invest New Drugs, 2015. **33**(3): p. 652-63.

156. Shi, D.S., et al., *Proteasome function is required for platelet production.* J Clin Invest, 2014. **124**(9): p. 3757-66.

157. Argyriou, A.A., G. Iconomou, and H.P. Kalofonos, *Bortezomib-induced peripheral neuropathy in multiple myeloma: a comprehensive review of the literature.* Blood, 2008. **112**(5): p. 1593-9.

158. Arastu-Kapur, S., et al., *Non-proteasomal targets of the proteasome inhibitors bortezomib and carfilzomib: a link to clinical adverse events.* Clin Cancer Res, 2011.

159. Raedler, L.A., *Ninlaro (Ixazomib): First Oral Proteasome Inhibitor Approved for the Treatment of Patients with Relapsed or Refractory Multiple Myeloma.* Am Health Drug Benefits, 2016. **9**(Spec Feature): p. 102-5.

160. Siegel, D.S., et al., *A phase 2 study of single-agent carfilzomib (PX-171-003-A1) in patients with relapsed and refractory multiple myeloma.* Blood, 2012. **120**(14): p. 2817-25.

161. Lu, S., et al., *Overexpression of the PSMB5 gene contributes to bortezomib resistance in T-lymphoblastic lymphoma/leukemia cells derived from Jurkat line.* Exp Hematol, 2008. **36**(10): p. 1278-84.

162. Oerlemans, R., et al., *Molecular basis of bortezomib resistance: proteasome subunit beta5 (PSMB5) gene mutation and overexpression of PSMB5 protein.* Blood, 2008. **112**(6): p. 2489-99.

163. Huber, E.M., W. Heinemeyer, and M. Groll, *Bortezomib-resistant mutant proteasomes: structural and biochemical evaluation with carfilzomib and ONX 0914.* Structure, 2015. **23**(2): p. 407-17.

164. Li, X., et al., *Effect of noncompetitive proteasome inhibition on bortezomib resistance.* J Natl Cancer Inst, 2010. **102**(14): p. 1069-82.

165. Chapman, M.A., et al., *Initial genome sequencing and analysis of multiple myeloma.* Nature, 2011. **471**(7339): p. 467-72.

166. Lichter, D.I., et al., *Sequence analysis of beta-subunit genes of the 20S proteasome in patients with relapsed multiple myeloma treated with bortezomib or dexamethasone.* Blood, 2012. **120**(23): p. 4513-6.

167. Barrio, S., et al., *Parallel Evolution of Multiple PSMB5 mutations in a Myeloma Patient Treated with Bortezomib.* Blood, 2016. **128**(22): p. 3282-3282.

168. Verbrugge, S.E., et al., *Inactivating PSMB5 mutations and P-glycoprotein (multidrug resistance-associated protein/ATP-binding cassette B1) mediate resistance to proteasome inhibitors: ex vivo efficacy of (immuno)proteasome inhibitors in mononuclear blood cells from patients with rheumatoid arthritis.* J Pharmacol Exp Ther, 2012. **341**(1): p. 174-82.

169. Ao, L., et al., *Development of Peptide-based reversing agents for p-glycoprotein-mediated resistance to carfilzomib.* Mol Pharm, 2012. **9**(8): p. 2197-205.

170. Besse, A., et al., *Carfilzomib resistance due to ABCB1/MDR1 overexpression is overcome by nelfinavir and lopinavir in multiple myeloma.* Leukemia, 2017.

171. Epstein, J., H.Q. Xiao, and B.K. Oba, *P-glycoprotein expression in plasma-cell myeloma is associated with resistance to VAD.* Blood, 1989. **74**(3): p. 913-7.

172. Grogan, T.M., et al., *P-glycoprotein expression in human plasma cell myeloma: correlation with prior chemotherapy.* Blood, 1993. **81**(2): p. 490-5.

173. Suzuki, E., et al., *Molecular mechanisms of bortezomib resistant adenocarcinoma cells.* PLoS One, 2011. **6**(12): p. e27996.

174. Niewerth, D., et al., *Interferon-gamma-induced upregulation of immunoproteasome subunit assembly overcomes bortezomib resistance in human hematological cell lines.* J Hematol Oncol, 2014. **7**: p. 7.

175. Niewerth, D., et al., *Proteasome subunit expression analysis and chemosensitivity in relapsed paediatric acute leukaemia patients receiving bortezomib-containing chemotherapy.* J Hematol Oncol, 2016. **9**(1): p. 82.

176. Niewerth, D., et al., *Higher ratio immune versus constitutive proteasome level as novel indicator of sensitivity of pediatric acute leukemia cells to proteasome inhibitors.* Haematologica, 2013. **98**(12): p. 1896-904.

177. Chen, Y. and F. Brandizzi, *IRE1: ER stress sensor and cell fate executor.* Trends Cell Biol, 2013. **23**(11): p. 547-55.

178. Lee, A.H., et al., *Proteasome inhibitors disrupt the unfolded protein response in myeloma cells.* Proc Natl Acad Sci U S A, 2003. **100**(17): p. 9946-51.

179. Leung-Hagesteijn, C., et al., *Xbp1s-negative tumor B cells and pre-plasmablasts mediate therapeutic proteasome inhibitor resistance in multiple myeloma.* Cancer Cell, 2013. **24**(3): p. 289-304.

180. Gambella, M., et al., *High XBP1 expression is a marker of better outcome in multiple myeloma patients treated with bortezomib.* Haematologica, 2014. **99**(2): p. e14-6.

181. Choi, S.Y., et al., *Lessons from patient-derived xenografts for better in vitro modeling of human cancer.* Adv Drug Deliv Rev, 2014. **79-80**: p. 222-37.

182. *Velcade(R) (bortezomib) for injection, Full Prescribing Information.*

183. Moreau, P., et al., *Pharmacokinetic, pharmacodynamic and covariate analysis of subcutaneous versus intravenous administration of bortezomib in patients with relapsed multiple myeloma.* Clin Pharmacokinet, 2012. **51**(12): p. 823-9.

184. Pekol, T., et al., *Human metabolism of the proteasome inhibitor bortezomib: identification of circulating metabolites.* Drug Metab Dispos, 2005. **33**(6): p. 771-7.

185. Labutti, J., et al., *Oxidative deboronation of the peptide boronic acid proteasome inhibitor bortezomib: contributions from reactive oxygen species in this novel cytochrome P450 reaction.* Chem Res Toxicol, 2006. **19**(4): p. 539-46.

186. Clemens, J., et al., *Cellular uptake kinetics of bortezomib in relation to efficacy in myeloma cells and the influence of drug transporters.* Cancer Chemother Pharmacol, 2015. **75**(2): p. 281-91.

187. Minchinton, A.I. and I.F. Tannock, *Drug penetration in solid tumours.* Nat Rev Cancer, 2006. **6**(8): p. 583-92.

188. Williamson, M.J., et al., *The relationship among tumor architecture, pharmacokinetics, pharmacodynamics, and efficacy of bortezomib in mouse xenograft models.* Mol Cancer Ther, 2009. **8**(12): p. 3234-43.

189. Wang, Z., et al., *Clinical pharmacokinetics, metabolism, and drug-drug interaction of carfilzomib.* Drug Metab Dispos, 2013. **41**(1): p. 230-7.

190.   Carlisle, K.M., et al., *Estimation of total hepatic blood flow by duplex ultrasound.* Gut, 1992. **33**(1): p. 92-7.

191.   Yang, J., et al., *Pharmacokinetics, pharmacodynamics, metabolism, distribution, and excretion of carfilzomib in rats.* Drug Metab Dispos, 2011. **39**(10): p. 1873-82.

192.   Richardson, P.G., et al., *Phase 1 study of twice-weekly ixazomib, an oral proteasome inhibitor, in relapsed/refractory multiple myeloma patients.* Blood, 2014. **124**(7): p. 1038-46.

193.   Lum, R.T., et al., *A new structural class of proteasome inhibitors that prevent NF-kappa B activation.* Biochem Pharmacol, 1998. **55**(9): p. 1391-7.

194.   Lum, R.T., et al., *Selective inhibition of the chymotrypsin-like activity of the 20S proteasome by 5-methoxy-1-indanone dipeptide benzamides.* Bioorg Med Chem Lett, 1998. **8**(3): p. 209-14.

195.   Koguchi, Y., et al., *TMC-95A, B, C, and D, novel proteasome inhibitors produced by Apiospora montagnei Sacc. TC 1093. Taxonomy, production, isolation, and biological activities.* J Antibiot (Tokyo), 2000. **53**(2): p. 105-9.

196.   Kohno, J., et al., *Structures of TMC-95A-D: novel proteasome inhibitors from Apiospora montagnei sacc. TC 1093.* J Org Chem, 2000. **65**(4): p. 990-5.

197.   Groll, M., et al., *Crystal structure of the 20 S proteasome:TMC-95A complex: a non-covalent proteasome inhibitor.* J Mol Biol, 2001. **311**(3): p. 543-8.

198.   Kazi, A., et al., *Discovery of a novel proteasome inhibitor selective for cancer cells over non-transformed cells.* Cell Cycle, 2009. **8**(12): p. 1940-51.

199.   Lawrence, H.R., et al., *Synthesis and biological evaluation of naphthoquinone analogs as a novel class of proteasome inhibitors.* Bioorg Med Chem, 2010. **18**(15): p. 5576-92.

200.   Gallastegui, N., et al., *Hydroxyureas as noncovalent proteasome inhibitors.* Angew Chem Int Ed Engl, 2012. **51**(1): p. 247-9.

201.   Ozcan, S., et al., *Oxadiazole-isopropylamides as potent and noncovalent proteasome inhibitors.* J Med Chem, 2013. **56**(10): p. 3783-805.

202.   Kazi, A., et al., *Discovery of PI-1840, a novel noncovalent and rapidly reversible proteasome inhibitor with anti-tumor activity.* J Biol Chem, 2014. **289**(17): p. 11906-15.

203.   Siegel, R.L., K.D. Miller, and A. Jemal, *Cancer statistics, 2016.* CA Cancer J Clin, 2016. **66**(1): p. 7-30.

204.   Macdonald, S. and F. Mair, *Tackling cancers of unmet need: the pancreatic cancer pathway.* Lancet Gastroenterol Hepatol, 2016. **1**(4): p. 266-267.

205.   Bupathi, M., et al., *Hepatocellular carcinoma: Where there is unmet need.* Mol Oncol, 2015. **9**(8): p. 1501-9.

206.   Miller, Z., et al., *Proteasome inhibitors with pyrazole scaffolds from structure-based virtual screening.* J Med Chem, 2015. **58**(4): p. 2036-41.

207.   Lei, B., H. Adel, and C.-G. Zhan, *Structural features and binding free energies for non-covalent inhibitors interacting with immunoproteasome by molecular modeling and dynamics simulations.* Theoretical Chemistry Accounts, 2012. **131**(4): p. 1203.

208.   Furet, P., et al., *Entry into a new class of potent proteasome inhibitors having high antiproliferative activity by structure-based design.* J Med Chem, 2004. **47**(20): p. 4810-3.

209.   Harshbarger, W., et al., *Crystal structure of the human 20S proteasome in complex with carfilzomib.* Structure, 2015. **23**(2): p. 418-24.

210. Kisselev, A.F., A. Callard, and A.L. Goldberg, *Importance of the different proteolytic sites of the proteasome and the efficacy of inhibitors varies with the protein substrate.* J Biol Chem, 2006. **281**(13): p. 8582-90.

211. Winter, M.B., et al., *Immunoproteasome functions explained by divergence in cleavage specificity and regulation.* Elife, 2017. **6**.

212. Kim, K.B., et al., *Proteasome inhibitors*. 2016, Google Patents.

213. Snodin, D.J. and S.D. McCrossen, *Mutagenic impurities in pharmaceuticals: a critique of the derivation of the cancer TTC (Threshold of Toxicological Concern) and recommendations for structural-class-based limits.* Regul Toxicol Pharmacol, 2013. **67**(2): p. 299-316.

214. Kasam, V., et al., *Selective immunoproteasome inhibitors with non-peptide scaffolds identified from structure-based virtual screening.* Bioorg Med Chem Lett, 2014. **24**(15): p. 3614-7.

215. Miller, Z., et al., *Inhibitors of the immunoproteasome: current status and future directions.* Curr Pharm Des, 2013. **19**(22): p. 4140-51.

216. Britton, M., et al., *Selective inhibitor of proteasome's caspase-like sites sensitizes cells to specific inhibition of chymotrypsin-like sites.* Chem Biol, 2009. **16**(12): p. 1278-89.

217. Fabre, B., et al., *Subcellular distribution and dynamics of active proteasome complexes unraveled by a workflow combining in vivo complex cross-linking and quantitative proteomics.* Mol Cell Proteomics, 2013. **12**(3): p. 687-99.

218. Liu, C.W., et al., *ATP binding and ATP hydrolysis play distinct roles in the function of 26S proteasome.* Mol Cell, 2006. **24**(1): p. 39-50.

219. Copeland, R.A., et al., *Impact of enzyme concentration and residence time on apparent activity recovery in jump dilution analysis.* Anal Biochem, 2011. **416**(2): p. 206-10.

220. Patching, S.G., *Surface plasmon resonance spectroscopy for characterisation of membrane protein-ligand interactions and its potential for drug discovery.* Biochim Biophys Acta, 2014. **1838**(1 Pt A): p. 43-55.

221. Shabaneh, T.B., et al., *Molecular basis of differential sensitivity of myeloma cells to clinically relevant bolus treatment with bortezomib.* PLoS One, 2013. **8**(2): p. e56132.

222. Chiba, M., Y. Ishii, and Y. Sugiyama, *Prediction of hepatic clearance in human from in vitro data for successful drug development.* AAPS J, 2009. **11**(2): p. 262-76.

223. Chauhan, D., et al., *A novel orally active proteasome inhibitor ONX 0912 triggers in vitro and in vivo cytotoxicity in multiple myeloma.* Blood, 2011. **116**(23): p. 4906-15.

224. Moreno, L. and A.D. Pearson, *How can attrition rates be reduced in cancer drug discovery?* Expert Opin Drug Discov, 2013. **8**(4): p. 363-8.

225. Tonkens, R., *An overview of the drug development process.* Physician Exec, 2005. **31**(3): p. 48-52.

226. Strovel, J., et al., *Early Drug Discovery and Development Guidelines: For Academic Researchers, Collaborators, and Start-up Companies*, in *Assay Guidance Manual*, G.S. Sittampalam, et al., Editors. 2004: Bethesda (MD).

227. Gallastegui, N. and M. Groll, *Analysing properties of proteasome inhibitors using kinetic and X-ray crystallographic studies.* Methods Mol Biol, 2012. **832**: p. 373-90.

228. Frueh, D.P., et al., *NMR methods for structural studies of large monomeric and multimeric proteins.* Curr Opin Struct Biol, 2013. **23**(5): p. 734-9.

229. Sprangers, R., et al., *TROSY-based NMR evidence for a novel class of 20S proteasome inhibitors.* Biochemistry, 2008. **47**(26): p. 6727-34.

230. Sprangers, R. and L.E. Kay, *Quantitative dynamics and binding studies of the 20S proteasome by NMR.* Nature, 2007. **445**(7128): p. 618-22.

231. Lightcap, E.S., et al., *Proteasome inhibition measurements: clinical application.* Clin Chem, 2000. **46**(5): p. 673-83.

232. de Groot, K.A., et al., *Pharmacodynamic monitoring of (immuno)proteasome inhibition during bortezomib treatment of a critically ill patient with lupus nephritis and myocarditis.* Lupus Sci Med, 2015. **2**(1): p. e000121.

233. Luker, G.D., et al., *Imaging 26S proteasome activity and inhibition in living mice.* Nat Med, 2003. **9**(7): p. 969-73.

234. Momose, I., et al., *In vivo imaging of proteasome inhibition using a proteasome-sensitive fluorescent reporter.* Cancer Sci, 2012. **103**(9): p. 1730-6.

235. Day, C.P., G. Merlino, and T. Van Dyke, *Preclinical mouse cancer models: a maze of opportunities and challenges.* Cell, 2015. **163**(1): p. 39-53.

236. Bowes, J., et al., *Reducing safety-related drug attrition: the use of in vitro pharmacological profiling.* Nat Rev Drug Discov, 2012. **11**(12): p. 909-22.

237. Zimmermann, J., et al., *Proteasome inhibitor induced gene expression profiles reveal overexpression of transcriptional regulators ATF3, GADD153 and MAD1.* Oncogene, 2000. **19**(25): p. 2913-20.

238. Tang, Z.Y., et al., *Effects of the proteasome inhibitor bortezomib on gene expression profiles of pancreatic cancer cells.* J Surg Res, 2008. **145**(1): p. 111-23.

239. Lamb, J., *The Connectivity Map: a new tool for biomedical research.* Nat Rev Cancer, 2007. **7**(1): p. 54-60.

240. Subramanian, A., et al., *A Next Generation Connectivity Map: L1000 Platform and the First 1,000,000 Profiles.* Cell, 2017. **171**(6): p. 1437-1452 e17.

241. Wu, X., et al., *In vitro ADME profiling using high-throughput rapidfire mass spectrometry: cytochrome p450 inhibition and metabolic stability assays.* J Biomol Screen, 2012. **17**(6): p. 761-72.

242. Volpe, D.A., *Transporter assays as useful in vitro tools in drug discovery and development.* Expert Opin Drug Discov, 2016. **11**(1): p. 91-103.

243. Sevin, E., et al., *Accelerated Caco-2 cell permeability model for drug discovery.* J Pharmacol Toxicol Methods, 2013. **68**(3): p. 334-9.

ZACHARY CHARLES MILLER

PLACE OF BIRTH

Dodgeville, Wisconsin, USA

EDUCATION

2005-2011   Bachelor of Science, Pharmacology and Toxicology
              University of Wisconsin-Madison, Madison, WI

PUBLICATIONS

Zachary Miller, Lin Ao, Kyung-Bo Kim, and Wooin Lee. "Inhibitors of the Immunoproteasome: Current Status and Future Directions". Current Pharmaceutical Design. 2013; 19(22):4140-4151.

Jieun Park, Lin Ao, **Zachary Miller**, Kyungbo Kim, Ying Wu, Eun Ryoung Jang, Eun Young Lee, Kyung-Bo Kim, and Wooin Lee. "PSMB9 Codon 60 Polymorphisms Have No Impact on the Activity of the Immunoproteasome Catalytic Subunit B1i Expressed in Multiple Types of Solid Cancer". PLoS One. 2013 Sep 9; 8(9):e73732.

Park Jieun, Ying Wu, Kimberly Carmony, **Zachary Miller**, Lalit Sharma, Do-Min Lee, Doo-Young Kim, Wooin Lee, and Kyung-Bo Kim. "A FRET-Based Approach for Identification of Proteasome Catalytic Subunit Composition". Molecular Biosystems. 2014 Feb; 10(2):196-200.

Zachary Miller, Wooin Lee, and Kyung-Bo Kim. "The Immunoproteasome as a Therapeutic Target for Hematological Malignancies". Current Cancer Drug Targets. 2014; 14(6):537-548.

Zachary Miller, Keun-Sik Kim, Do-Min Lee, Vinod Kasam, Si Eun Baek, Kwang Hyun Lee, Yan-Yan Zhang, Lin Ao, Kimberly Carmony, Na-Ra Lee, Shou Zhou, Qingguan Zhao, Yujin Jang, Hyun-Young Jeong, Chang-Guo Zhan, Wooin Lee, Dong-Eun Kim, and Kyung-Bo Kim. "Proteasome Inhibitors with Pyrazole Scaffolds from Structure-Based Virtual Screening". Journal of Medicinal Chemistry. 2015 Feb 26; 58(4):2036–2041.

Ji Eun Park, **Zachary Miller**, Yearin Jun, Wooin Lee, Kyung Bo Kim. "Next-generation proteasome inhibitors for cancer therapy". Translational Research. 2018; https://doi.org/10.1016/j.trsl.2018.03.002.